NOTICE

AVIS

The quality of this microform is heavily dependent upon the quality of the original thesis submitted for microfilming. Every effort has been made to ensure the highest quality of reproduction possible.

La qualité de cette microforme dépend grandement de la qualité de la thèse soumise au microfilmage. Nous avons tout fait pour assurer une qualité supérieure de reproduction.

If pages are missing, contact the university which granted the degree.

S'il manque des pages, veuillez communiquer avec l'université qui a conféré le grade.

Some pages may have indistinct print especially if the original pages were typed with a poor typewriter ribbon or if the university sent us an inferior photocopy.

La qualité d'impression de certaines pages peut laisser à désirer, surtout si les pages originales ont été dactylographiées à l'aide d'un ruban usé ou si l'université nous a fait parvenir une photocopie de qualité inférieure.

Reproduction in full or in part of this microform is governed by the Canadian Copyright Act, R.S.C. 1970, c. C-30, and subsequent amendments.

La reproduction, même partielle, de cette microforme est soumise à la Loi canadienne sur le droit d'auteur, SRC 1970, c. C-30, et ses amendements subséquents.

Canada

UNIVERSITY OF ALBERTA

JET FLOW ON STEPPED SPILLWAYS AND DR⌐⌐S

by

MOHAMMAD R. CHAMANI

©

A THESIS

SUBMITTED TO THE FACULTY OF GRADUATE AND
RESEARCH IN PARTIAL FULFILLMENT OF THE
REQUIREMENT FOR THE DEGREE

of

MASTER OF SCIENCE

in

WATER RESOURCES

DEPARTMENT OF CIVIL ENGINEERING

EDMONTON, ALBERTA

FALL, 1993

The author has granted an irrevocable non-exclusive licence allowing the National Library of Canada to reproduce, loan, distribute or sell copies of his/her thesis by any means and in any form or format, making this thesis available to interested persons.

L'auteur a accordé une licence irrévocable et non exclusive permettant à la Bibliothèque nationale du Canada de reproduire, prêter, distribuer ou vendre des copies de sa thèse de quelque manière et sous quelque forme que ce soit pour mettre des exemplaires de cette thèse à la disposition des personnes intéressées.

The author retains ownership of the copyright in his/her thesis. Neither the thesis nor substantial extracts from it may be printed or otherwise reproduced without his/her permission.

L'auteur conserve la propriété du droit d'auteur qui protège sa thèse. Ni la thèse ni des extraits substantiels de celle-ci ne doivent être imprimés ou autrement reproduits sans son autorisation.
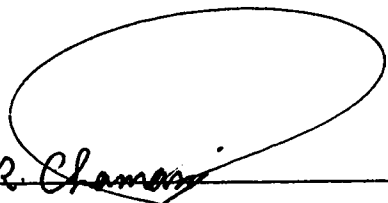
ISBN 0-315-88149-6

Canada

UNIVERSITY OF ALBERTA

RELEASE FORM

NAME OF AUTHOR: Mohammad Reza Chamani

TITLE OF THESIS: Jet Flow on Stepped Spillways and Drops

DEGREE: MASTER OF SCIENCE

YEAR THIS DEGREE GRANTED: FALL 1993

Permission is hereby granted to THE UNIVERSITY OF ALBERTA LIBRARY to reproduce single copies of this thesis and to lend or sell such copies for private, scholarly or scientific research purposes only.

The author reserves other publication rights, and neither the thesis or extensive extracts from it may be printed nor otherwise reproduced without the author's written permission.

Mohammad Reza Chamani

191 Haghparasty Lane

Sadi St., Najafabad

Isfahan, IRAN   85137

Date: June 1993

THE UNIVERSITY OF ALBERTA

FACULTY OF GRADUATE STUDIES AND RESEARCH
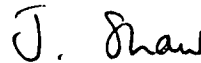
The undersigned certify that they have read, and recommend to the Faculty of Graduate Studies and Research, for acceptance, a thesis entitled JET FLOW ON STEPPED SPILLWAYS AND DROPS submitted by Mohammad R. Chamani in partial fulfillment of the requirement for the degree of MASTER OF SCIENCE.

Dr. N. Rajaratnam, Supervisor

Dr. P. M. Steffler

Dr. J. Shaw

Date: 17th June 93

ABSTRACT

The first part of this study considers jet flow on stepped spillways. Using the experimental results of Horner (1969), a method has been developed to estimate the energy loss on a stepped spillway. It appears that the energy loss in jet flow regime is mainly due to jet circulation in the pool beneath the nappe. An equation for the energy loss is presented based on the idea of the proportion of energy loss on each step, α. Equations are derived to evaluate α for horizontal and inclined steps. It is found that the energy dissipation of maximum discharge in jet flow regime is a function of step geometry and number of steps.

Since the drop is the basic element of a stepped spillway, the flow characteristics of a drop were evaluated by model study, to develop a better understanding of flow in a stepped spillway. The plane jet model is also studied because of its similarity to the drop flow. Flow visualization shows that the nappe oscillation is an important factor in the flow exchanging process between the pool and the jet. It appears that the flow circulation in the pool is a major cause for energy dissipation. Laboratory measurements show that the energy loss at the base of a drop is significant at lower discharges and decreases as the discharge increases. The relative energy loss for plane jet is approximately constant and equal to about 11%. Empirical equations are derived to estimate some of the flow characteristics of the drop based on the experimental data of the present contribution and previous studies.

ACKNOWLEDGMENTS

TABLE OF CONTENTS

LIST OF FIGURES

LIST OF PLATES

LIST OF TABLES

LIST OF SYMBOLS

a, b	Constants
a_1, b_1	Constants
c, d	Constants
D	Drop number
D_r	Pool depth ratio
E	Energy
E_0	Energy at the upstream of a stepped spillway or a drop or a plane jet
E_1	Specific energy at the base of a drop or a plane jet
E_N	Energy number
E_s	Specific energy at the base of a stepped spillway
F_N	Force number
F_s	Specific force at the base of a steeped spillway
g	Gravity acceleration
H	Height of a step.
h	Total height of spillway
L	Length of a step
L_N	Length number
L_p	Pool length
L_r	Pool length ratio
l	Characteristic length
N	Number of steps
Q	Flow discharge
Q_c	Circulating discharge

Q_b	Backward flow in a plane jet
Q_{br}	Backwater discharge ratio
Q_f	Forward flow in a plane jet
Q_r	Circulating discharge ratio
q	Discharge per unit width
r^2	Correlation factor
U	Mean velocity
V	Mean velocity of the free falling jet before the mixing zone
V_1	Mean velocity at the base of drop or plane jet
V_m	Mean velocity of the sliding jet
V_p	Velocity of the sliding jet in mixing zone just below the pool level
V_x	Horizontal mean velocity component of free falling jet.
v_0	Average point velocity at the upstream channel
v_1	Average point velocity at the base of a drop
Y_0	Depth of flow at the upstream channel
Y_1	Depth of flow at the base of a drop
Y_2	Depth of flow in downstream channel if the hydraulic jump begins at the toe of the nappe
Y_b	Depth of backward flow in a plane jet
Y_f	Depth of forward flow in a plane jet
Y_c	Critical depth
Y_p	Pool depth
y_1	Energy loss per unit height
α	Proportion of energy loss on each step
β	Jet inclination at the bed

ΔA	Area element
ΔE	Energy loss
φ	Jet inclination at the pool level
θ	Inclination of a step

Subscripts

m	model
p	prototype
l	loss
u	upstream
r	remaining

Chapter 1

INTRODUCTION

The problem of dissipating the energy of the flow that passes down a spillway is important in hydraulic engineering to reduce the scour downstream of the structure. A stepped spillway can dissipate an appreciable part of this energy. A stepped spillway consists of a series of steps or drops, built into the face of the spillway. When water flows down the steps, turbulent mixing and diffusion can produce more energy dissipation compared to that on a standard spillway.

The use of stepped spillways is not new and, in the past, it was generally used in masonry structures. As far as the writer is aware, the Allahverdi-Khan diversion dam (Plate 1.1), built on Zayandeh-roud River in 15th century in Isfahan, Iran, is one of the oldest masonry dams featuring three dimensional steps (the steps are not continuous across the width of the river). The first step is two meters high while each of the other eight steps measures 0.35 meter in height. The tips of the steps follow a curved line that might be similar to the WES (Waterways Experiment Station) standard profile for ogee spillways. Gausmann and Madden (1923) designed a stepped spillway for the Gilboa dam, a 49 meter embankment dam. The downstream side of the 404 meter masonry part was cut into large steps. The step heights vary from 3.1 meters at the top to 5.8 meters at the bottom. The tread or length of the steps varies from 3.1 to 5.5 meters and the steps are inclined downward. There was no discussion of the energy dissipation characteristics of the Gilboa spillway.
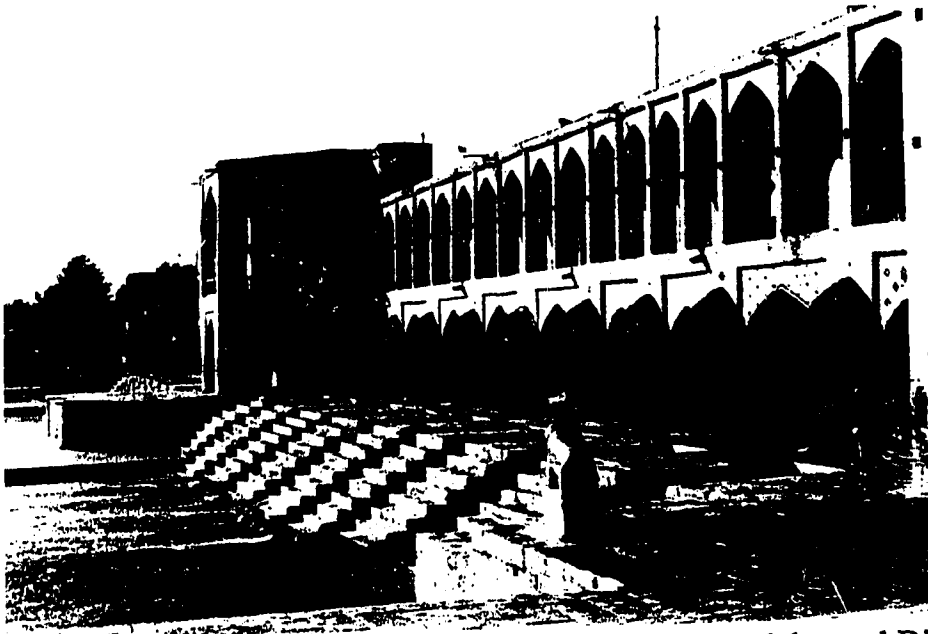
Plate 1.1 The Allahverdi-Khan diversion dam on Zayandeh-roud River, built in 15th century, Isfahan, Iran
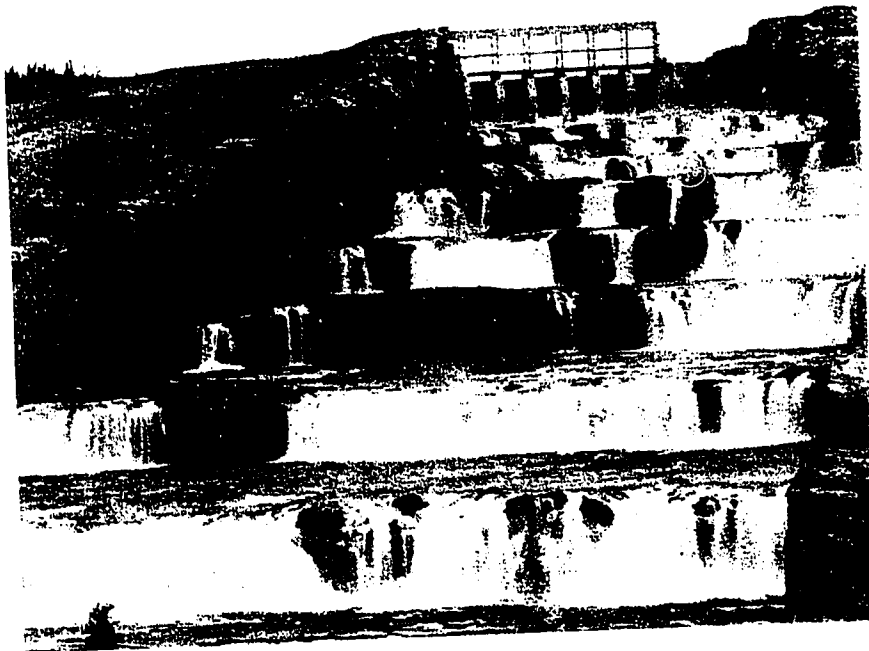
Plate 1.2 The spillway and stepped outlet channel, la Grande 2 development, Quebec

As concrete technology progressed, smooth spillway chutes replaced stepped spillways. Currently, considerable interest is shown on stepped spillways mainly because of the technical advances in the building of RCC (Roller-Compacted Concrete) dams. In addition, the U.S. Bureau of Reclamation is considering the use of stepped spillways as an alternative for rehabilitating old dams. It has been suggested to use the stepped spillway as a protective cover for embankment dams that are not able to pass their design flow without overtopping. Frizell (1992) listed the most recent dams that used the stepped spillway either for regular or emergency overflow (Table 1.1). The stepped outlet channel of la Grande 2 development project in Quebec, completed in 1979, is perhaps the largest in the world. The Societe d' energie de la Baie James (1988) outlines the design specification of the outlet channel that carries a flow of 17,600 cubic meters per second. The stepped channel, cut into solid rock, is 1,500 meters long and 122 meters wide (Plate 1.2). The total drop is 110 meters and consists of 10 steps that range from 127 to 200 meters in length and 9.1 to 12.2 meters in height.

The flow over a stepped spillway can be classified into jet (nappe) or skimming flow regimes, based on the discharge (Figure 1.1). At lower discharges, the jet flow strikes the tread of the steps and its energy is mainly dissipated by jet circulation in the pool beneath the nappe and sometimes by the formation of a partial hydraulic jump on every step. In the skimming flow regime, which occurs at higher discharges, the steps become completely submerged and the flow skims over the steps. In this case, the circulating flow also contributes to the energy loss.

At this time, it is difficult to quantify the energy dissipation for a

Dam and location (Reference, date)	Design unit discharge (m³/s/m)	Hydraulic Height (m)	Downstream Slope (H:V)
Upper Stillwater, U.S.A (Houston, 1987)	11.5	61.6	0.32:1 top 0.60:1 toe
Monksville, U.S.A (Sorensen, 1985)	9.3	36.6	0.78:1
Stagecoach, U.S.A (Stevens)	3.6	42.7	0.80:1
De Mist Kraal, South Africa (Jordaan, 1986)	10.2	18	0.60:1
Zaaihoek, South Africa	5.1	36.6	0.62:1
Lower Chase Creek, U.S.A	3.3	18	0.70:1
Milltown Hill, U.S.A (Frizell, 1990)	14.3	54.9	0.75:1
Middle Fork, U.S.A	overtops for events >500 yrs.	37.8	0.80:1
Knellport, South Africa	8.4	43.1	0.60:1
Santa Cruz, U.S.A	4	36.6	0.65:1
Bucca Weir, Australia	55.6	11.9	0.50:1
Jequitai, Brazil	9.2	36.2	0.80:1
Junction Falls Dam, U.S.A	11.4	9	0.875:1
Les Olivettes, France	7.2	31.5	0.75:1
Cedar Falls, U.S.A	2.8	7.6	0.80:1

Table 1.1 RCC or Rehabilitated Concrete dams with stepped spillway (adapted from Frizell, 1992)

(a) Jet Flow

(b) Skimming Flow
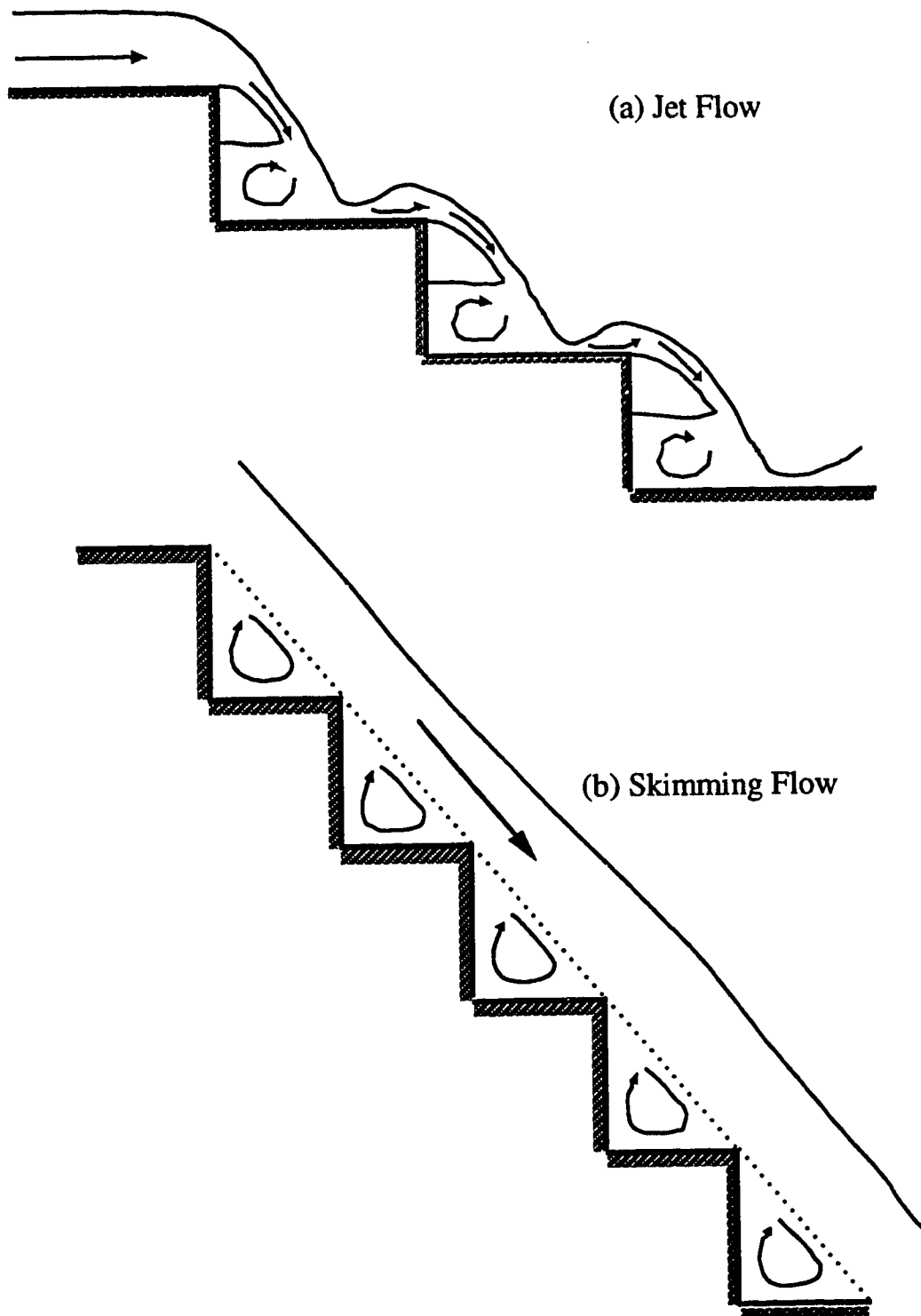
Figure 1.1 Definition sketches for flow on stepped spillways

given discharge and step geometry. Some model studies were carried out by Sorensen (1985), Houston (1987), and Young (1986) to investigate the best step geometry. Sorensen (1985) showed that the kinetic energy at the toe of spillway was reduced to about 6 to 12% of that which would exist at the toe of the corresponding standard spillway. In all the models, the WES standard spillway profile was chosen to pass through the tips of the steps with very little modification. Rajaratnam (1990) developed a method of analyzing skimming flow and showed that, under some conditions, the relative energy loss could be as much as 88%. For his doctoral research, Horner (1969) built a series of hydraulic models to investigate the flow patterns on stepped spillways. In all the models, the envelope of the tips of steps followed a straight line down to the toe of spillway. In this extensive experimental study, graphical solutions for energy and specific forces at the spillway toe, based on non-dimensional parameters for a wide range of step geometry and discharges, were presented for the jet flow regime. However, Horner did not develop any theoretical or other predictive solutions.

The main objective of this study is to develop a general method of estimating the energy dissipation in the jet flow regime. The extensive data of Horner (1969) were used to evaluate the energy loss. Because a stepped spillway is simply a series of steps or drops, to develop a better understanding of hydraulic characteristics of flow over stepped spillway, a detailed examination of flow below a drop (or free overfall) was attempted in this study. Although experimental studies have been carried out by Moore (1943), Rand (1955), and Gill (1982) on drops, very few detailed observations has been made on the nature

and pattern of flow connected with the drop. Hence, a few drop models were built in the T. Blench Hydraulic Laboratory to obtain more information regarding the mechanism of energy dissipation and velocity profiles of the jet flow.

Chapter 2 presents a method to evaluate the energy loss over stepped spillway in the jet flow regime, which uses the considerable amount of experimental data collected by Horner (1969). In chapter 3, a review of earlier studies on the hydraulics of flow over a drop is presented. Chapter 4 describes the present experimental work and present results. The discussion of experimental results, modification of White's theory, and a new analysis are also presented in this chapter. Finally, the conclusions of the present investigation are presented in chapter 5.

Chapter 2

JET FLOW ON STEPPED SPILLWAYS

2.1. Introduction

It was stated earlier that the flow over stepped spillway can be mainly classified into two types, jet (or nappe) flow and skimming flow. Peyras et al. (1992) include the partial jet flow as a transition state to the above classification. In the jet regime, the flow impinges on the tread of the lower step at small discharges. Then the sub or supercritical flow with or without the formation of a hydraulic jump will leave the step and this phenomenon repeats itself on every step. As the discharge increases, the impact point of the jet flow will move towards the end of the step thus starting the partial jet flow. In this stage, the flow does not completely strike the step surface. The upper part of the jet overshoots the tips of the steps and it disperses with considerable turbulence. At higher discharges, the steps become completely submerged and a relatively smooth current skims the steps. In this situation, the spillway may be described as a steep open channel with large roughness elements.

In this study, the term jet flow refers to the jet and partial jet flows. First, a brief description of flow pattern for skimming flow is presented in this chapter. Then, the experimental studies on jet flow by Horner (1969) are reviewed. Later, a new method of estimating the energy loss for the jet flow is presented.

2.2. Skimming Flow

2.2.1. Description

As previously mentioned, skimming flow occurs at high discharge intensities. There is no visible nappe and the smooth coherent stream proceeds down the spillway (Figure 2.1). An added feature of this type of flow is the occurrence of air entrainment. The air entrainment is possibly caused by the spraying, surface break-up and turbulence.

Horner (1969) divided the flow reach into two segments. At the beginning, there is a 'clear water' reach where the flow begins to accelerate down the spillway and has no air entrainment. As the flow descends, the velocity increases with a subsequent reduction in depth of flow and air entrainment commences. The ejection of water slugs from the water surface downstream of this section into the adjacent air layer causes air entrainment. The reach downstream of this section is referred to as 'white water'. The surface drag of the high velocity stream causes the adjacent air layer to move parallel to the main stream. The turbulent component of velocity normal to the surface causes ejection of water slugs into the air that aids in bringing air into the main stream. These bubbles diffuse through the main flow and a mixture of air and water flows down to the base of spillway.

In his model study of the new Monksville dam, Sorensen (1985) studied the skimming flow over stepped spillway. It was shown that with or without air entrainment, a roller or vortex developed in every step, surrounded by the step and the main flow. His observation revealed that the flow entered the vortex, stayed in the vortex for a short time, and then returned to the main flow to descend to the next step. The
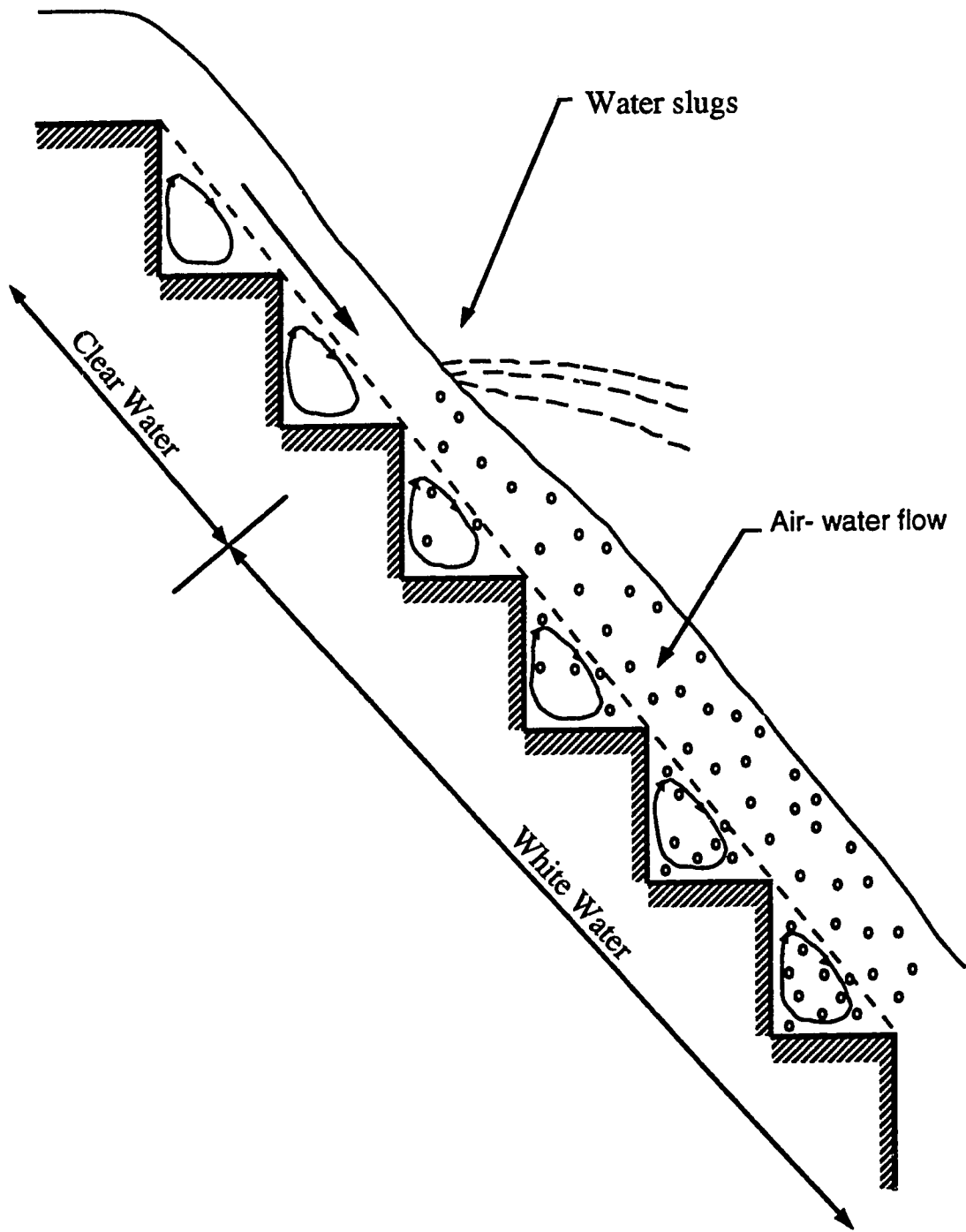
Figure 2.1 Flow patterns for skimming flow

data showed that flow depth decreased as the flow proceeded down the spillway to the point where air entrainment started. Beyond this point, air entrainment caused some bulking of the flow.

Peyras et al. (1992) studied the flow behavior and energy dissipation of stepped spillway made of gabions. This study showed that, after the first two steps, the flow reached its maximum velocity at which air entrainment started. This is in contrast to Sorensen's results which show that the location of air entrainment moves down as the discharge increases. It was also confirmed that some flow entered the roller in every step and the air bubbles gyrated in the roller.

2.2.2. Energy Dissipation

Because of the complexity of flow over a stepped spillway, no general solution has been developed for predicting the energy loss. Sorensen (1985), Frizell (1987 and 1991), and Rajaratnam (1990) have conducted some investigations to quantify the energy loss for any given step geometry.

Sorensen (1985) presented the results of a model study of stepped spillway with a slope of 0.78 on 1. In addition, an ogee spillway model was also built for comparison. The observed data revealed that the kinetic energy of flow at the toe of stepped spillway was reduced to about 6 to 12 percent of that existing at the toe of the standard spillway.

Frizell (1987) presented the results of the model study for the upper stillwater stepped spillway. There was no data on energy loss, but the author mentioned that 72 percent of the energy was dissipated down the spillway. In 1991, Frizell investigated the design criteria for stepped spillways over embankment dams that were unable to pass their design

flows without overtopping. The results for a step slope of 2 on 1 revealed a 45 to 75 percent energy dissipation, based on discharge intensities.

The only theoretical solution for skimming flow is presented by Rajaratnam (1990). In this study, the method used to develop flow equation for fishways was followed. The flow was assumed to be uniform except for the few first steps and the shear stress between the roller formed on each step and the main flow was introduced as the retarding force. Equations were developed to predict the coefficient of friction and the energy loss. The analysis showed that, in some cases, the energy loss could be as much as 88 percent. The assumption of uniform flow associated with constant depth over stepped spillway is in contrast to the observed data by Sorensen (1985) which show that the variation of flow depths could be significant. This implies that the drag coefficient of shear stress on each step, and hence the energy loss, could have a wide range of variation. For example, the flow depth on the crest for run C-6 of Sorensen data was 48 mm. and decreased to 34 mm on step 6. Beyond this point, the flow depth increased until it reached a maximum value of 60 mm on step 51. Using his expression, the drag coefficient for step 51 is 7.7 times the value of step 6.

2.2.3. Onset of Skimming Flow

As mentioned earlier, skimming flow occurs at higher discharges. The approximate range of skimming flow was investigated by Horner (1969) and Rajaratnam (1990). In a graphical solution for energy loss, presented by Horner, the approximate boundary at which skimming regime started was shown. This boundary varied based on step

geometry and discharge intensities. Rajaratnam (1990), using the data of Horner, suggested an average value of Y_c/H equal to 0.8 for the onset of skimming flow where Y_c is the critical depth and H is the height of the step.

2.3. Jet Flow

2.3.1. Description

In the jet flow regime, the jet hits the tread of the step immediately below. It is believed that two main features contribute to the energy loss. These are firstly, the jet circulation in the pool beneath the nappe retards the main flow, and secondly, the partial hydraulic jump that may be formed downstream of the point of jet impact.

Three types of steps, including horizontal step, inclined step, and pooled or rising lip step could be developed for stepped spillway (Figure 2.2). It seems that the inclined and pooled types dissipate more energy than the horizontal one. The results of Horner (1969) confirmed the enhanced energy loss on the inclined step.

2.3.2. Review of earlier investigations

2.3.2.1. General

Horner (1969) has performed the most comprehensive experimental study on jet flows. Other investigators like Peyras et al. (1992), Diez-Cascon et al. (1991), and Stephenson (1991) did not separate the jet flow from the skimming flow. These researchers presented graphical solutions that showed the energy loss versus drop number for a limited range of slopes.

For a gabion spillway, Peyers et al (1992) presented the following

relationship for energy lost based on experimental results:

$$\frac{1}{1-y_1} = a_1 \cdot D^{b_1}$$ (2.1)

where:

$$y_1 = \frac{E_0 - E_s}{h}$$ (2.2.a)

$$D = \frac{q^2}{g h^3}$$ (2.2.b)

y_1 is the energy loss per unit height

D is the drop number

g is the gravity acceleration

E_0 is the total upstream energy

E_s is the total energy at the base of spillway

q is the discharge per unit width, and

h is the total height of spillway

The coefficients a_1 and b_1 are given in Table 2.1.

This relationship covers apparently both the skimming and jet flow regimes. A brief explanation of the state of flow was also given. It was concluded that the energy loss drops sharply as the drop number increases or as the flow changes from jet to skimming flow. It was found that the considerable energy dissipation for this kind of spillway could save 10-30% on stilling basin length and 5-10% on project cost.

15

Horizontal step

Inclined step

Pooled step
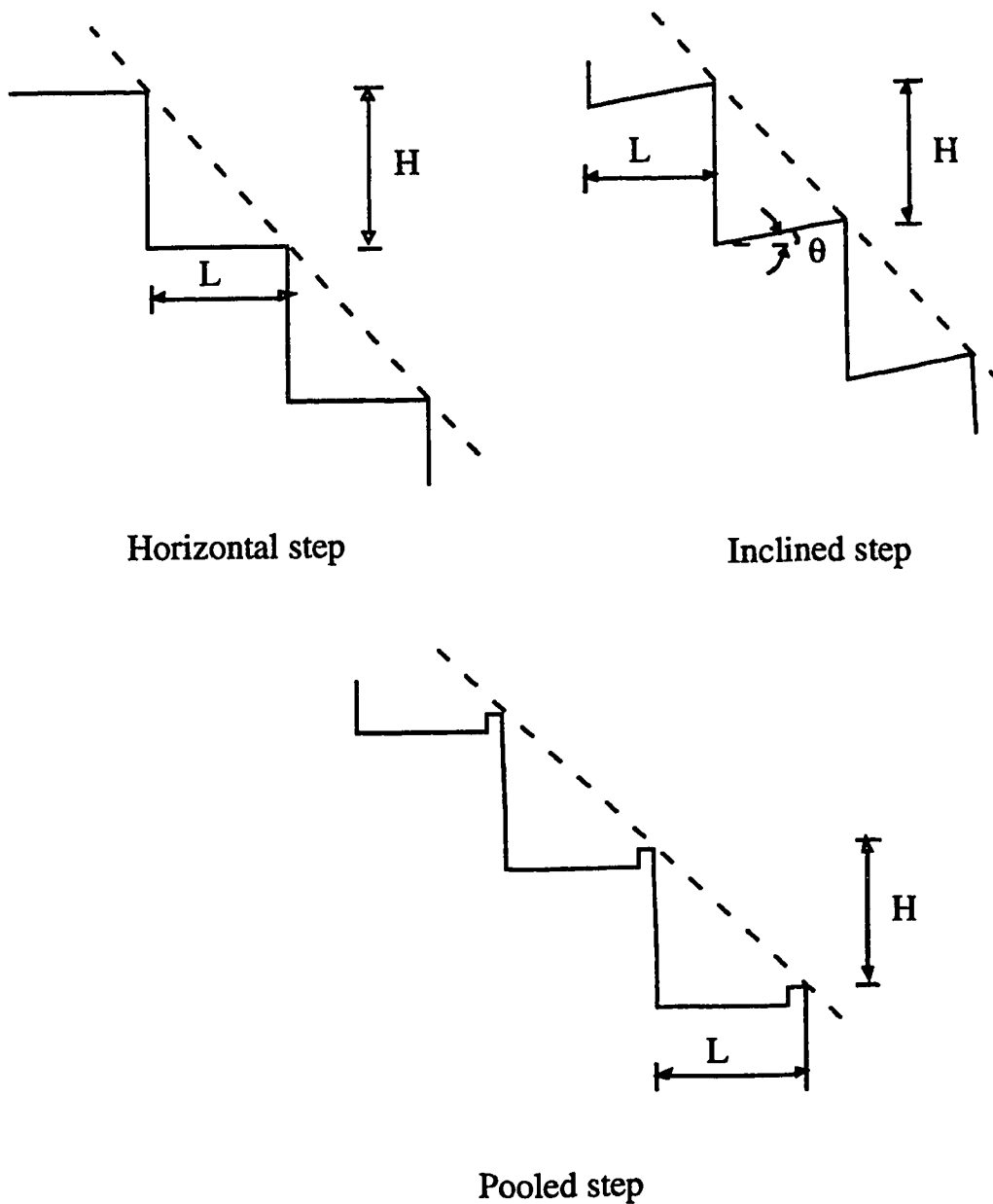
Figure 2.2 Different types of steps

Horner (1969) built a series of hydraulic models to investigate the flow patterns on stepped spillway. Both skimming and jet flows were extensively studied for a wide range of step geometry and discharges.

Some graphical solutions based on non-dimensional parameters were presented for energy and specific forces at the toe of spillway. Some of

Slope	Number of pairs	$\ln(a_1)$	b_1	r^2 Correlation factor
1/3	16	-1.568	-0.647	0.904
1/2	25	-1.778	-0.654	0.964
1/1	28	-1.434	-0.526	0.874

Table 2.1 Coefficients a_1 and b_1 for Equation 2.1 (after Peyras et al., 1992)

the flow characteristics such as flow geometry, state of flow, mechanism of momentum transfer, and air entrainment were also described.

2.3.2.2. Horner's Work (1969)

2.3.2.2.1. Hydraulic Similitude

Gravity was assumed as the major force acting on fluid motion on a stepped spillway. So, the Froude number was the criterion for similarity between the model and prototype. For the Froude model,

$$U_r = \sqrt{l_r} \qquad\qquad (2.3.a)$$

$$U_r = \frac{U_m}{U_p} \qquad\qquad (2.3.b)$$

$$l_r = \frac{l_m}{l_p} \qquad (2.3.c)$$

where U is the mean velocity and l is the characteristic length. Suffixes m, p, r refer to the model, prototype, and ratio, respectively.

Overall slope of the spillway, size and shape of each step, the discharge, and gravity were considered to be the main factors influencing the specific energy and specific force at the base of a stepped spillway. Hence, the analysis showed that

$$E_s = f(\frac{H}{L}, L, \theta, N, q, g) \qquad (2.4)$$

$$F_s = \phi(\frac{H}{L}, L, \theta, N, q, g) \qquad (2.5)$$

where:

F_s is the specific force

L is the length of a step

θ is the inclination of a step

N is the number of steps

Using dimensional analysis, Horner showed that

$$E_N = f'(\frac{H}{L}, \theta, N, L_N) \qquad (2.6)$$

$$F_N = \phi'(\frac{H}{L}, \theta, N, L_N) \qquad (2.7)$$

where:

$$E_N = \frac{E_s}{L} \tag{2.8.a}$$

$$F_N = \frac{\sqrt{F_s}}{L} \tag{2.8.b}$$

$$L_N = \frac{Y_c}{L} \tag{2.8.c}$$

E_N is the energy number

F_N is the force number

L_N is the length number

Because uniform flow was established on the spillway, it was assumed that the number of steps did not effect the specific energy and specific force. So, equations (2.6) and (2.7) were further reduced to

$$E_N = f''(\frac{H}{L}, \theta, L_N) \tag{2.9}$$

$$F_N = \phi''(\frac{H}{L}, \theta, L_N) \tag{2.10}$$

2.3.2.2.2. Hydraulic Models

Five sets of models featuring thirty, twenty, ten, eight, and three steps were built. In each set, the height, length, and inclination of steps

were varied to cover a wide range of step configurations. The height of each step ranged from 1067 mm for three step model to 29 mm for thirty step model. The step length was varied from 1067 mm for three step model to 69 mm for thirty step model. These ranges covered the ratio of drop height to step length from 0.421 to 0.842. Except for the twenty step model, the steps were inclined at zero, five, ten, fifteen, and twenty degrees to the horizontal. Tables 2.2 and 2.3 provide the details of the models and step geometry together with the number of tests made on each model.

2.3.2.2.3. Experimental Results and Analysis

The experimental results included the measurement of velocity and depth of flow by pitot traverse at the base of the spillway. With these, the specific force and specific energy over a wide range of discharge intensities were calculated. No measurements were performed in the upstream channel or on the steps. From dimensional analysis, for each set of H/L and θ, the value of E_N and F_N were plotted against L_N. Figures 2.3 and 2.4 show typical plots for horizontal and inclined steps, respectively, established for a H/L value of 0.421. The experimental results extracted from similar graphs for various step configurations are given in Appendix I.

The main objectives of the analysis were

(i)   To show the influence of step geometry and discharge on the specific force and specific energy at the base of the spillway.

(ii)   To represent the results in a dimensionless form that allows the specific force and energy force to be easily predicted for a prototype spillway.

H (mm)	L (mm)	H/L	N	Number of Tests
29	69	0.421	30	12
51	121	"	20	9
102	241	"	10	8
449	1067	"	8	10
36	69	0.526	30	10
127	241	"	10	13
152	241	0.631	10	10
51	69	0.736	30	13
178	241	"	10	18
58	69	0.842	30	12
203	241	"	10	13

Table 2.2 Details of step geometry and tests on horizontal steps

H (mm)	L (mm)	θ (degrees)	H/L	N	Number of Tests
29	69	5	0.421	30	7
"	"	10	"	"	"
"	"	15	"	"	"
"	"	20	"	"	"
102	241	5	"	10	14
"	"	10	"	"	13
"	"	15	"	"	11
"	"	20	"	"	8
36	69	5	0.526	30	10
"	"	10	"	"	"
"	"	15	"	"	"
"	"	20	"	"	9
127	241	5	"	10	16
"	"	10	"	"	15
"	"	15	"	"	"
"	"	20	"	"	16
152	241	5	0.631	30	8
"	"	10	"	"	7
"	"	15	"	"	"
"	"	20	"	"	6
51	69	5	0.736	30	13
"	"	10	"	"	15
"	"	15	"	"	14
"	"	20	"	"	18
178	241	5	"	10	"
"	"	10	"	"	"
"	"	15	"	"	"
"	"	20	"	"	"
58	69	5	0.842	30	13
"	"	10	"	"	"
"	"	15	"	"	12
"	"	20	"	"	13
203	241	5	"	10	8
"	"	10	"	"	"
"	"	15	"	"	6
"	"	20	"	"	7

Table 2.3 Details of step geometry and tests on inclined steps

To achieve the first objective, some graphs demonstrating the influence of discharge, overall slope of the spillway, step size, and step inclination on specific force and specific energy were plotted. For the second objective, the dimensionless Equations (2.9) and (2.10) were used. Plots of H/L versus L_N with E_N and F_N considered as parameters for each value of θ were considered to be the most appropriate form to represent the experimental results. A typical plot is shown in Figure 2.5 for H/L and θ equal to 0.421 and zero, respectively. There are no generalized equations for predicting specific force and specific energy. Attempts made to establish relationships between the ratio of mean depth to step length and L_N were not successful.

2.3.3. Present Analysis

2.3.3.1. Introduction

In conclusion, even though Horner had performed some extensive experiments, his analysis of the results appears to be rather inadequate. This investigation attempts to provide a method of predicting the energy loss on a stepped spillway for the jet flow regime. The extensive experimental results of Horner (1969) were used to form the basis for such a method. The idea of assessing the proportion of energy loss per step (α) helped to formulate equations for estimating energy loss.

2.3.2.2. Dimensionless Analysis

As mentioned earlier, the energy at the base of a stepped spillway depends on the size and shape of steps, the number of steps, the discharge per unit width, and acceleration of gravity. Hence, we can write

23

Figure 2.3 Relationship established between energy number and length number for horizontal steps (after Horner, 1969)
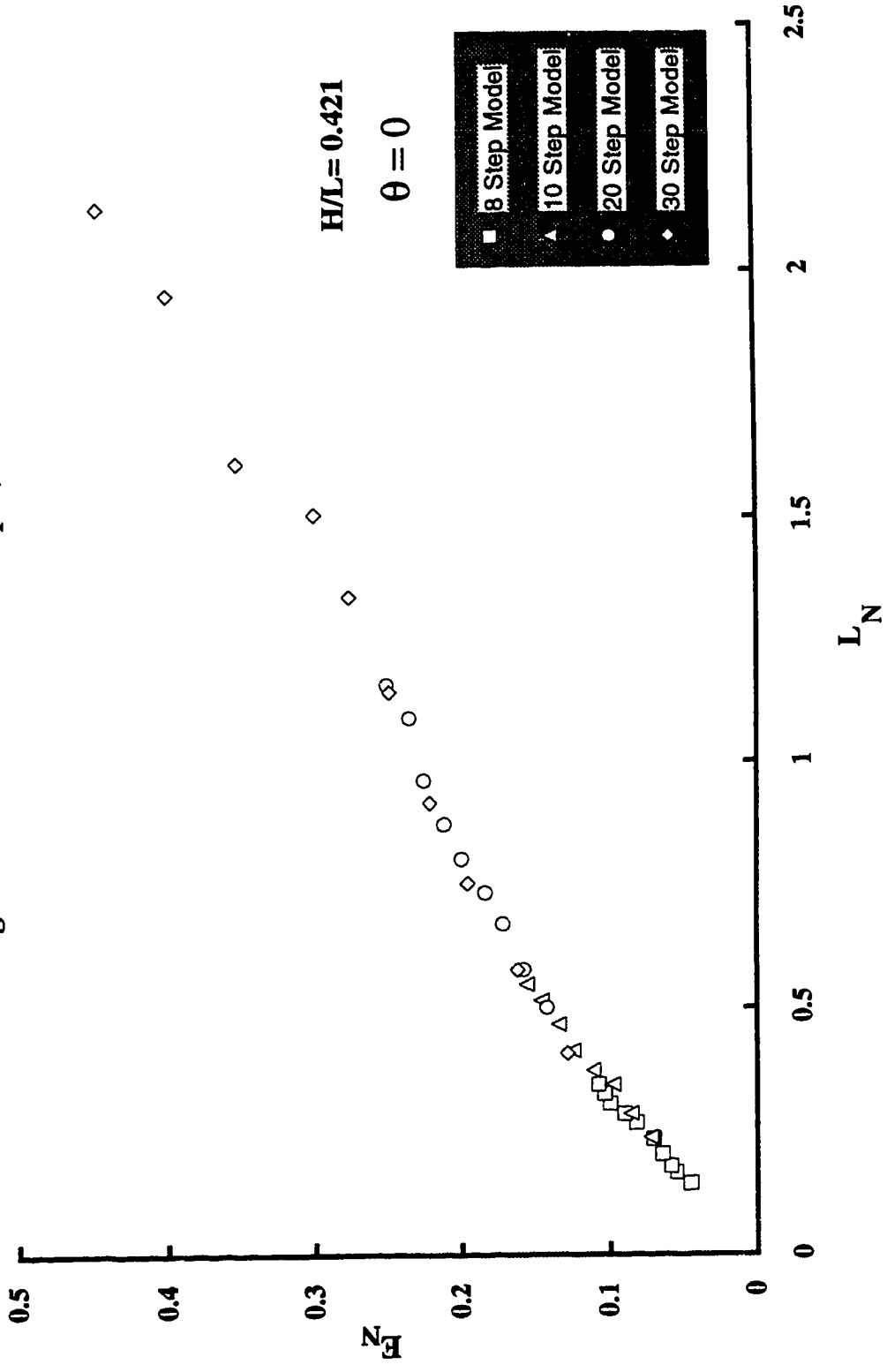
Figure 2.4 Relationship established between energy number and length number for inclined steps (after Horner, 1969)
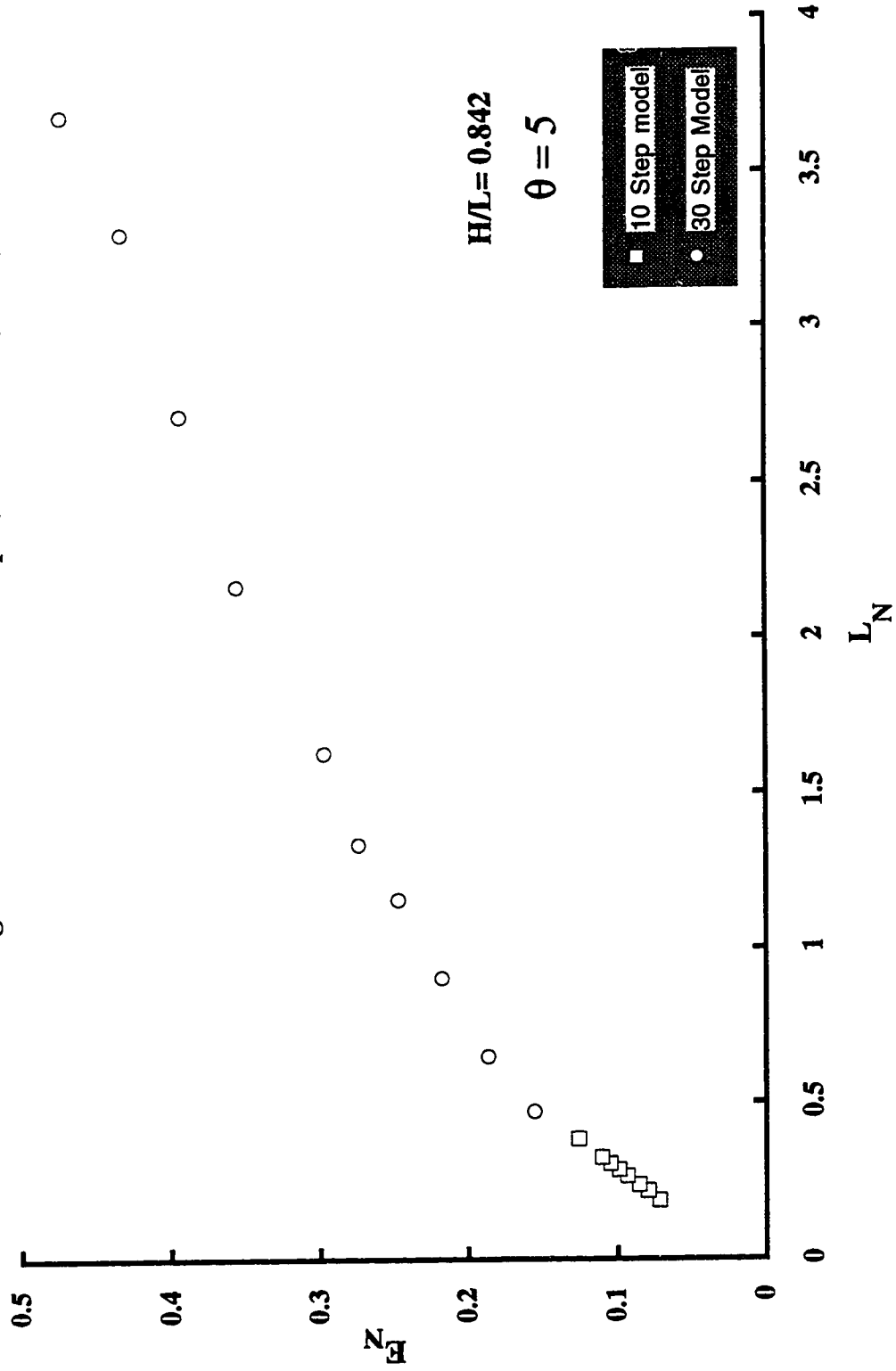
Figure 2.5 Dimensionless Relationship for energy number for horizontal steps (after Horner, 1969)
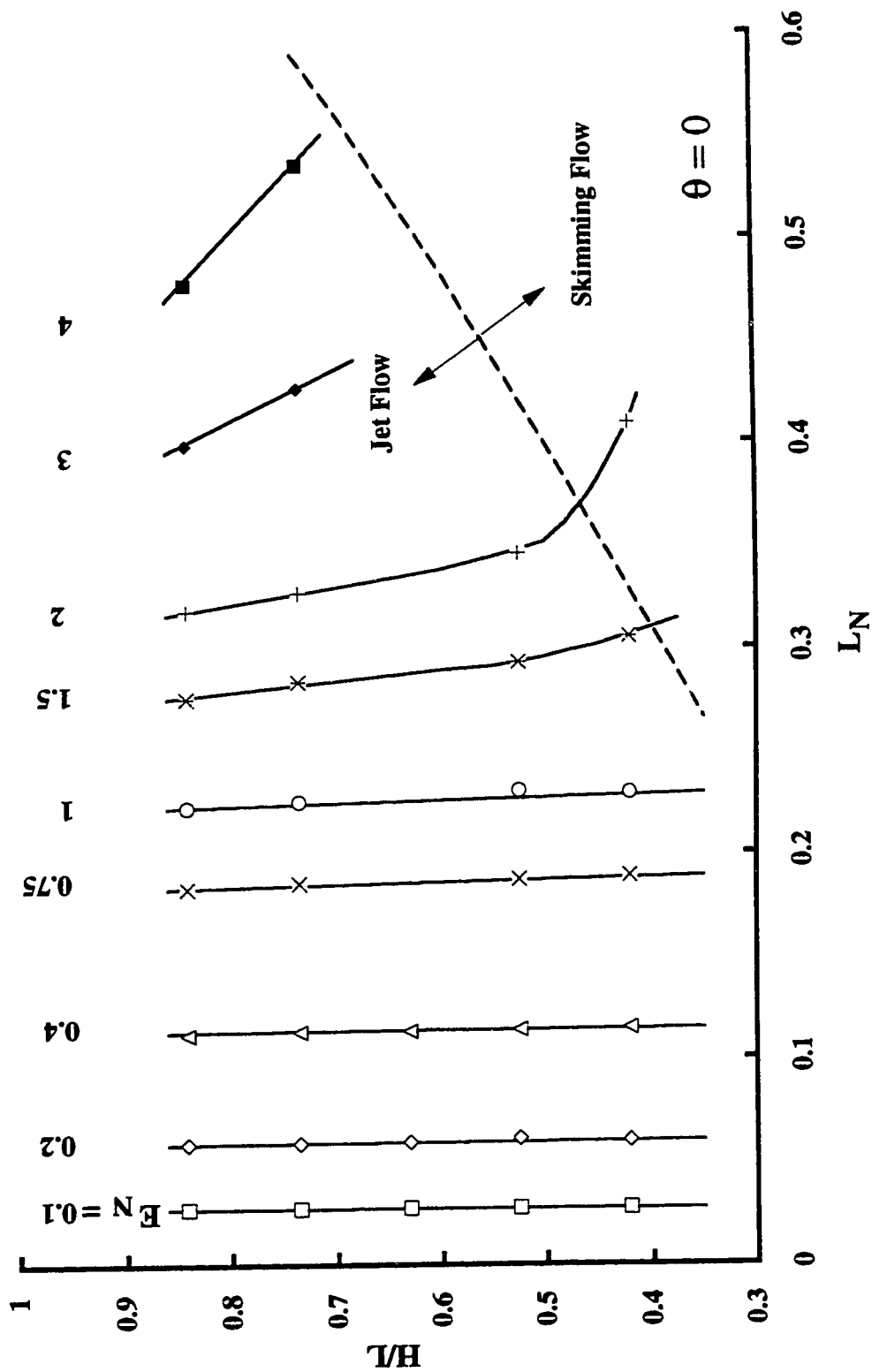
$$E_s = f(H, L, N, \theta, q, g) \tag{2.11}$$

To make Equation (2.11) dimensionless, it must be decided whether L or H is the more important factor. In Equation (2.6), Horner (1969) chose L as the length scale to make specific energy dimensionless. The author believes that in a stepped spillway, the step height is a more relevant factor to influence the energy dissipation rather than the length of step. In addition, it is more convenient to evaluate the energy loss instead of the remaining energy.

Hence, Equation (2.11) can be rewritten as

$$\frac{E_s}{H} = f'(\frac{H}{L}, N, \theta, \frac{q^{2/3}}{g^{1/3} H}) \tag{2.12}$$

It is obvious that

$$Y_c = \frac{q^{2/3}}{g^{1/3}} \tag{2.13}$$

Since, no measurements were made in the upstream channel, the following assumptions are made to evaluate the flow energy:

(i) The upstream flow is subcritical and approaches the spillway at critical depth.

(ii) The energy correction factor at critical section is assumed to be one, that is, uniform velocity distribution.

Hence, the upstream total energy, E_0, is

$$E_0 = N.H + \frac{3}{2}Y_c \qquad\qquad (2.14)$$

and the relative energy loss is

$$\frac{\Delta E}{E_0} = 1 - \frac{E_s}{E_0} \qquad\qquad (2.15)$$

where ΔE is the energy loss.

Substituting Equation (2.13) in Equation (2.12) and considering Equations (2.14) and (2.15), the following expression can be obtained:

$$\frac{\Delta E}{E_0} = f'(\frac{H}{L}, \theta, N, \frac{Y_c}{H}) \qquad\qquad (2.16)$$

As it will be shown in the following section, Equation (2.16) does not yield a method to obtain a generalized equation for predicting the energy loss.

If α is assumed to be the proportion of energy lost on each step (which is defined in the next section),

$$\alpha = \phi(\frac{H}{L}, \theta, \frac{Y_c}{H}) \qquad\qquad (2.17)$$

Substituting Equation (2.17) in Equation (2.16)

$$\frac{\Delta E}{E_0} = f''(\alpha, N, \frac{Y_c}{H}) \qquad\qquad (2.18)$$

2.3.3.3. Method of Analysis

2.3.3.3.1. Horizontal Steps

The energy loss on a stepped spillway with horizontal steps is determined by considering Equations (2.14) and (2.15). Horner (1969) presented experimental results, from which the value of energy loss can be calculated for stepped spillways, for H/L= 0.421 (8,10,20 & 30 steps), 0.526 (10 & 30 steps), 0.736 (10 & 30 steps), 0.842 (10 & 30 steps). Using Equation (2.15), the results of this calculation are shown in Figures 2.6(a-d). For any given value of Y_c/H, as the number of steps increases, more energy is dissipated. Figures 2.6(a-d) show significant energy dissipation that varies from 80% to 97% for the specified range of H/L. This shows that the need for stilling basin at the base of a stepped spillway could be eliminated. As H/L increases, the energy loss decreases for any given value of Y_c/H.

Horner (1969) mentioned that the flow is similar on the steps except for the first few steps. It is a reasonable approximation to assume that the proportion of energy lost on each step is approximately the same. Let α be the proportional loss, defined for each step as the ratio of the heads of the flow entering and leaving the step. From Figure 2.7, it can be easily deduced that the upstream energy for first step is

$$E_u^1 = H + 1.5 Y_c \tag{2.19}$$

The energy loss on the first step is

$$E_l^1 = \alpha(H + 1.5 Y_c) \tag{2.20}$$

Figure 2.6(a) Variation of relative energy loss over several models for H/L= 0.421
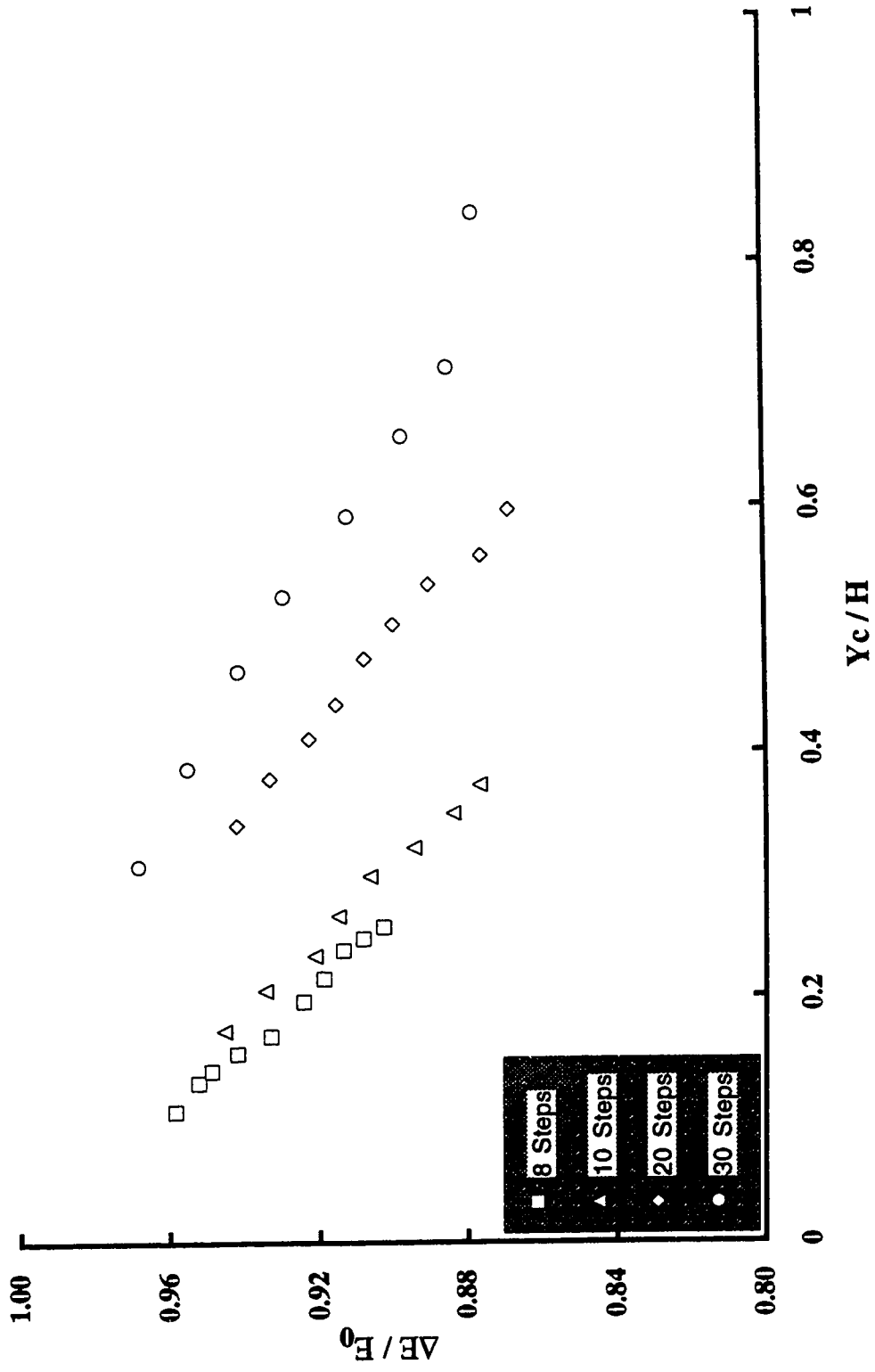
Figure 2.6(b) Variation of relative energy loss over several models for H/L= 0.526
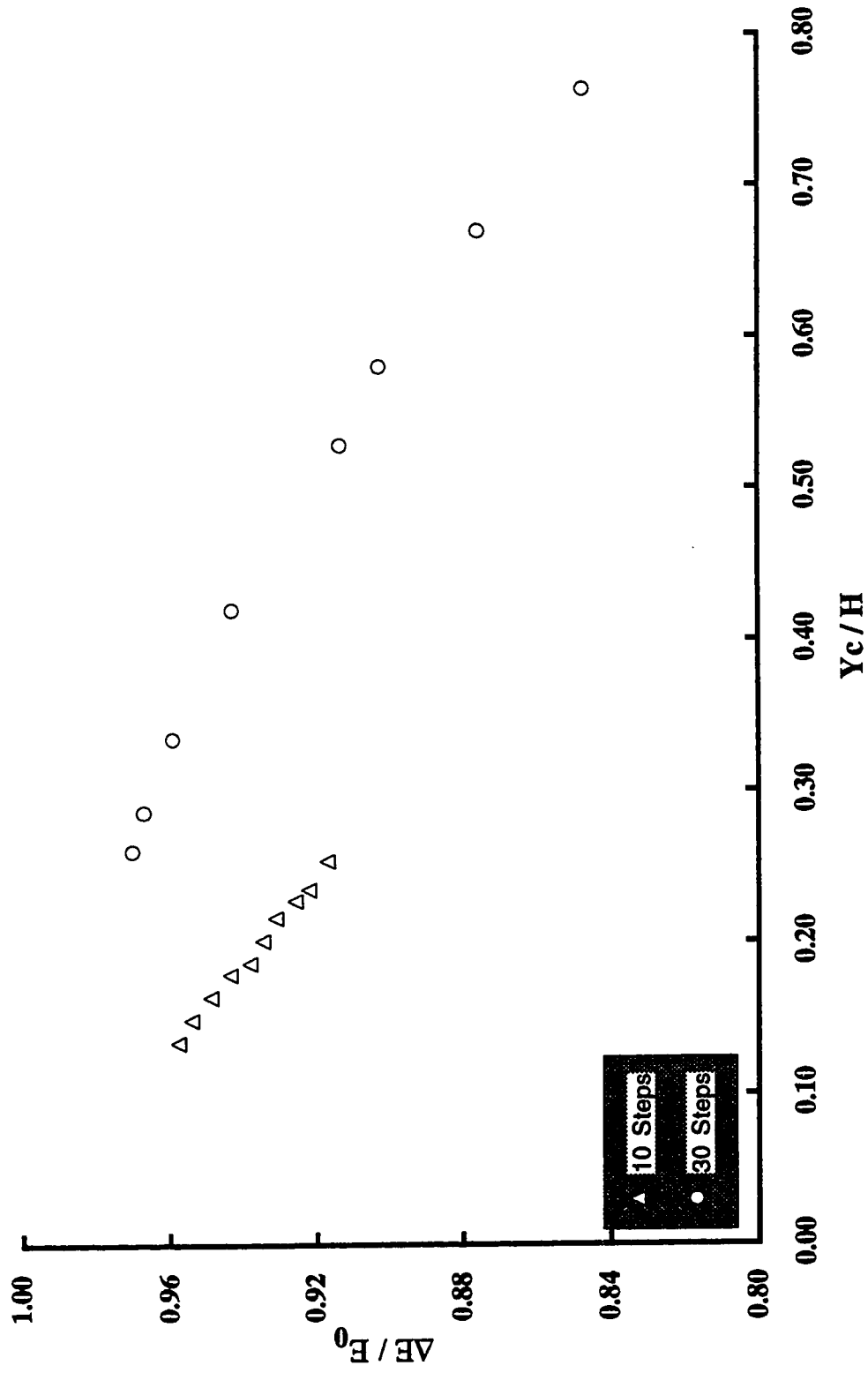
Figure 2.6(c) Variation of relative energy loss over several models for H/L= 0.736
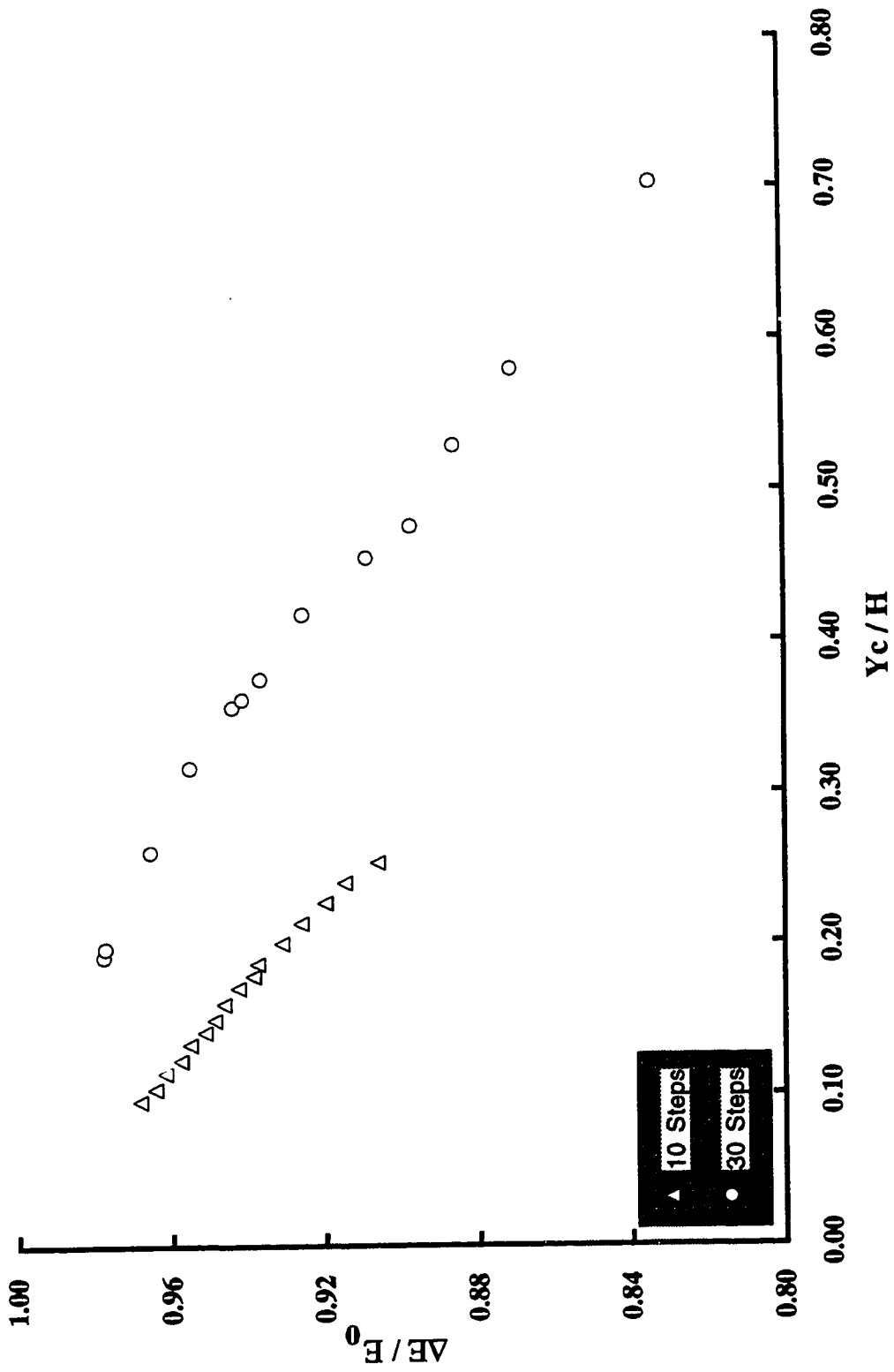
Figure 2.6(d) Variation of relative energy loss over several models for H/L= 0.842
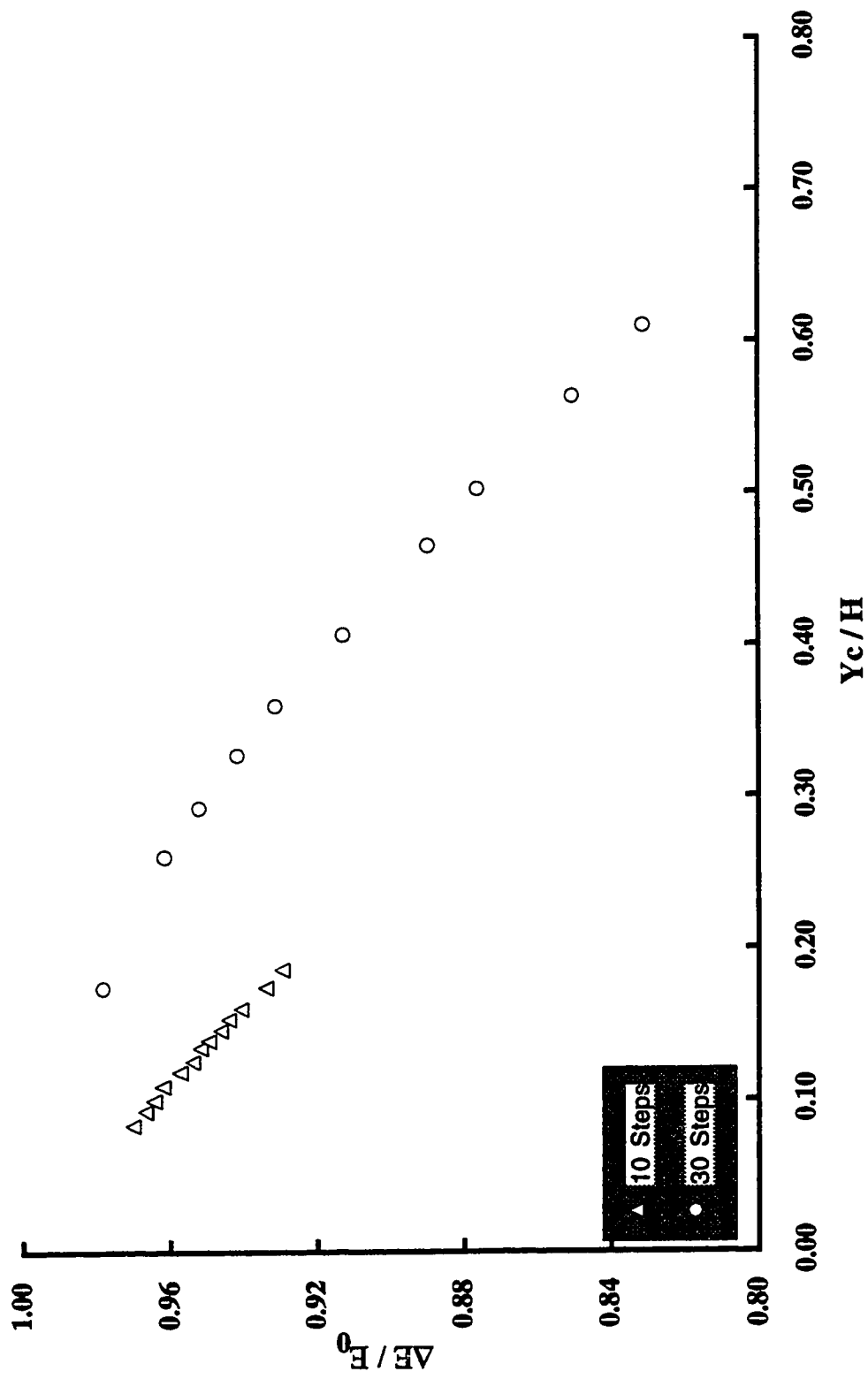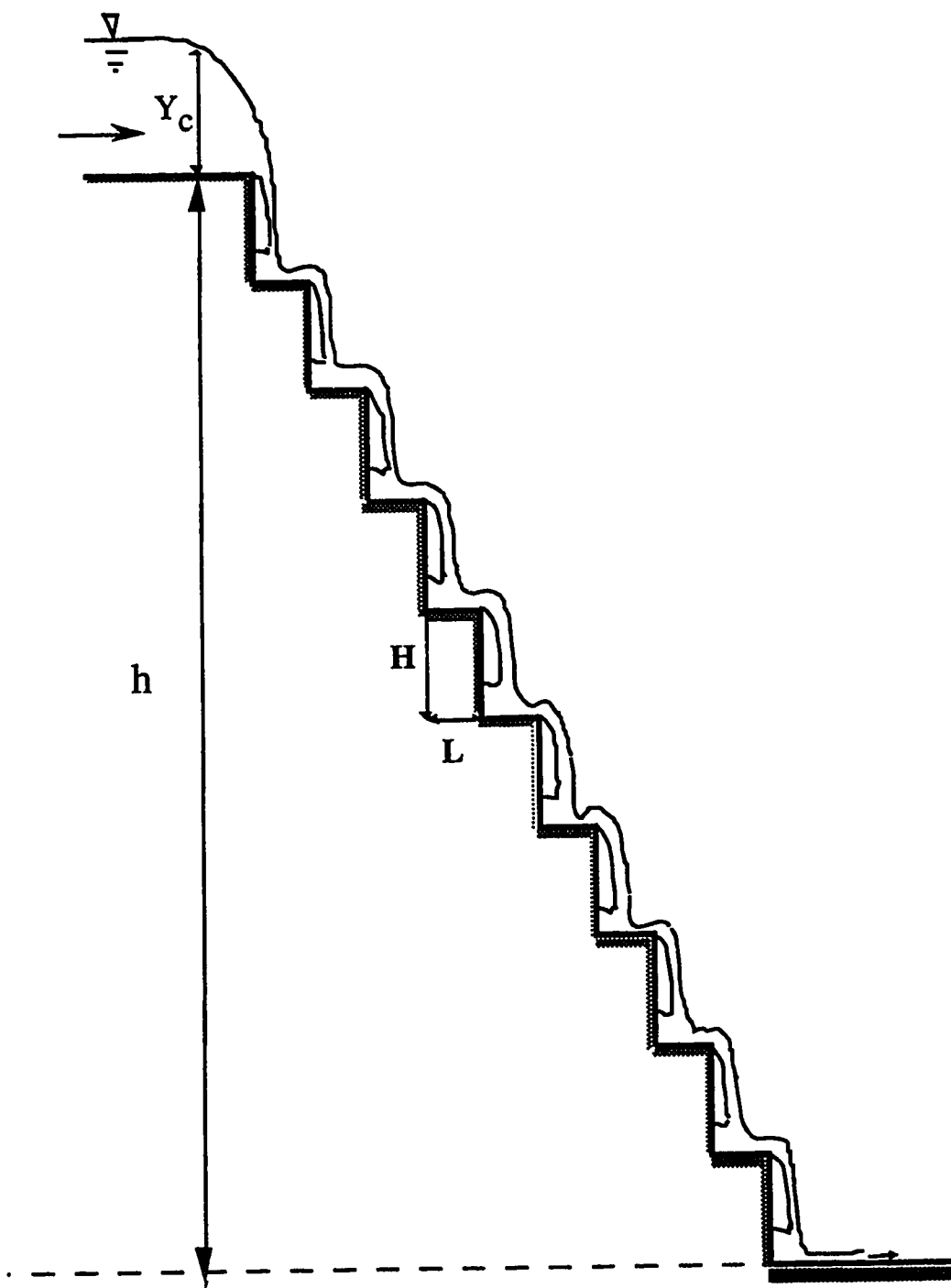
Figure 2.7 Definition sketch for a stepped spillway

and the remaining energy is

$$E_r^1 = (1-\alpha)(H + 1.5Y_c)$$ (2.21)

Hence, the upstream energy, the energy loss, and the remaining energy for second step are, respectively,

$$E_u^2 = (1-\alpha)(H + 1.5Y_c) + H$$ (2.22.a)

$$E_l^2 = \alpha\big[(1-\alpha)(H + 1.5Y_c) + H\big]$$ (2.22.b)

$$E_r^2 = (1-\alpha)^2(H + 1.5Y_c) + H(1-\alpha)$$ (2.22.c)

Following this argument further, at the bottom of the spillway with N steps, the remaining energy can be shown to be

$$E_s = (1-\alpha)^N(H + 1.5Y_c) + H\sum_{i=1}^{N-1}(1-\alpha)^i$$ (2.23)

If ΔE is the energy loss over the spillway, the relative energy loss is

$$\frac{\Delta E}{E_0} = 1 - \frac{\left\{(1-\alpha)^N\big[1 + 1.5(Y_c/H)\big] + \sum_{i=1}^{N-1}(1-\alpha)^i\right\}}{N + 1.5(Y_c/H)}$$ (2.24)

Equation (2.24) is a non linear function of α and can be solved by the Secant method for all the data presented in Figures 2.6(a-d).

The results of these calculations are shown in Figures 2.8(a-d). The results for all the values of H/L are collected together in Figure 2.9. In addition, the results of Horner are presented in Figure 2.10 along with those of Moore (1943) for a single step. A detailed qualitative examination of Figures 2.8 and 2.9 shows the following results

(i) α decreases from a relatively large value of about 0.77 for $Y_c/H = 0.1$ to about 0.15 for Y_c/H approximately equal to 0.8. At this stage, the flow regime might change to skimming flow. This argument was supported by Rajaratnam (1990) who found the value of Y_c/H for onset of skimming flow to be about 0.8.

(ii) A close inspection of Figure 2.9 shows that for Y_c/H less than about 0.20, α is unaffected by parameter H/L in the range of 0.421 to 0.842. For Y_c/H larger than 0.20, α decreases as H/L increases with the data points beginning to fall off at progressively larger values of Y_c/H as H/L decreases. So, the separation point for each set of data depends on the value of H/L; the separation for $H/L=0.736$ occurred at $Y_c/H = 0.25$, while for $H/L=0.526$ it starts at about $Y_c/H = 0.50$. This is due to the formation of a partial jump on the deflected jet. It is known that all values of H/L are associated with the same step length. At lower values of Y_c/H, the step length is large enough for the partial hydraulic jump to form. As Y_c/H increases, the jet hits closer to the end of the step for higher H/L and the partial hydraulic jump does not form. As a result, α decreases as H/L increases.

Figure 2.8(a) Variation of α with Y_c/H for H/L= 0.421
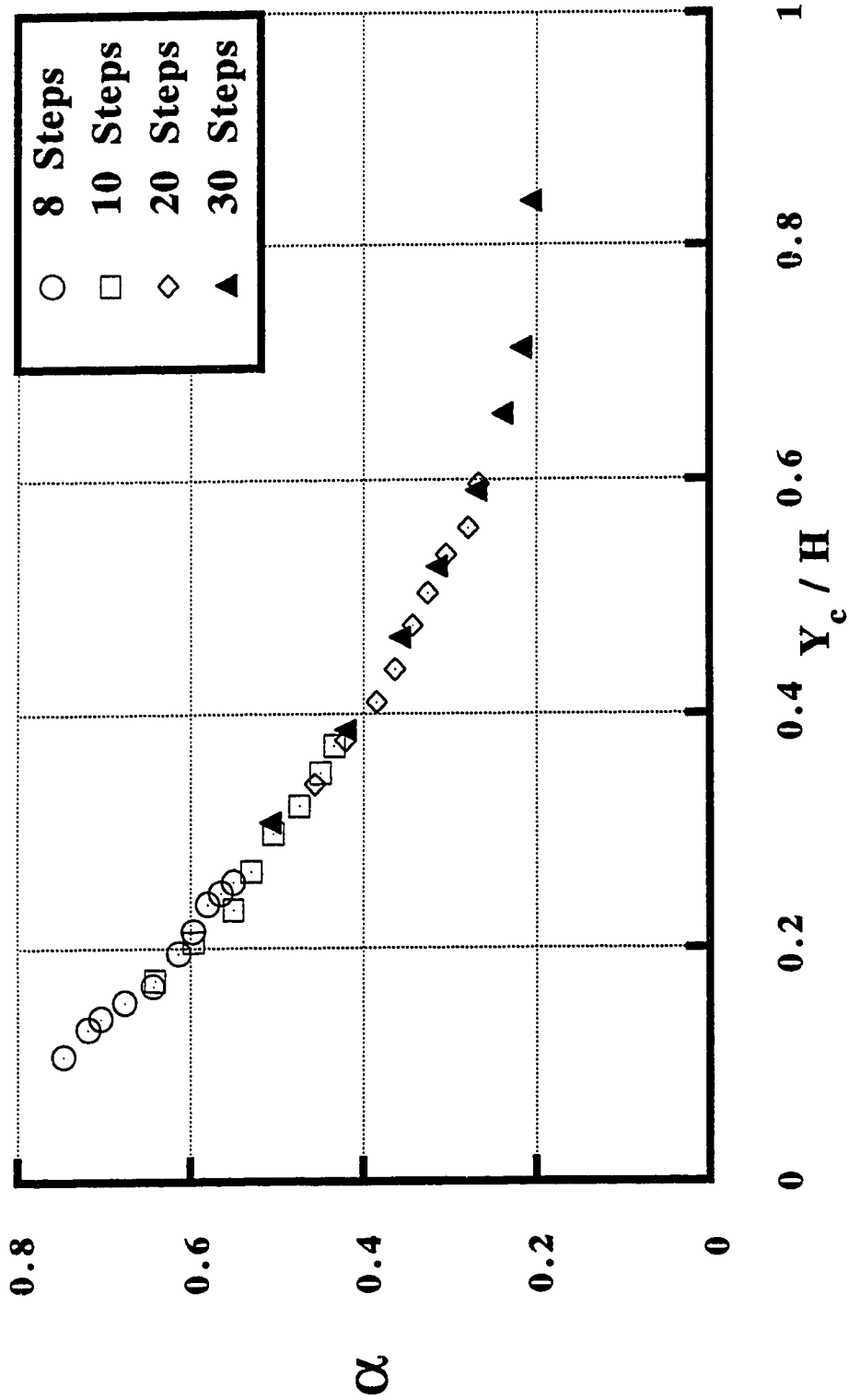
Figure 2.8(b) Variation of α with Y_c/H for H/L= 0.526
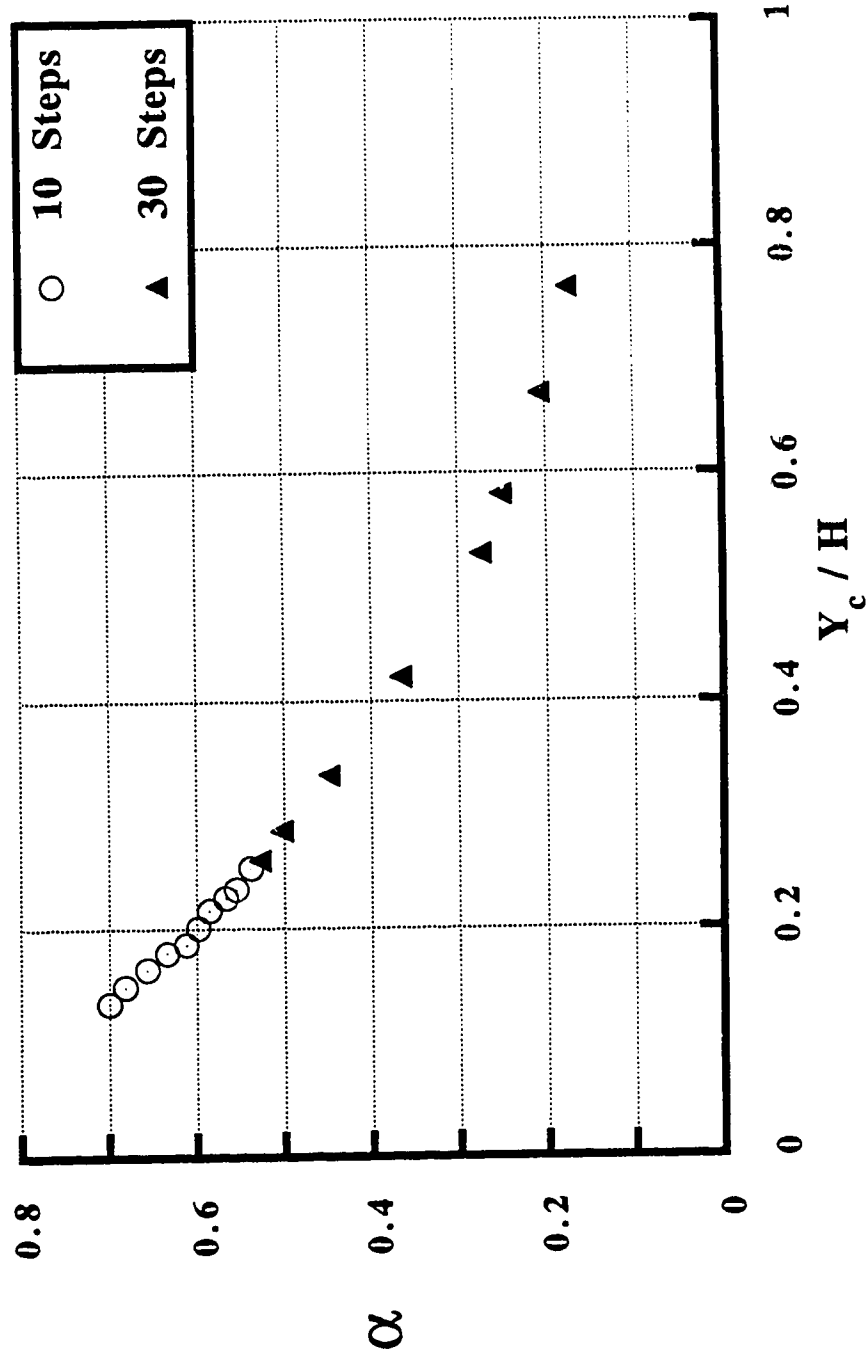
Figure 2.8(c) Variation of α with Y_c/H for H/L= 0.736
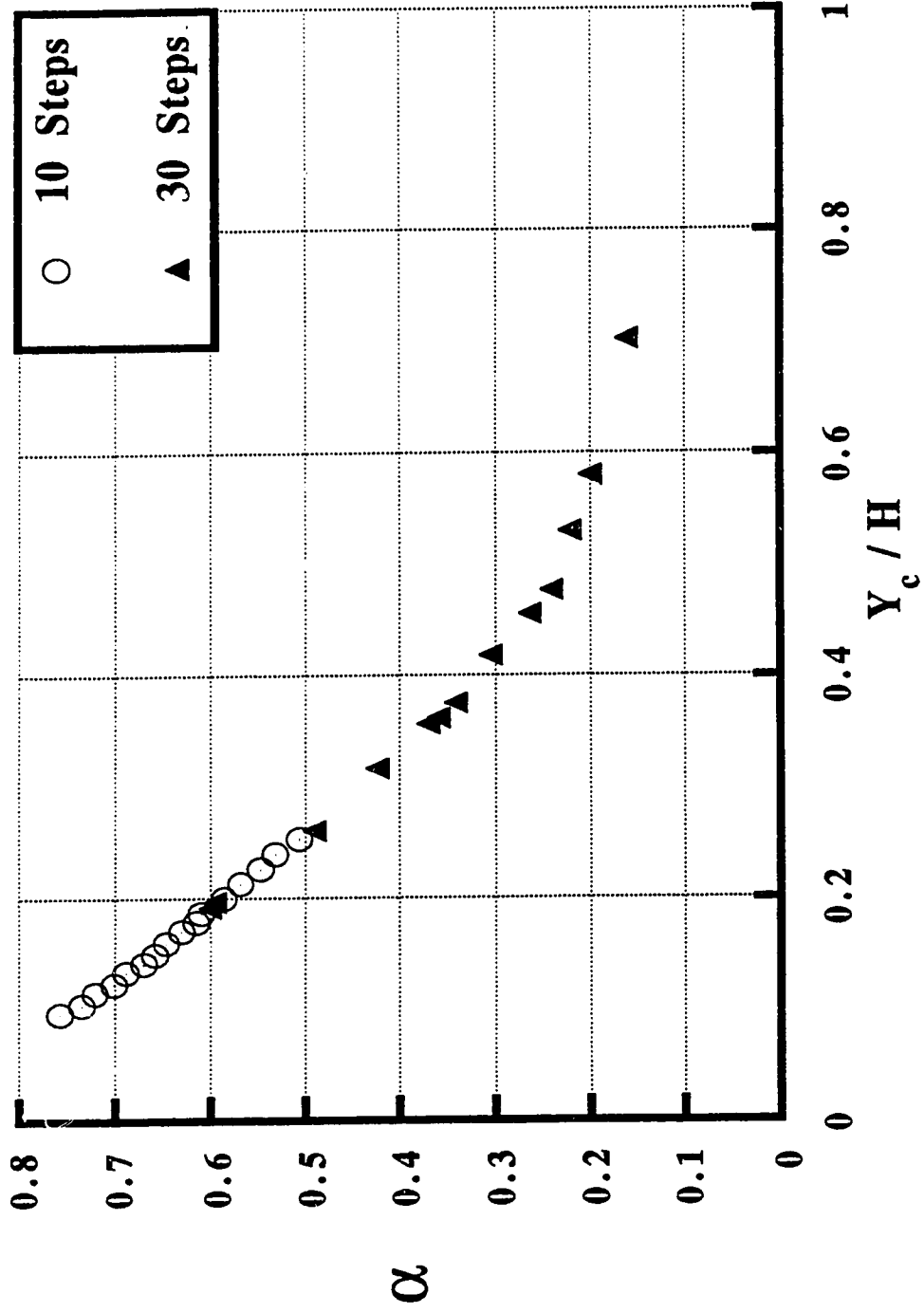
Figure 2.8(d) Variation of α with Y_c/H for H/L= 0.842
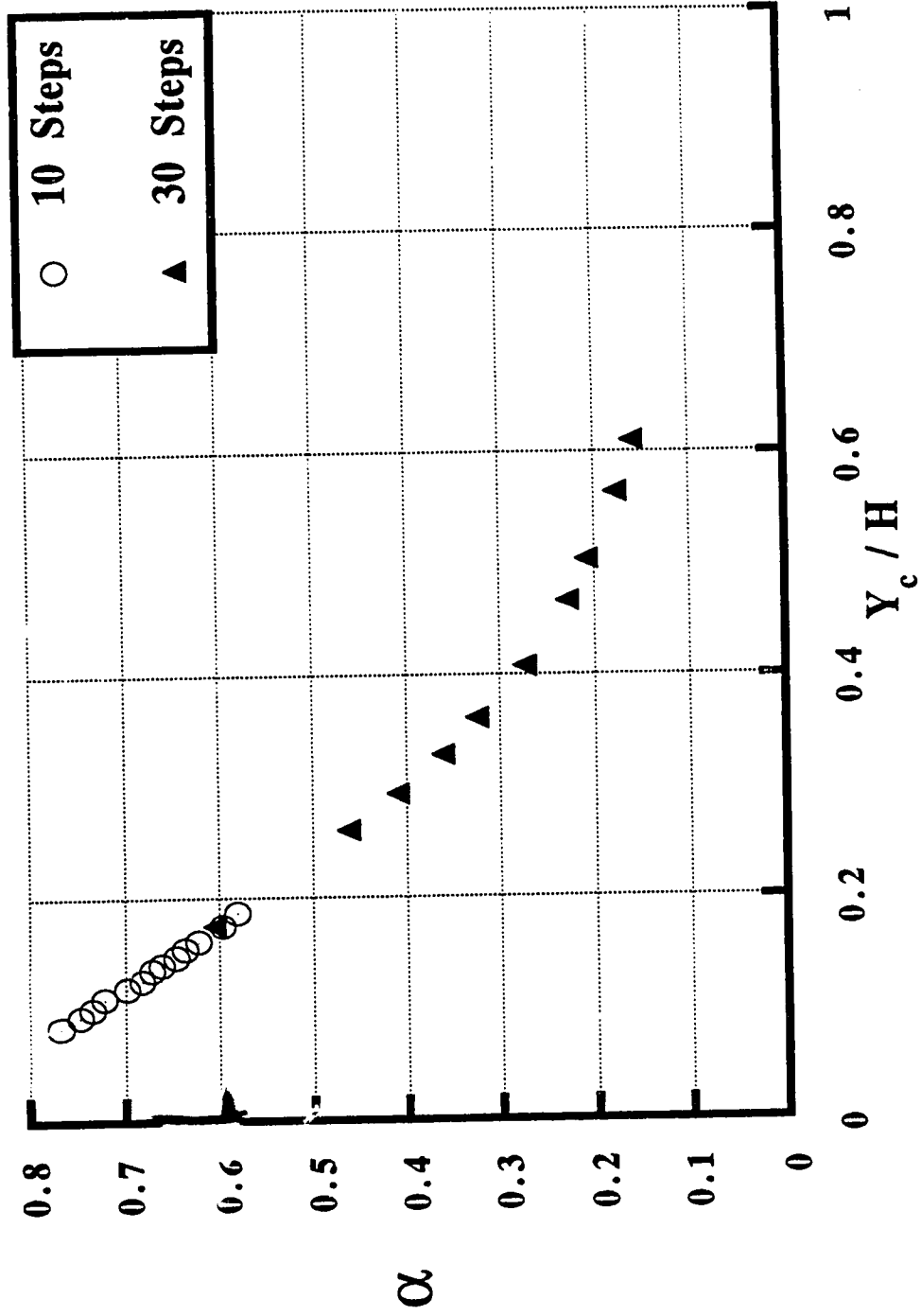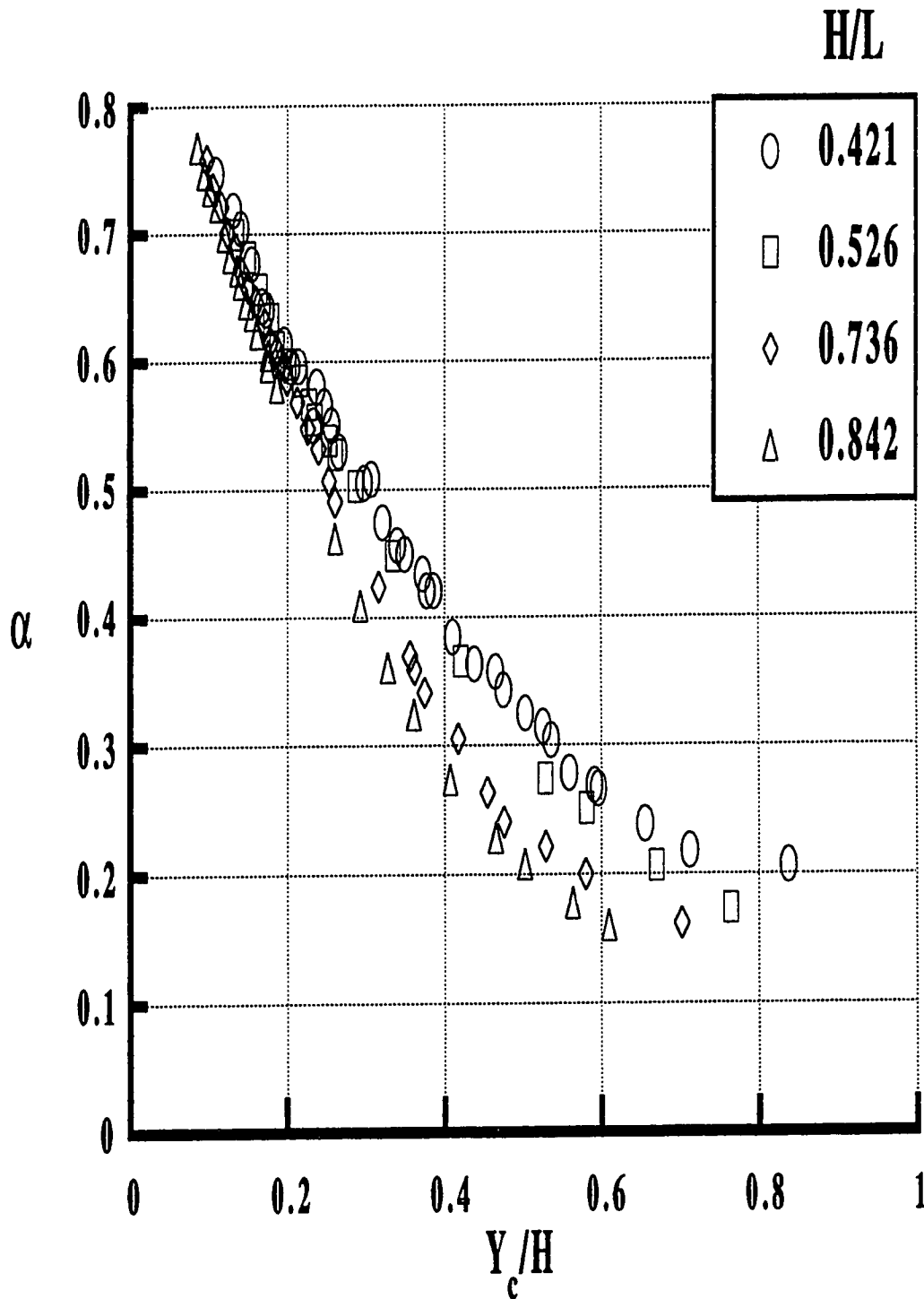
Figure 2.9 Consolidated results on the variation of α with Y_c/H

(iii) For any given value of Y_c/H, α is larger for multiple steps than for a single step which again points to the influence of the partial jump. Perhaps the state of the approaching flow could be partly responsible for this difference. The upstream flow in Moore's experiment was subcritical whereas in Horner's set up, the flow became supercritical after the first few steps.

From Figure 2.8, it was found that the variation of α with H/L can be well described by the following equation

$$\alpha = a - b\log(Y_c / H) \tag{2.25}$$

Table 2.4 shows the coefficients a and b for different values of H/L. It is realized that with the increase of H/L, a decreases while b increases. Figure 2.11 shows the relationship between these coefficients and H/L. It appears that the relationship between the coefficients a and b and H/L can be described by the following equations

$$a = 0.25 - 0.30(H / L) \tag{2.26}$$

$$b = 0.61 + 0.19(H / L) \tag{2.27}$$

Substituting Equations (2.26) and (2.27) in Equation (2.25) results in

$$\alpha = 0.25 - 0.30(H / L) - [0.61 + 0.19(H / L)]\log(Y_c / H) \tag{2.28}$$

H/L	a	b	r
0.421	0.132	0.676	0.995
0.526	0.089	0.729	0.997
0.736	0.035	0.754	0.992
0.842	-0.003	0.761	0.995

Table 2.4 Variation of coefficients of Equation (2.25) with H/L

Figure 2.12 shows the comparison between the value α calculated from Equation (2.28) and that obtained from experimental data. The regression coefficient is 0.993.

Returning to the relative energy loss equation (Equation (2.24)), an attempt was made to develop an asymptotic value for small values of Y_c / H. For relatively smaller values of Y_c / H, α is large and $(1 - \alpha)^N$ becomes negligible when the number of steps N is large. Under such a condition, Equation (2.24) can be further reduced to show the relative energy loss approaches unity. This argument is supported by observations for $H/L = 0.421$ shown in Figure 2.6(a), where for the case with 30 steps and Y_c / H approximately equal to 0.3, the relative energy loss is about 0.97.

Considering the experimental data and the above discussion, it can be concluded that the term $(1-\alpha)^N \left[1 + 1.5(Y_c/H)\right]$ in Equation (2.24) can be neglected as compared to the other terms. Hence, Equation (2.24) can be reduced to

Figure 2.11 Variation of coefficients of Equation (2.25) with H/L
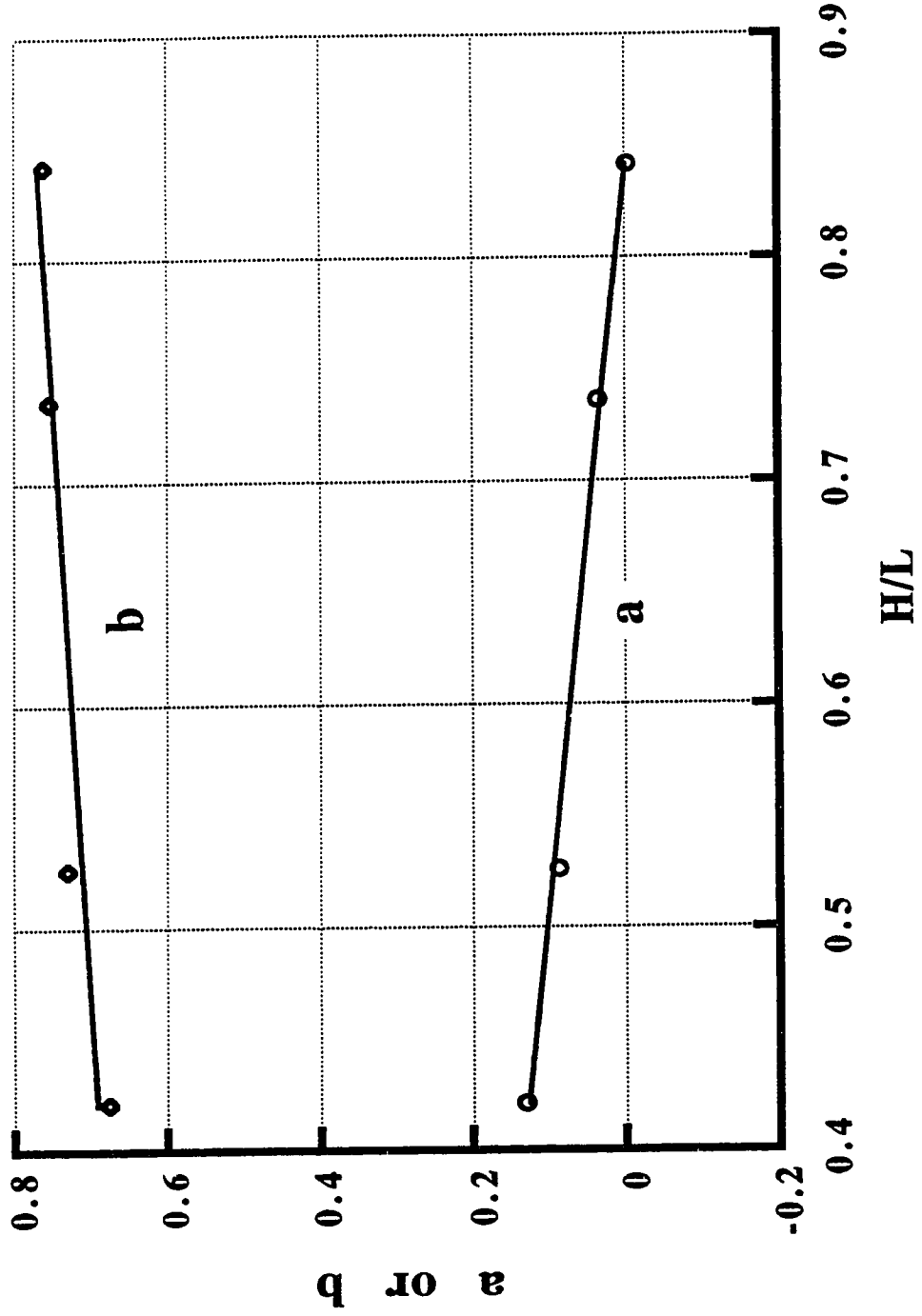
Figure 2.12 Comparison between values of α obtained from experimental data and Equation (2.28) for horizontal steps
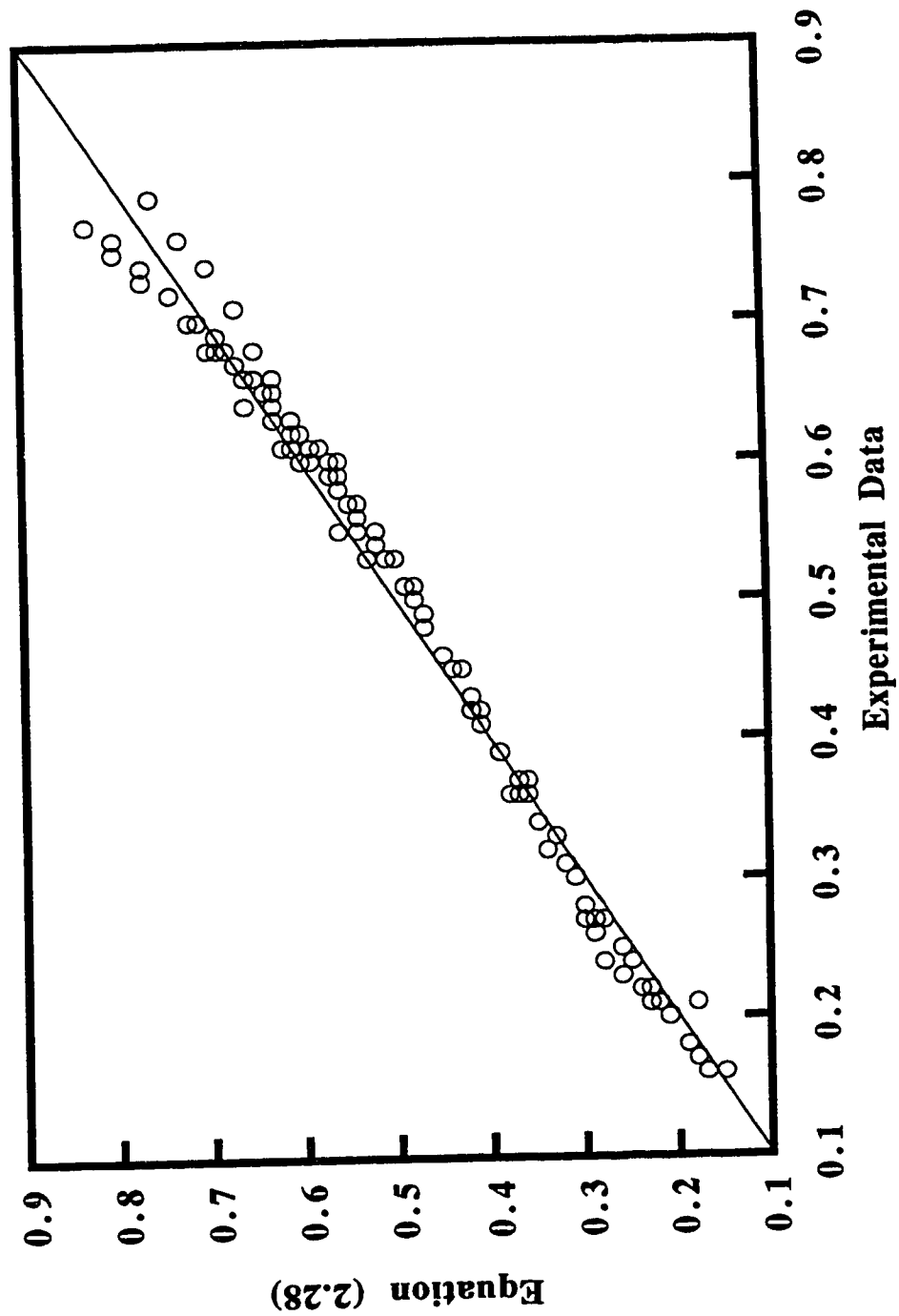
$$\frac{\Delta E}{E_0} = 1 - \frac{\sum_{i=1}^{N-1}(1-\alpha)^i}{N +1.5(Y_c/H)} \tag{2.29}$$

It can be further deducted that for the range of experimental data, the term $1.5(Y_c/H)$ is negligible as compared to N. Therefore, Equation (2.29) can be further approximated to

$$\frac{\Delta E}{E_0} = 1 - \frac{\sum_{i=1}^{N-1}(1-\alpha)^i}{N} \tag{2.30}$$

Substituting the value of α from Equation (2.28), the resulting equation is,

$$\frac{\Delta E}{E_0} = 1 - \frac{1}{N}\sum_{i=1}^{N-1}\left(\begin{array}{l}0.70 + 0.35(H/L) + \\ [0.54 + 0.27(H/L)]\log(Y_c/H)\end{array}\right)^i \tag{2.31}$$

The comparison between calculated relative energy loss from Equation (2.31) and from experimental data is shown in Figure 2.13. The regression coefficient is 0.9995, indicating an excellent agreement for such a relatively simple expression.

It is also desirable to derive an equation for estimating the relative energy loss in a stepped spillway of a particular geometry in jet flow for maximum discharge. Considering Figure 2.5 of Horner, it is found that the maximum value of Y_c / H in jet regime varies from 0.79 to 0.82 for

Figure 2.13 Comparison between values of energy loss
obtained from experimental data and Equation (2.31)
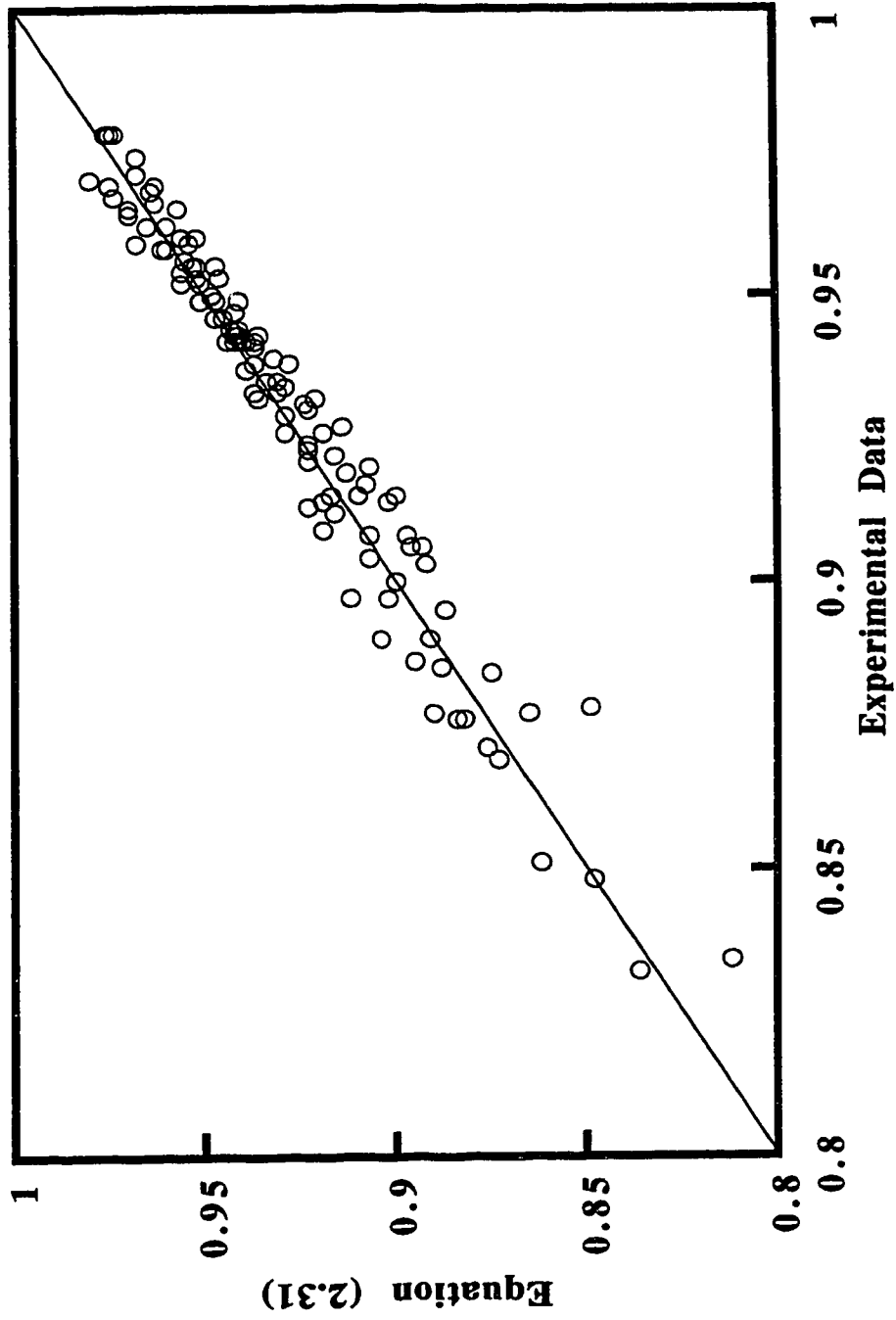
H/L in the range of 0.35 to 0.75. So, the value of Y_c / H where the flow changes from jet flow to skimming flow can be approximated to be 0.80. Substituting the value of 0.80 for Y_c / H in Equation (2.31), the relative energy loss for a stepped spillway in jet flow regime for maximum discharge ... essed as

$$\left(\frac{\Delta E}{E_0}\right)_{\substack{max \\ discharge}} = 1 - \frac{1}{N}\sum_{i=1}^{i}[0.65 + 0.32(H/L)]^i \qquad (2.32)$$

Figure 2.14 shows the variation of the relative energy loss with H/L for five values of $N= 8, 10, 15, 20,$ & 30 steps. An examination of Figure 2.14 shows that $\left(\Delta E/E_0\right)_{\substack{max \\ discharge}}$ decreases as H/L increases for a given N. Finally, it must be borne in mind that Equations (2.30) to (2.32) are empirical relationships and so should not be extended to conditions outside those for which they were developed.

2.3.3.3.2. Inclined Steps

In this category, the steps were inclined upward to provide a pool on the tread of each step. This geometry forced the jet to plunge into a turbulent pool, thereby dissipating more energy.

The experimental data obtained for step inclinations of zero, five, ten, fifteen, and twenty degrees are used to evaluate the energy loss. The results for inclined steps are presented in the same manner as that for horizontal steps. This means that the proportion of energy lost on each step α can be calculated, using Equation (2.24). For each value of H/L, plots of α against Y_c/H are used for developing predictive

Figure 2.14 Variation of relative energy loss for maximum discharge of jet flow
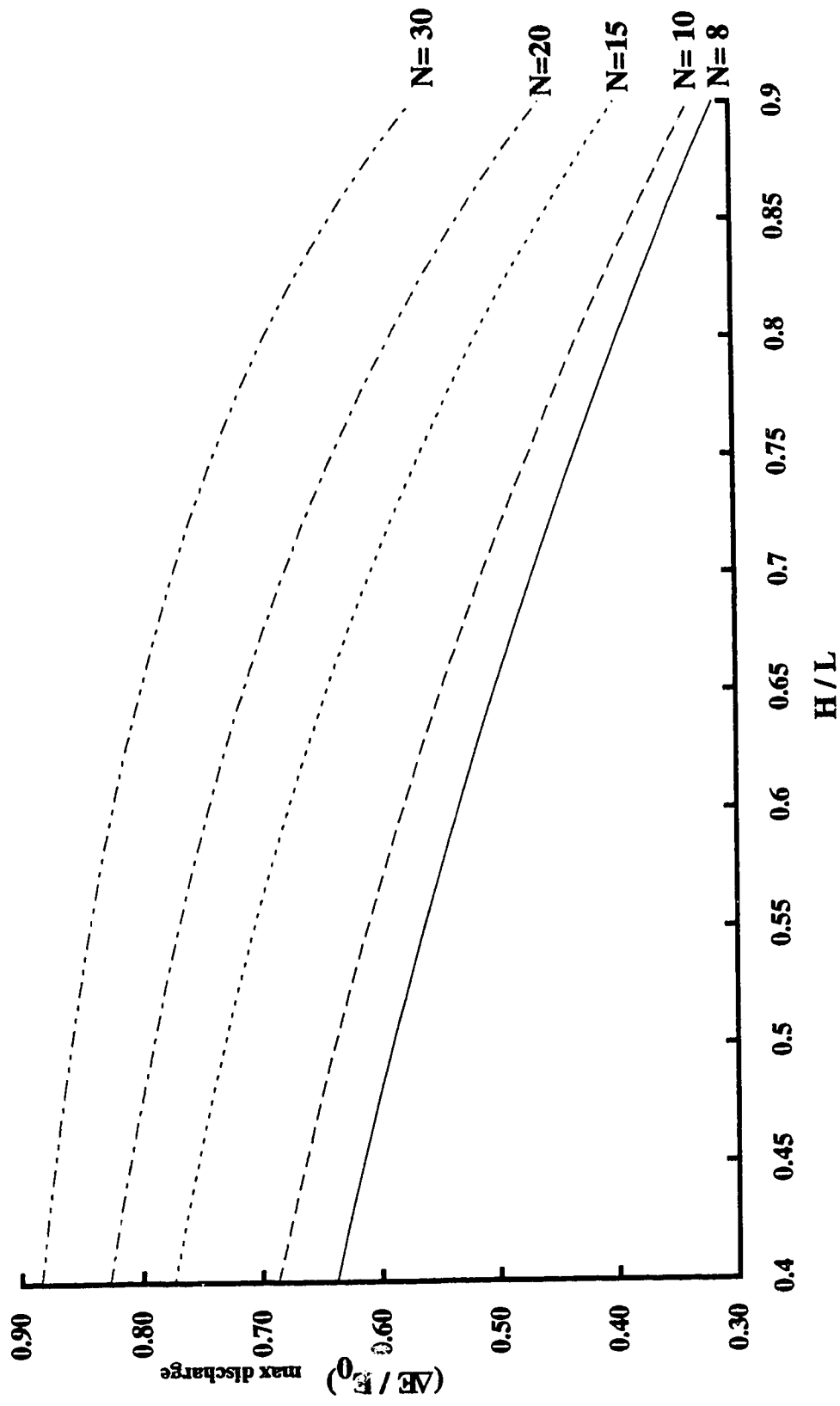
equations.

Figures 2.15(a-d) show the variation of α with Y_c/H for four values of H/L for several values of θ, where θ is the inclination angle of steps. These figures show that for smaller values of H/L, α increases with increasing θ for a given value of Y_c/H. For larger values of H/L, the increase in α is relatively small, which supports the argument of an additional energy loss when a partial jump occurs on an inclined step. At higher discharges, the jet front approaches the brink of the step where the depth of plunge pool decreases, thereby minimizing the energy dissipation. This point is supported by Figure 2.15 for any value of H/L, wherein α for several values of θ are approximately the same for higher values of Y_c/H. This argument suggests that the inclination of steps does not increase the energy dissipation capacity for maximum discharge.

A closer inspection of Figure 2.15 revealed that the variation of α with H/L for inclined steps can be described by the equation

$$\alpha = c + d\log(Y_c / H) \tag{2.33}$$

wherein the coefficients c and d are described by the following equations

$$c = 0.476 + 0.431\cos(\theta) + [-2.043 + 1.585\cos(\theta)]\log(H/L) \tag{2.34}$$

$$d = -0.795 - 0.223(\theta) + [-0.187 + 1.657(\theta)]\log(H/L) \tag{2.35}$$

Figure 2.15(a) Variation of α with Y_c/H for H/L= 0.421

Figure 2.15(b) Varaition of α with Y_c/H for H/L= 0.526

52
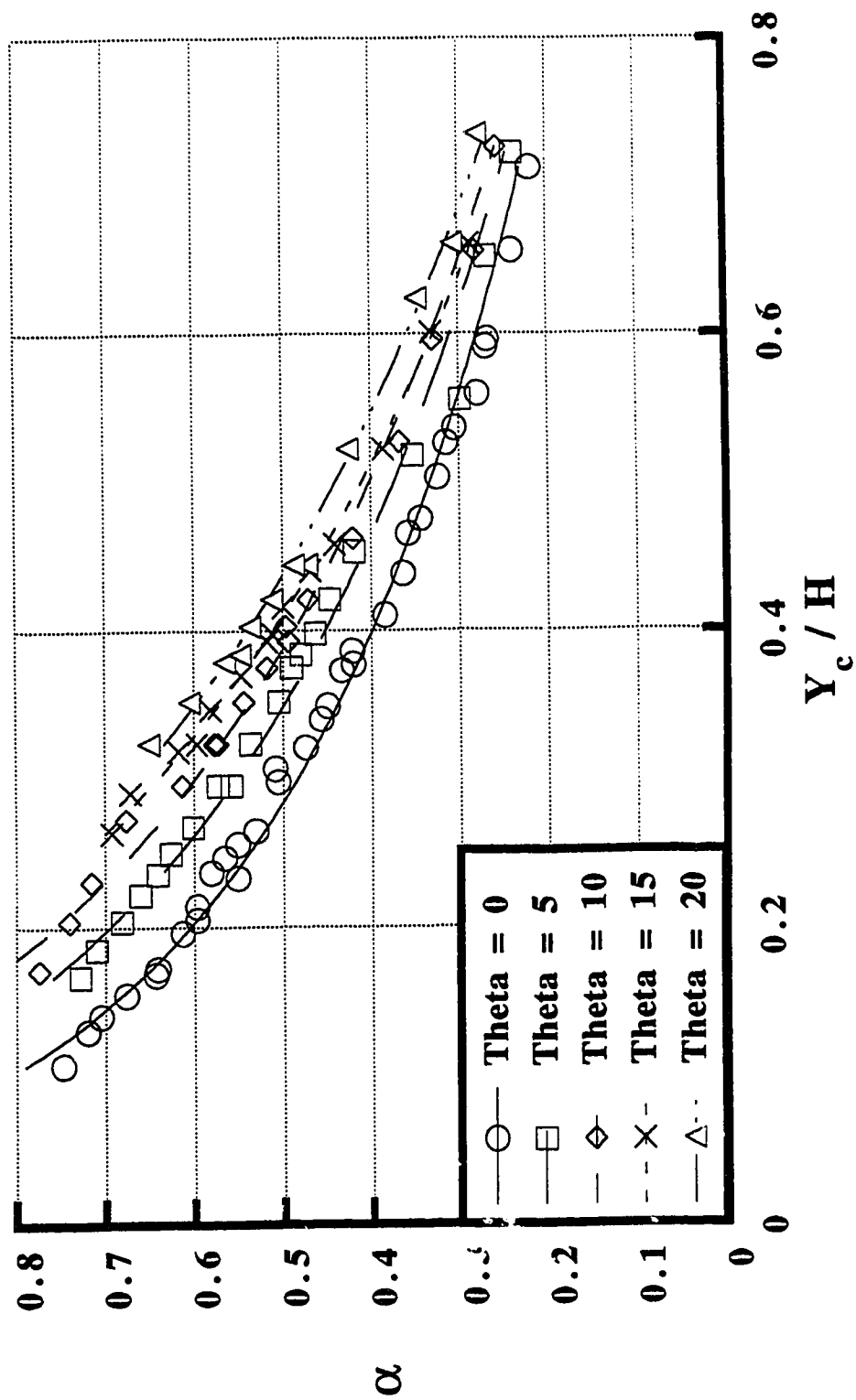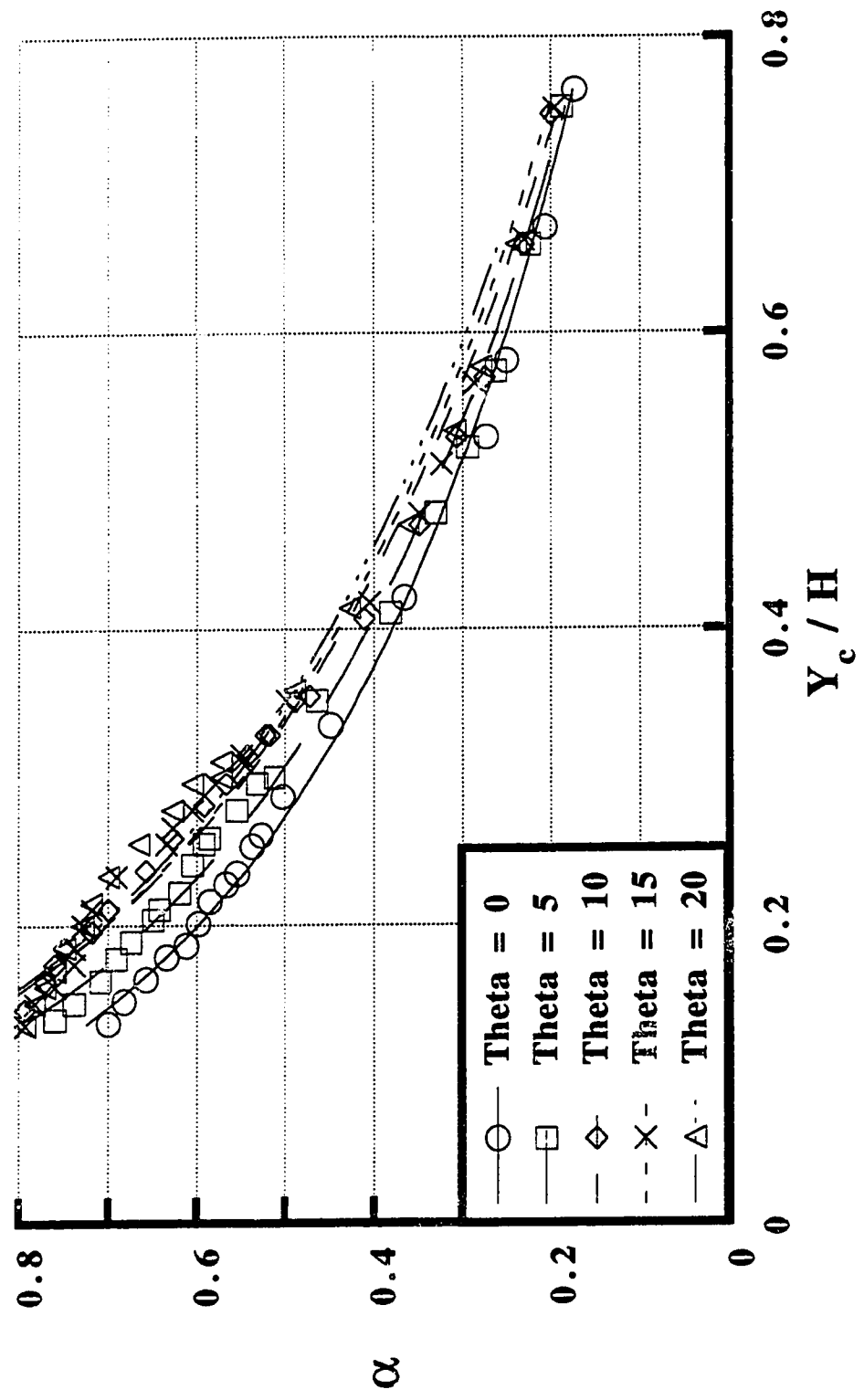
Figure 2.15(c)   Variation of α with Y_c/H for H/L= 0.736
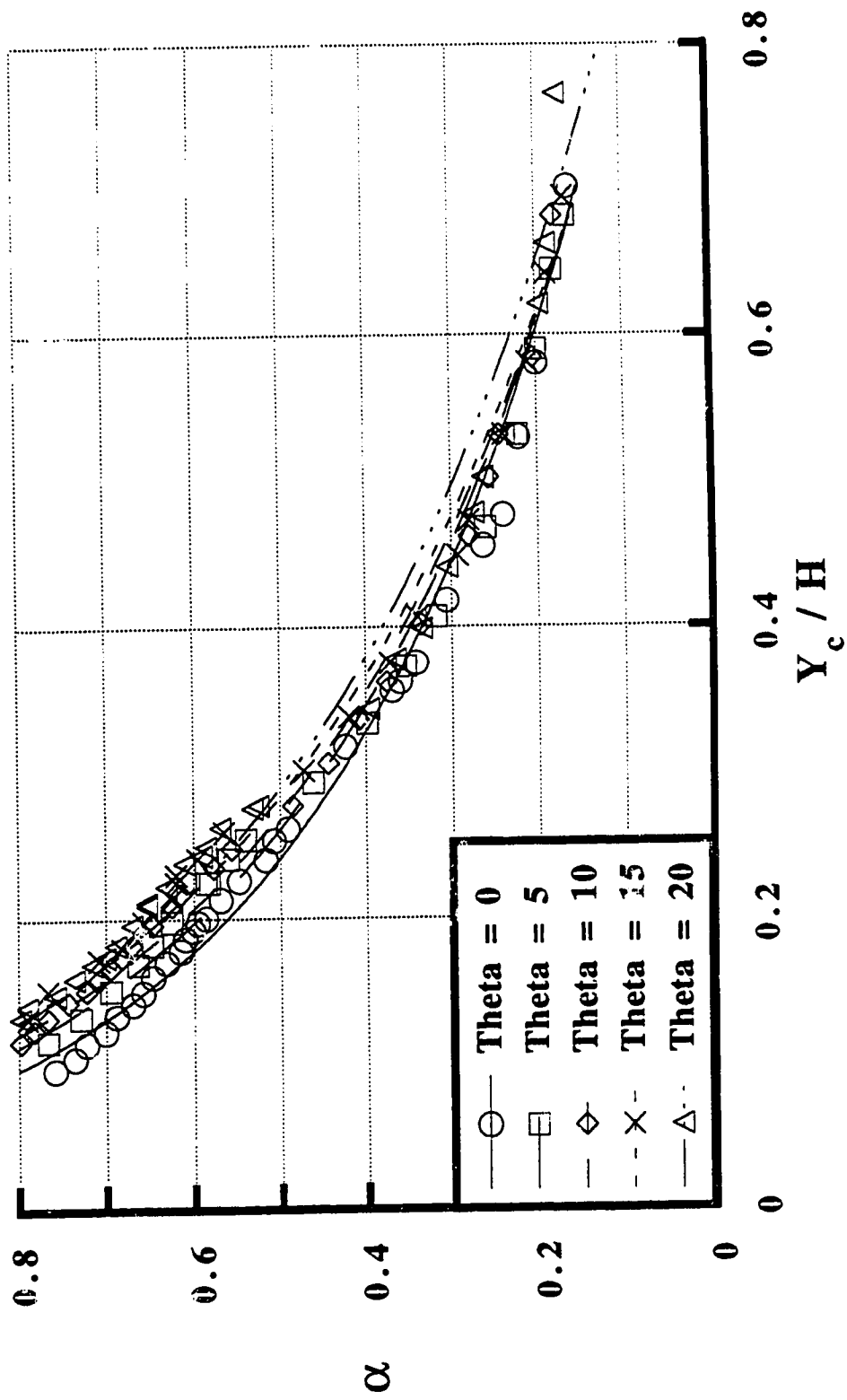
Figure 2.15(d)   Variation of α with Y_c/H for H/L= 0.842
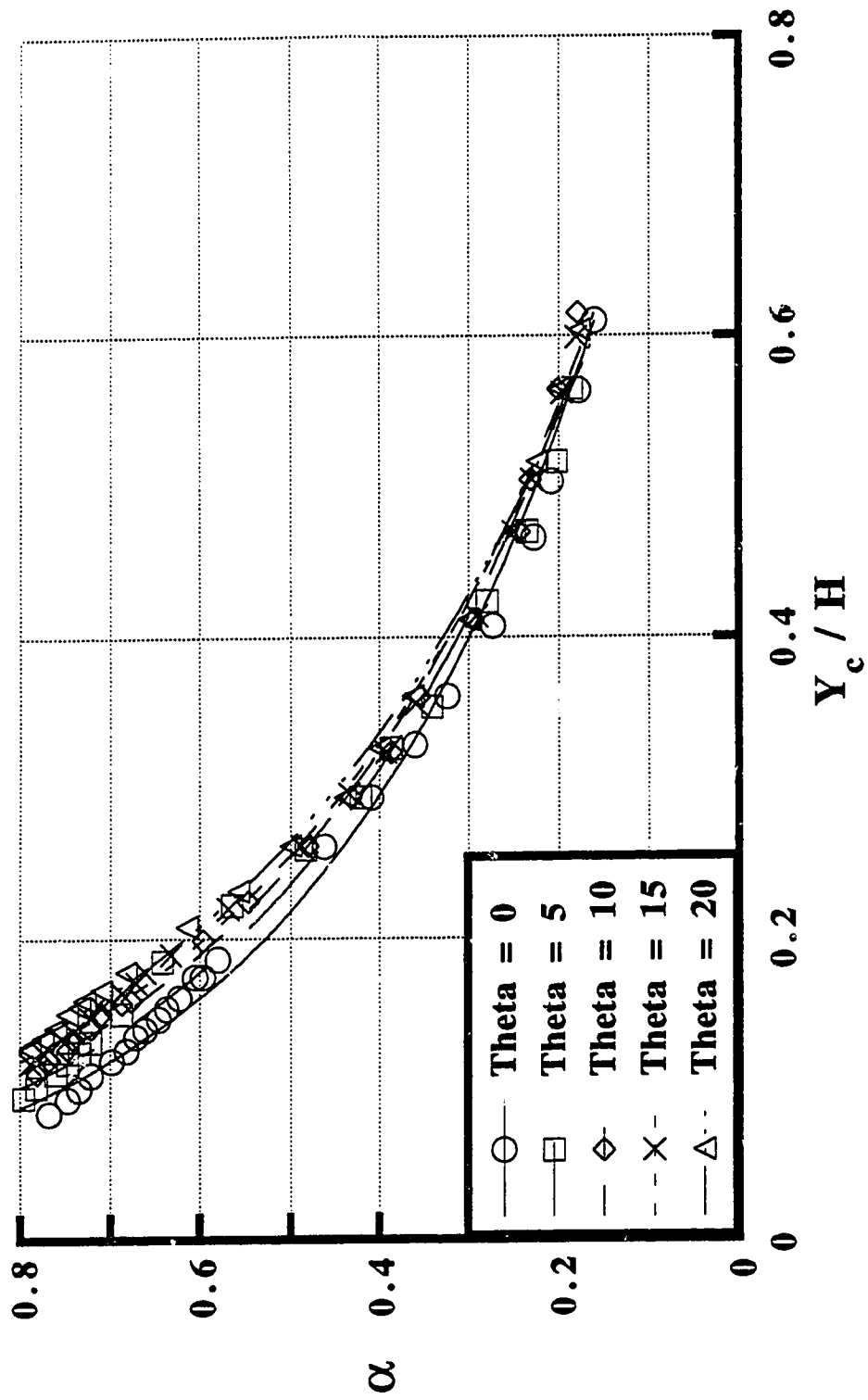
By substituting Equations (2.34) and (2.35) in Equation (2.33), the proportion of energy loss can be calculated. Then, Equation (2.24) or (2.30) is used to determine the relative energy loss. Figure 2.16 shows the comparison between calculated relative energy loss from Equation (2.33) and from experimental results. The regression coefficient is found to be 0.99994 using 430 experimental data. There were no attempts made to estimate the relative energy loss for maximum discharge because the limit of jet flow for inclined steps is approximately the same as for horizontal steps. Finally, it must be stressed that Equation (2.33) is an empirical relationship and should not be extended to conditions outside those for which it was obtained.

Figure 2.16 Comparison between values of relative energy loss obtained from observed data and Equation (2.33) for inclined steps
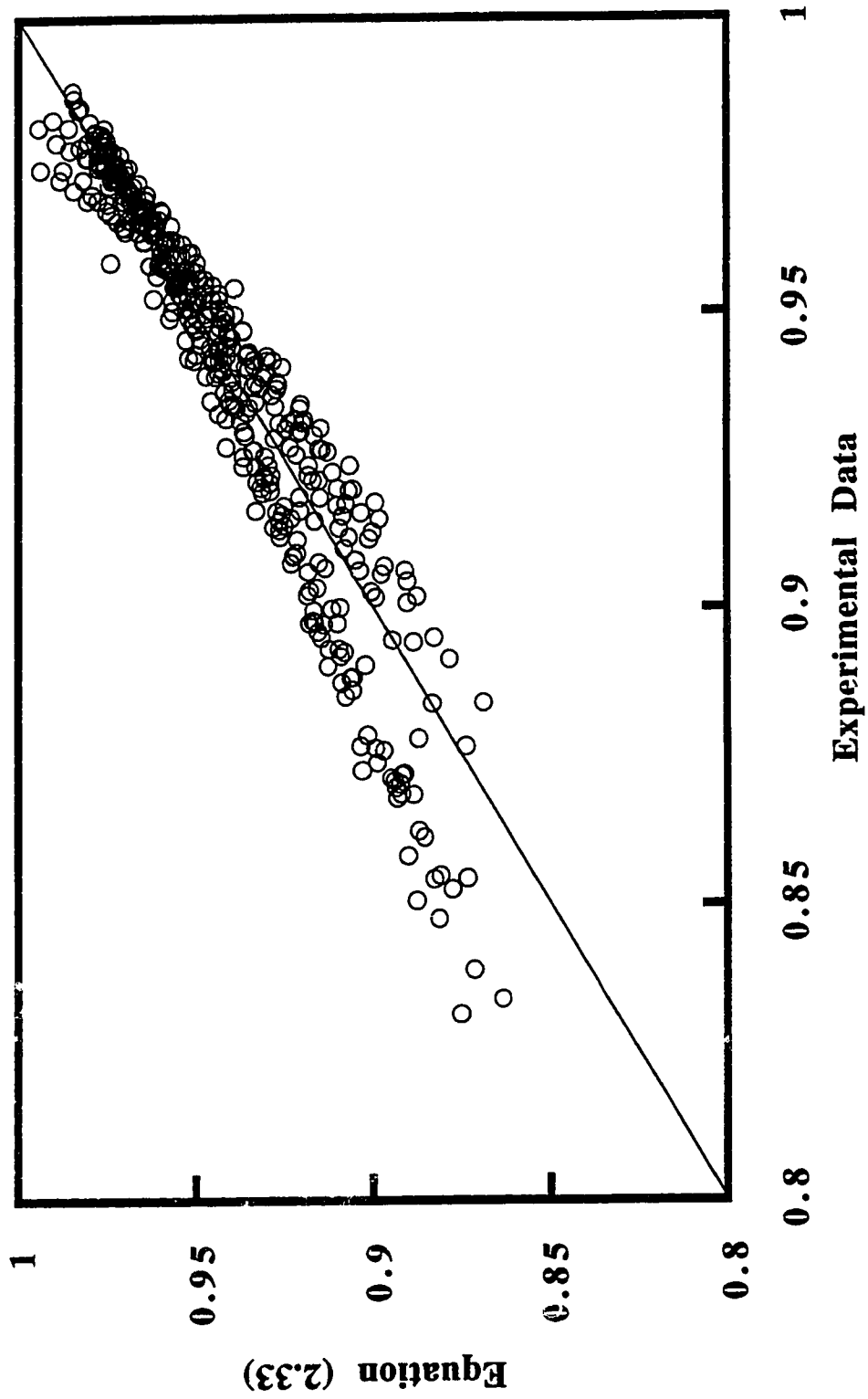
Chapter 3

LITERATURE REVIEW OF HYDRAULICS OF DROPS

3.1. Introduction

The approach to the study of hydraulic characteristics of drop or free overfall can be classified in two categories. Some investigators have studied the form of the nappe in the air. Others have concentrated on the flow patterns and energy dissipation. Although, it is beyond the scope of this investigation to provide a review of all the studies performed in this area, an attempt is made to briefly review some of the basic investigations. This will perhaps help to appreciate the mechanism of flow and the present investigation.

Blaisdell (1954) developed an equation for the flow profile of the aerated nappe using the data of earlier investigators. Schwartz (1963) developed a solution for the nappe profile considering the pressure difference across the nappe.

A basic contribution in the second category was made by Moore (1943) followed by the discussions of White (1943) and five others. These discussions were mainly on the energy loss at the base of drop. White (1943) developed a theoretical solution for energy loss that was later modified by Gill (1979). Rand (1955) developed empirical equations for some of the characteristics of the flow in terms of dimensionless parameters. Robinson (1989 and 1992) measured the shear stress and stagnation pressure along the bed and wall of drops with a non-aerated nappe. It appears that the mechanism of energy dissipation and velocity distribution of the falling jet have not been

studied so far. The next section presents a discussion of the significant papers in the second category, with some consideration of the nappe profile.

3.2. Nappe Profile

3.2.1. Blaisdell (1954)

In accordance with earlier studies, it is assumed that the horizontal velocity of flow is constant and the only force acting on the nappe is gravity. Ignoring air friction and fluid viscosity, equations were derived based on the trajectory of a particle to predict the form of free falling nappe. Then, coefficients of these equations were empirically determined using the experimental data. These equations are valid for subcritical approach velocity and varied approach channel depth. The formulae derived for the upper and lower nappe are not valid in the vicinity of the crest where it is believed that the pressure within the nappe is greater than atmospheric pressure. Blaisdell's equations agree very well with the experimental data of earlier investigators.

3.2.2. Schwartz (1963)

A general analysis was performed to predict the trajectory of projected nappe considering the influence of discharge, initial thickness and velocity of nappe, angle of projection, and the difference in pressure across the nappe. Equations of motion in the horizontal and vertical directions were used along with the continuity equation to develop a formula for the profile of the nappe. The relative influence of the governing parameters can be determined by checking the derived equations. An excellent agreement was reached between the suggested

numerical method and analytical solutions. A relatively small pressure difference plays a significant role in the nappe profile. This may explain the mechanics of the nappe oscillation caused by pressure difference across the nappe. It was suggested that the nappe may be used as a device for measuring small pressure because of the sensitivity of the thin nappe to pressure difference.

3.3. Flow Patterns

3.3.1. Moore (1943)

This distinguished work was performed to obtain information that would be of value in the design of drops. In this comprehensive study, some flow characteristics including energy loss and depth of flow at the base of a drop, pool depth, and the effect of tailwater on the hydraulic jump were carefully examined.

The experiments were performed on drops with different heights of $H = 0.45$ and 0.15 meter (Figure 3.1(a)). The upstream flow was subcritical and, hence, the flow approached the drop at critical depth. The inaccurate measurement of the flow depth because of the presence of heavy water spray near the base of the drop necessitated measurement of the velocity profile to determine the energy loss. The specific energy at the base of the drop E_1 was calculated by applying the relation

$$E_1 = Y_1 + \frac{\sum v_1^3 \Delta A}{2g \sum v_1 \Delta A} \tag{3.1}$$

where Y_1 is the depth of flow, v_1 is the average point velocity, and ΔA

is the element area associated with v_1. The upstream energy was predicted in a way similar to Equation (2.14) and the same assumptions were taken into consideration. Then, the energy loss ΔE is easily found by the difference between the upstream and downstream energies. Totally eleven runs were made covering a range of Y_c/H from 0.068 to 1. A plot of $\Delta E/Y_c$ against Y_c/H showed that, contrary to common belief, the relative energy dissipation could be as much as 50% for smaller discharges.

By using the momentum relation, it was shown that the pool depth Y_p, can be expressed by the relation

$$\frac{Y_p}{Y_c} = \sqrt{\left(\frac{Y_1}{Y_c}\right)^2 + 2\left(\frac{Y_c}{Y_1}\right) - 3} \tag{3.2}$$

Because of the inaccuracy encountered with the measurement of Y_1 for the reason mentioned previously, Y_1 was calculated from experimental value of E_1 by converting Equation (3.1) as a function of Y_1 and Y_c. The author believes that Y_1 calculated from the continuity equation could be more accurate rather than using the energy equation because the velocity distributions were carefully determined. Then, Equation (3.2) is used to determine the values of Y_p. A plot of Y_p/Y_c against Y_1/Y_c showed a good agreement between the calculated and experimental values of Y_p.

The second part of his investigation included a study of the vertical elements of the downstream jump and the longitudinal characteristics of the flow influenced by the tailwater.

3.3.2. White (1943)

In this remarkable discussion of Moore's work, a theoretical equation is developed for energy loss. It is assumed that the flow condition of drop can be approximated to the condition of plane jet (Figure 3.1(b)), where the jet strikes a flat surface. The energy loss at impact and the friction of the bed are ignored and therefore, the velocities of flow in the forward and backward directions are assumed to be the same as the velocity of jet before it strikes the floor. The conservation of momentum and continuity principles were applied to yield the relation

$$\frac{Q_b}{Q_f} = \frac{Y_b}{Y_f} = \frac{1 - \cos\beta}{1 + \cos\beta} \tag{3.3}$$

where Q_b, Q_f, Y_b, Y_f, and β are defined in Figure 3.1(b).

In the drop situation (Figure 3.1(c)), the backwater flows into the standing pool, causing clockwise rotation and the same flow passes back from the pool into the jet. This mixing process was believed to be responsible for energy loss. In this condition, the incoming and forward flows are equal to Q. It is further assumed that the velocity of flow V_m in the thickened mixing zone remains constant and is equal to the forward velocity V_1. So, the ratio of pool discharge Q_c to forward discharge Q is the same as the ratio of plane jet, that is

$$\frac{Q_c}{Q} = \frac{1 - \cos\beta}{1 + \cos\beta} \tag{3.4}$$

If the momentum of flow that enters the pool is assumed to be equal to that of the return flow, it is argued that the total momentum of the jet would not be changed in the mixing process. Therefore, the momentum equation between any two sections across and before the mixing zone gives

$$V_m = V_1 = \frac{V}{2}(1 + \cos\beta)$$ (3.5)

where V_m is the average velocity in the mixing zone, V_1 is the average velocity of the jet at the base of the drop, V and α are the velocity and inclination of the free falling jet before the mixing zone, respectively. Applying the momentum principle between the critical section and any section in the free jet and ignoring frictional resistance gives the relation

$$V_x = V\cos\beta = \frac{3}{2}\sqrt{gY_c}$$ (3.6)

where V_x is the horizontal component of free falling jet. The velocity V is then obtained by applying energy equation to the plane jet between the critical section and the section just before turning, as

$$V = \sqrt{2g(H + 1.5Y_c)}$$ (3.7)

Substituting Equation (3.7) in Equation (3.6) and introducing the continuity equation, the following relations can be deduced

(a) Drop

(b) Plane jet

(c) Jet including pool flow
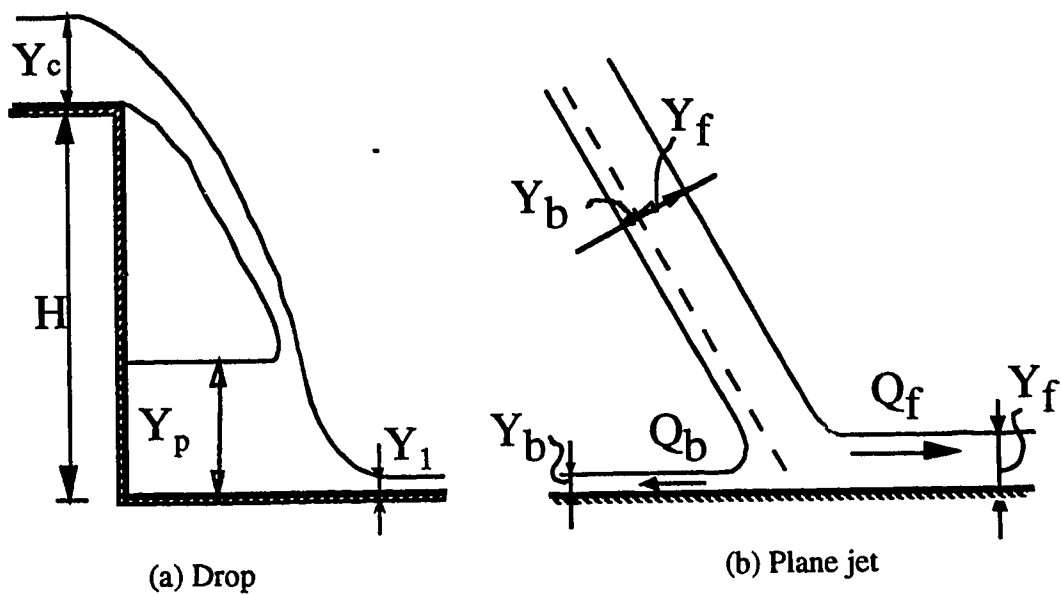
Figure 3.1 Definition sketches of plane jet and drop

$$\cos \alpha = \frac{1.06}{\sqrt{\dfrac{H}{Y_c}} + 1.5} \tag{3.8}$$

$$\frac{Y_1}{Y_c} = \frac{\sqrt{2}}{1.06 + \sqrt{\dfrac{H}{Y_c} + 1.5}} \tag{3.9}$$

The remaining energy of flow at the toe of the drop can be expressed by following equation

$$E_1 = Y_1 + \frac{q^2}{2gY_1^2} = Y_1 + \frac{Y_c^3}{2Y_1^2} \tag{3.10}$$

Using the value of Y_1 from Equation (3.9)

$$\frac{E_1}{Y_c} = \frac{\sqrt{2}}{1.06 + \sqrt{\dfrac{H}{Y_c} + 1.5}} + \frac{1}{4}\left(1.06 + \sqrt{\frac{H}{Y_c} + 1.5}\right)^2 \tag{3.11}$$

The calculated values of E_1/Y_c show a reasonable agreement with the experimental results of Moore.

3.3.3. Rand (1955)

The purpose of this investigation was to evaluate empirically the basic characteristic lengths of the drop. These terms are the depth of flow at the toe of the drop Y_1, the depth of flow in downstream channel

Y_2 if the hydraulic jump begins at the toe of the nappe, and the depth of pool behind the nappe Y_p.

A vertical drop with the height of $H = 197.9$ mm was built and well aerated to assure the atmospheric pressure under the nappe. Similar to Moore's experiment, the upstream flow was subcritical. The measurement of different lengths and surface elevations was repeated twenty times to minimize the error and the average values were recorded.

The data of Moore are also considered as a supplement to his experiment results to cover a wide range of variable values. As an independent variable, the drop number $D = q^2 / gH^3 = (Y_c / H)^3$ is introduced to represent the variation of dependent terms. Plots of Y_1/H, Y_2/H, and Y_p/H against D resulted in the following relations

$$\frac{Y_1}{H} = 0.54 \, D^{0.425} \tag{3.12}$$

$$\frac{Y_p}{H} = D^{0.22} \tag{3.13}$$

$$\frac{Y_2}{Y_1} = \frac{3.07}{D^{0.155}} \tag{3.14}$$

It is obvious that the ratio Y_2/Y_1 can be accurately evaluated by the theoretical jump equation rather than Equation (3.14). It is reported that the surface of the pool is slightly inclined downward to the nappe and the rotating flow is believed to be responsible for the inclination. A

brief explanation of stilling basin design for drop was also given according to the downstream flow condition.

3.3.4. Gill (1979)

This study presented a modification to White's theory to mainly improve the prediction of the pool depth. It addition, an experiment was set up to measure some hydraulic lengths such as pool depth Y_p, the brink depth Y_0, and the inclination of jet β. The results of experiments were compared with White's theory and Rand's equations.

Equation (3.7) of White's theory was modified by considering the existing of the pool. In other words, the velocity V was assu. ed to be the velocity of the jet before entering the mixing zone and modified by the relation

$$V = \sqrt{2g(H + {}^{\cdot}.5Y_c - Y_p)}$$ (3.15)

It was argued that the velocity of the jet in the mixing zone could not be constant. If the velocity of jet in mixing zone just below the pool level is V_p, Equation (3.5) is converted into

$$V_p = \frac{V}{2}(1 + \cos\beta)$$ (3.16)

Further V_p is assumed to be equal to the horizontal component of the jet velocity above the pool V_x, that is

$$V_x = V_p \cos\beta$$ (3.17)

Rearranging E $_x$ $_x$ ns (3.15) to (3.17) and solving for β

$$\cos\beta\,(1 + \cos\beta)\sqrt{2g(H + 1.5Y - Y_p)} = 3\sqrt{gY_c} \qquad (3.18)$$

The energy equation is then applied between the toe section and the section just below the pool level

$$V_1 = \sqrt{V_p^2 + 2g(Y_p - Y_1)} \qquad (3.19)$$

The above relation is obtained by ignoring the energy loss in the mixing zone and it is assumed that the energy is only dissipated at the intersection of free falling jet and pool level (which appears to be a poor assumption). Introducing the continuity and energy equations, considering Equations (3.15) & (3.16), and solving for Y_1 and E_1

$$\frac{Y_1}{Y_c} = \frac{1}{\sqrt{\dfrac{(1 + \cos\beta)^2}{2}(\dfrac{H}{Y_c} + 1.5 - \dfrac{Y_p}{Y_c}) + 2(\dfrac{Y_p - Y_1}{Y_c})}} \qquad (3.20)$$

$$\frac{E_1}{Y_c} = \frac{Y_1}{Y_c} + \frac{1}{2}(\frac{Y_c}{Y_1})^2 \qquad (3.21)$$

The values of Y_p, β, Y_1, and E_1 can be evaluated by considering the above equations and Equation (3.2).

It is conceded that the angle β and the circulating discharge in the pool are smaller than the angle and the backwater discharge of a free

falling jet. Plots of Y_p/Y_c , Y_1/Y_c , and E_1/Y_c show that the pool depth obtained from modified theory and Rand's empirical equation agrees well in the range of Y_c/H from 0.20 to 0.70. The energy loss is less than that obtained from White's theory.

An experimental set up was arranged for drop heights of H =43, 74, 99.4, & 176.5 mm. The drops wer well utilized and the angle of lower nappe was used as a basis for jet inclination. Nothing was reported about the state of upstream flow, whether it is subcritical or supercritical. The discharge of each run was measured two or three times and the average was taken. To verify the angle of the jet and to obtain detailed measurement of the jet profile, some experiments were performed in a wider channel.

The experimental results along with the predictions of White's theory and Rand's empirical equations are given. The observed values of pool depth show satisfactory agreement with Gill's theory and are quite close to Rand's relation. White's theory predicts smaller values for pool depth than the observed ones and, for some runs, the differences are noticeable. A good agreement is obtained between the experimental values of jet inclination and those of Gill's theory. Greater values of jet inclination are predicted by White's theory compared to the observed results. As a complementary note, the ratio of brink depth to critical depth is compared with the results of previous investigations. Although this ratio should be close to 0.715, all runs showed higher values. It is reported that for higher drops the ratio is less than that for smaller drops.

3.4. Closing Comments

Although some flow characteristics have been studied earlier, there is still some uncertainty about the assumptions mentioned previously. Actually, any hypothesis must depend for its verification on observable evidence. It is difficult to decide which theory describes the mechanism of flow in the drop where only a few measurements are reported.

In the absence of any measurement in the mixing zone, the assumption introduced by White regarding the ratio of pool discharge to forward flow is a remarkable idea for further work. With the aid of this idea, Gill succeeded in modifying the White's theory with minor changes. There are three major factors that influence the flow in the mixing zone. While the gravity and the pool pressure tend to accelerate the flow, the shear stress exerted by the standing pool acts in an opposite way to slow down the flow. White assumed that the resultant force gives the thickened jet a constant velocity. Gill suggested a sudden change in jet velocity where it enters the pool. To develop his theory, Gill assumed that no energy is dissipated in the mixing zone except at the interface of pool level and free falling jet. Both theories, to some extent, are questionable. Unfortunately, no measurements of velocity in the mixing zone were reported to verify which assumption is relatively close to actual conditions. In addition, none of the previous works succeeded in evaluating the variation of velocity distribution downstream of the drop base.

In order to verify the theories mentioned before, some models are set up. The aim of this study is to investigate the mechanism of flow mixing in the standing pool, especially to provide a clear picture of

energy dissipation. It is also attempted to obtain information regarding the velocity distributions at the mixing zone and at the toe of the of drop.

Chapter 4

STUDY OF DROPS

4.1. Introduction

The main goal of this part of this study is to investigate the hydraulics of drops. More emphasis has been placed on the falling jet and pool sections for which are no previous measurements. The mechanism of energy dissipation is carefully studied with the aid of measurements and observations. The impinging plane jet is also studied because of its use in the analysis of drops.

This chapter is divided into three major parts. The first part describes the general experimental set-up as well as the measurement system. The experimental results are presented in the second part. The third part presents analysis of the data along with discussion of the previous investigations.

4.2. Definitions

The following terminology is used to describe most flow characteristics of the drop and plane jet models (Figure 4.1):

1) Upstream channel: the higher channel that is bounded by the brink of the drop or plane jet model.

2) Downstream channel: the part of channel that extends from the brink of models to the end of channel.

3) Intersection line: the line that defines the intersection of the free falling jet with pool surface.

4) Base of the drop or plane jet: refers to the channel section, where

the impinging jet becomes parallel to the downstream channel bed.

5) Jet inclination: the angle that jet makes with the horizontal line.

6) Free falling jet: includes the portion of the falling jet from the brink to the intersection line or the bed for drop and jet model, respectively.

7) Sliding jet: the segment of the jet from the intersection line to the base of the drop.

8) Jet inflection point: the point where the curvature of the sliding jet changes (point A, Figure 4.1).

9) Jet hitting point: the point at which the continuation of the sliding jet centerline intersects the bed.

10) Pool length L_p: the distance of jet hitting point from the drop wall.

11) Pool depth Y_p: the depth of standing water at the under-nappe pool.

12) Circulating discharge Q_c: the discharge that circulates in the pool.

4.3. Models and Experimental Equipment

4.3.1. General Description of Models

The model study was carried out in the T. Blench Hydraulics Laboratory at the University of Alberta. The models utilized in this study consisted of the following

(I) A drop model with a height equal to 618 mm

(II) A drop model with a height equal to 250 mm

(III) A plane jet model with a height of 250 mm

At the upstream end of all models, a stilling tank was provided to calm the flow coming from the supply reservoir. From the stilling tank,

the flow approaches the model through a short channel. This channel was set up at zero slope and had the same width ;s the models it served.
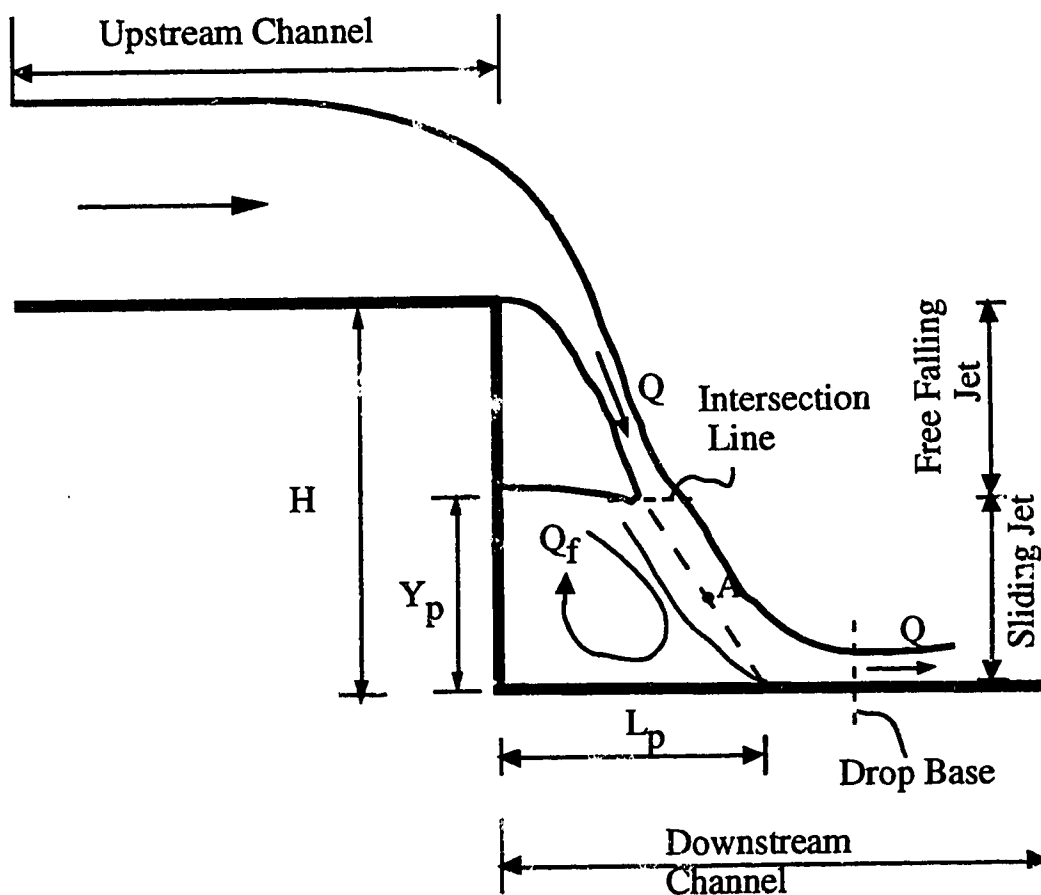
Figure 4.1 Definition sketch of a drop

The downstream channel of each model was equipped for making flow measurements. A more detailed explanation of the model arrangement is presented next.

4.3.2. Models

These models include; a supply reservoir and water supply line containing a magnetic flow meter and a control valve, a stilling tank, a short horizontal channel extending from the stilling tank to drops of variable heights, and a horizontal channel equipped with measuring devices. The diagrammatic sketches of these models are shown in Figures 4.2 and 4.3 and the general layout is also illustrated in Plates 4.1 to 4.3.

The water flows to the drops from a galvanized supply reservoir equipped with an overflow gate through a 0.16 meter diameter circular pipe. This pipe contains a magnetic flow meter near the supply reservoir to measure the discharge and a butterfly valve is located near the inlet of the stilling tank to control the discharge. To avoid air entrainment in the flow at high discharge, it is necessary to keep the supply reservoir in overflowing state.

The stilling tank was installed to calm the high velocity flow from the supply line so that a steady low velocity flow approaches the drop. The galvanized stilling tank is 1.60 meter long, 0.46 meter wide, and 0.60 meter deep. The operation of the stilling tank was improved very effectively by installing a metallic screen at the inlet normal to flow direction.

The upstream channel is 0.46 meter wide and contains a wooden platform projecting into the stilling tank to minimize the effect of end contraction on the drop flow patterns. The channel sides are constructed of Plexiglas except at the water inlet where they are made of steel. In order to make the flow subcritical, the wooden platform was furnished with plastic carpet having roughness elements to slow down the flow.
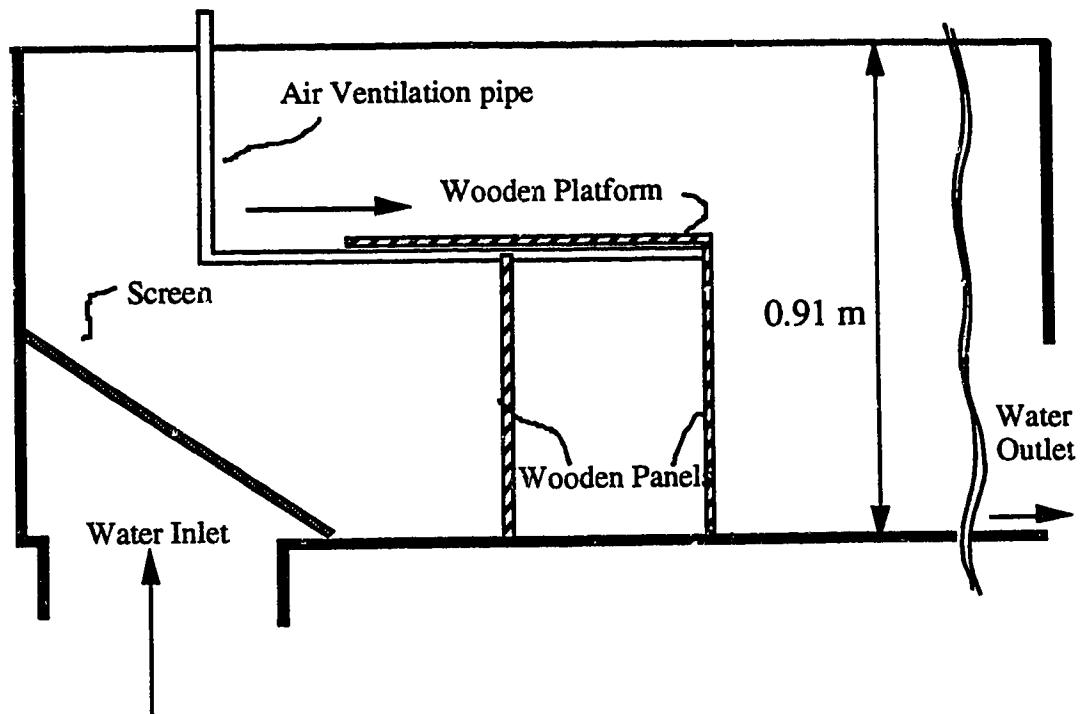
(a) Side View
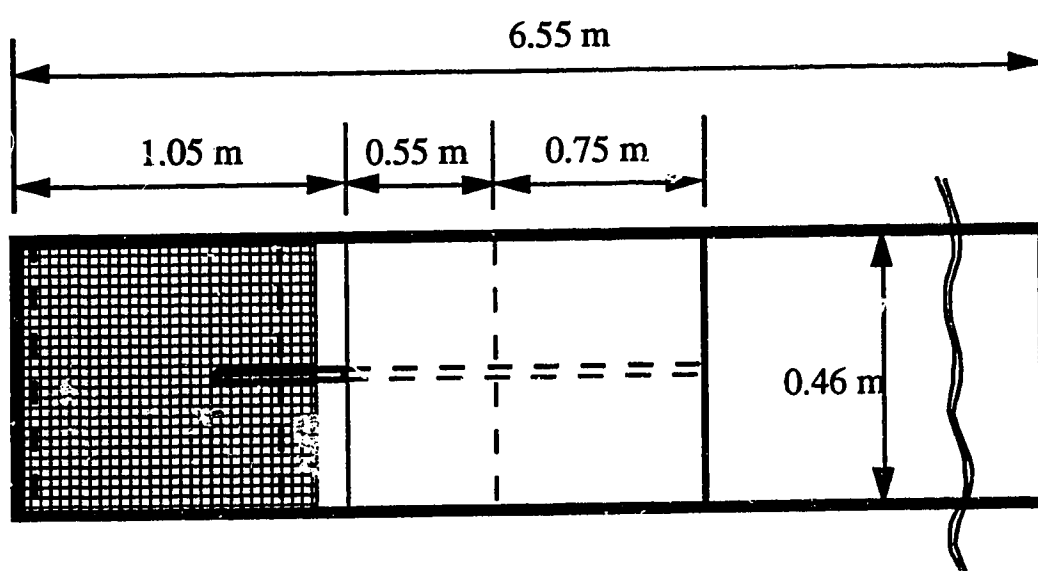
(b) Plan

Figure 4.2 Diagrammatic sketch of a drop model
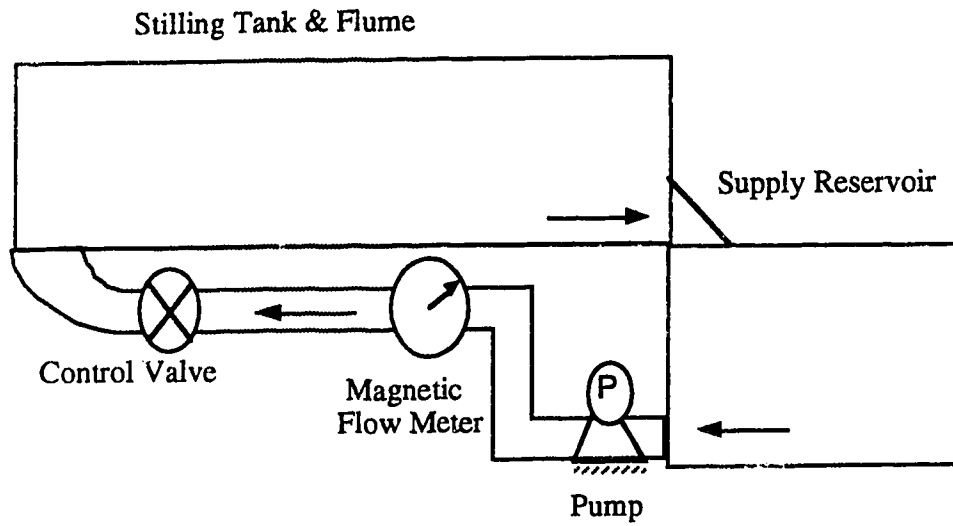
Figure 4.3 Diagrammatic layout of the general set-up
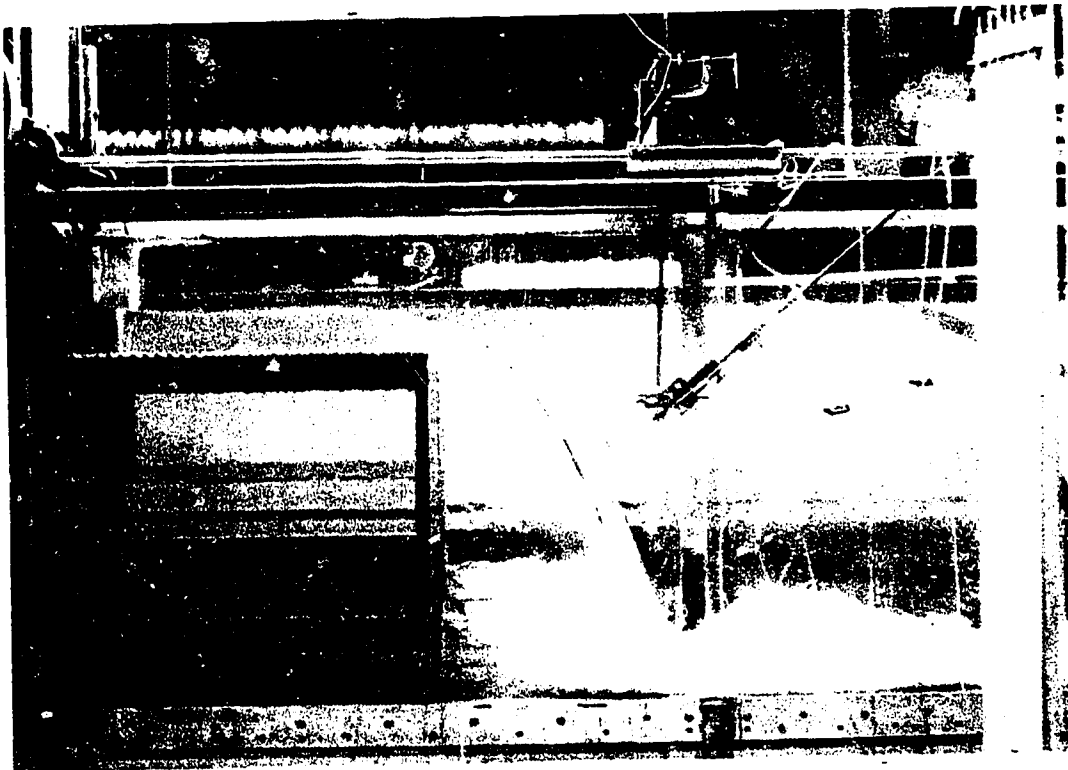
Plate 4.1 Drop Model of 618 mm height
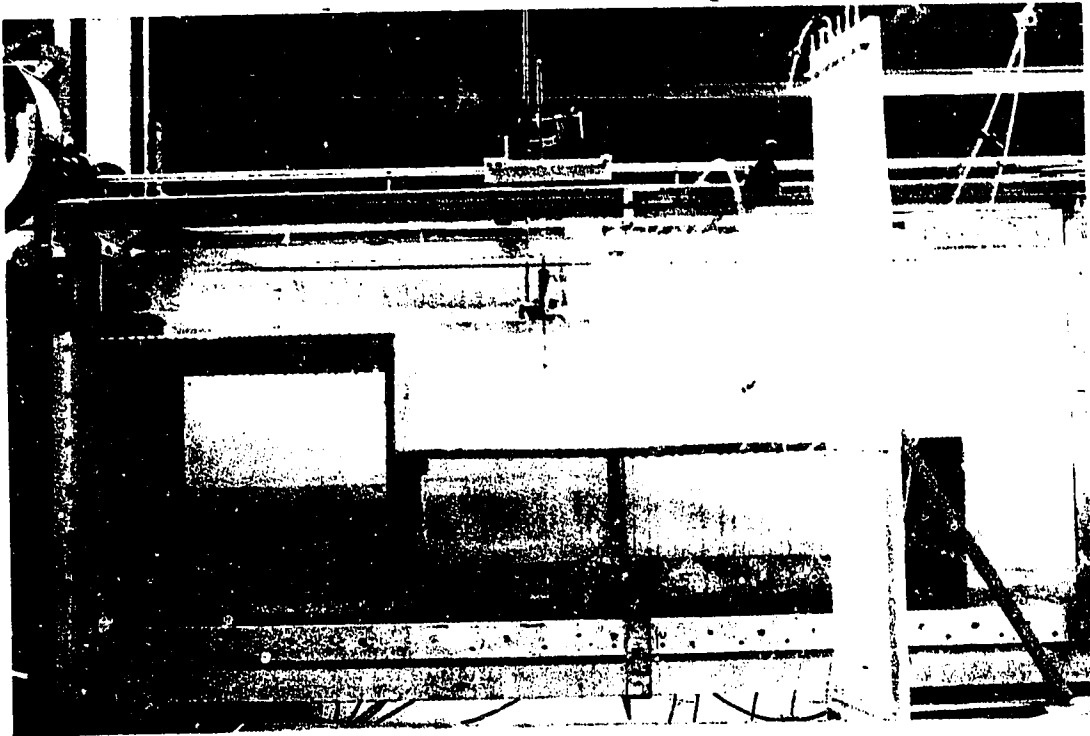
Plate 4.2 Drop Model of 250 mm height
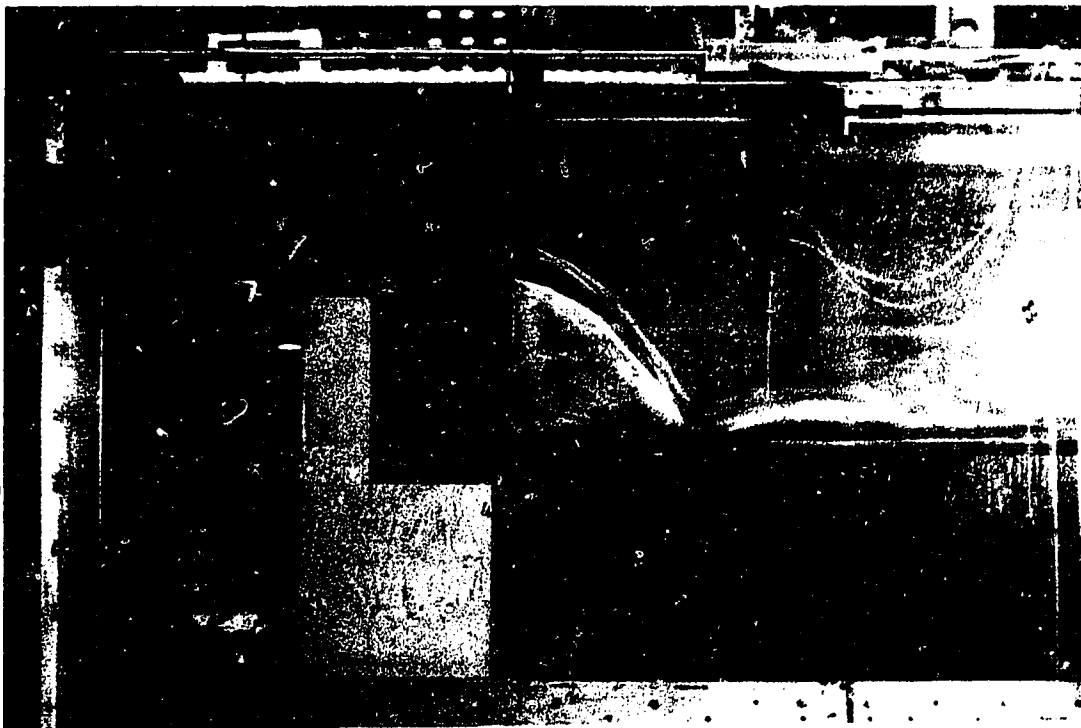
Plate 4.3 Jet model of 250 mm height

The first model consists of a drop with a width of 0.46 m and a height of 0.618 m. The channel bed is then raised with a wooden platform of a length of 1.5 m to set the second drop with 0.25 m height. The jet model is essentially an extension of the second model. A slot is cut into the vertical panel at the pool section to drain the backward flow into the main channel bed. Both models are well aerated by means of a steel pipe to ensure that the pressure underneath the nappe is atmospheric.

The downstream channel was located at the base of the drops. The channel sides are made of Plexiglas and like the upstream channel, the bed is made of galvanized steel. It has the same width as the drop and is 3.5 meter long and 0.91 meter deep.

4.3.3. Measurements

The measurements included the discharge, velocity, depth, and nappe coordinates. A magnetic flow meter, a Prandtl tube, a point gauge, and photographic work were used to obtain these measurements.

The flows to the models were measured by means of a magnetic flow meter installed in the supply line. The principle of the magnetic meter is that when a moving conductor crosses the lines of a magnetic field, a voltage is induced. If the dimensions of the conductor are constant, the voltage is proportional to the velocity. The flowing liquid itself is the moving conductor, therefore, the voltage varies directly with the variation in the velocity or discharge of the flowing flow. The voltage is then read by a voltmeter that is calibrated to read five litres per second for each volt. The voltage could be read to 0.01 volt that makes it possible to set the flow rate within 0.1% from 15 L/s to 45 L/s. To avoid air entrainment by the pump, the maximum discharge was set
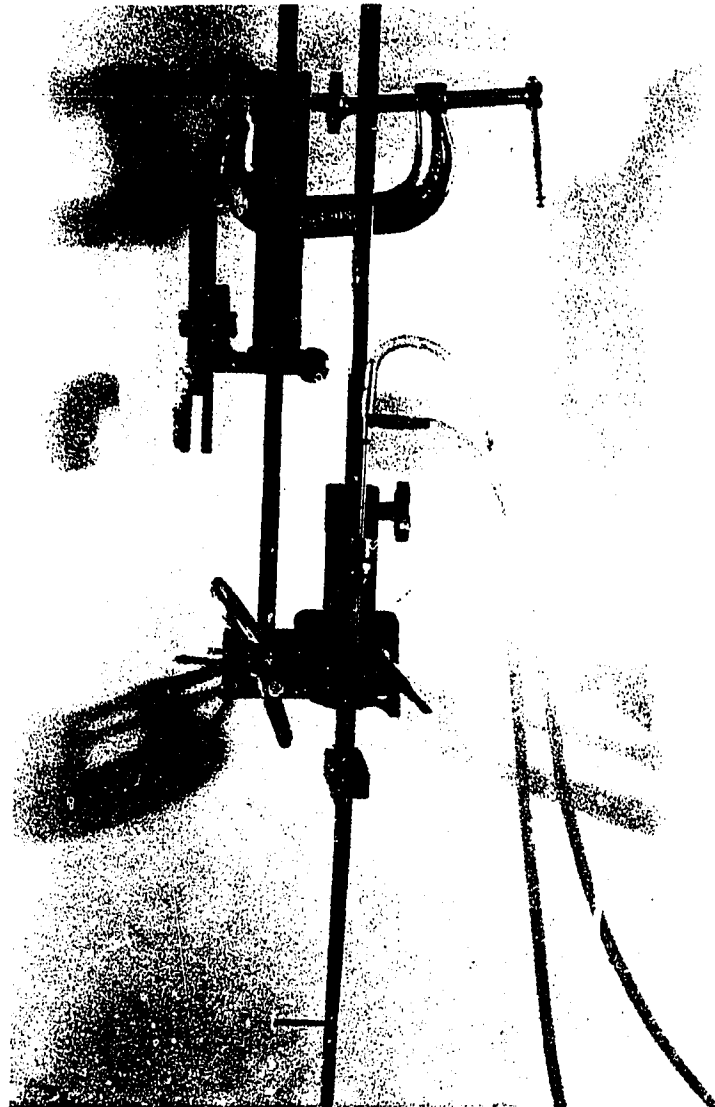
Plate 4.4 Prandtl tube assembled with point gauge

to about 43 L/s.

The velocity measurements were made with a standard Prandtl tube of external diameter of 3.2 mm, shown in Plate 4.4. A point gauge was used to measure the flow depth and nappe coordinates. It was mounted on an instrument carriage that can be rolled over the rails at

the top of the channel. The point gauge was assembled with a Prandtl tube, shown in Plate 4.4, and is accurate to 0.0005 m. Another measuring scale was located at the side wall of channel to measure the section coordinates of the Prandtl tube position.

4.3.4. Observations

Flow visualization is very useful in developing an understanding of the patterns of the flow. Most of the flow visualization was done in the mixing zone in the pool region of the drops. Flow visualization was performed by injecting dye upstream and using video to observe how the flow develops in the mixing zone. Photographic work was used to find the manner in which the air was entrained and mixed with the flow. The video film frames were converted into computer files to determine the factors that influence energy dissipation. The video film speed can be reduced to show 1/30 second frames that are useful in following the flow mixing process and the mechanism of nappe oscillation. More detailed explanation of this photographic analysis is presented in the next section.

4.4. Experimental Results

4.4.1. Experimental Procedure

The height of the drop for models I and II was varied to cover a wide range of Y_c/H. The variation can also be made by changing the discharge. Considering the drop heights and discharge limitation, a total of twelve runs was performed covering a Y_c/H range of 0.06 to 0.35. Two runs were eliminated because of end contraction effects on the drop and the approach flow being supercritical. For the plane jet model,

four runs were performed with the same arrangement as for the drop of 250 mm height. Details of the model configurations used in this study are given in Table 4.1 along with the details of the discharges.

Three types of measurement were recorded for drop models. These included the velocity profile, water surface elevation, nappe coordinates, and some characteristic lengths. For the jet model, velocity distribution at the base of the jet and jet inclination were measured. All

Model	Y_c/H	Y_c	Q
		mm	L/s
Drop $H = 0.618$ m	0.08	49.4	15.84
	0.10	61.8	22.13
	0.12	74.2	29.1
	0.14	86.5	36.67
	0.155	95.8	42.71
	0.165	102	46.91
Drop $H = 0.25$ m	0.2	50	16.11
	0.25	62.5	22.51
	0.3	75	29.59
	0.35	87.5	37.29
Plane Jet $H = 0.25$ m	0.2	50	16.11
	0.25	62.5	22.51
	0.3	75	29.59
	0.35	87.5	37.29

Table 4.1 Details of tests made on models

the measurements were made in the centerplane of the upstream or downstream channel.

The velocity distributions at different locations were measured by the Prandtl tube. These measurements were performed in the upstream channel, the brink of drop, the free falling jet, the pool, and at the base of the drop. An attempt was made to measure the resultant velocity at every section. However, at the brink of drop, the measurements included only the horizontal velocity. Since the Prandtl tube is somewhat sensitive to the angle of attack, it was held parallel to the flow at the free falling jet and pool locations. In the free falling jet region, the angle of Prandtl tube was set parallel to the lower nappe. The angular difference between the lower and the upper nappe was less than 5 degrees for the maximum discharge resulting in a maximum error of 1% in the velocity measurement. An attempt to measure the velocity near the intersection line failed because of air entrainment and unsteadiness. For each run, the velocity profiles at two sections of the free falling jet and two sections of the pool were measured. A Prandtl tube of external diameter of 2.6 mm was used in the pool region to avoid the air bubbles. The velocity profiles of the supercritical flow at the base of the models were obtained by taking measurements at one or two millimeter intervals because of the relatively small depth of flow.

The upstream water surface profile and the coordinates of the nappe at the drop were measured for each run. The nappe oscillation created some difficulties in measuring the upper and lower nappe geometry of the free falling jet. Therefore, the recorded profiles represent average values. No measurements were recorded for water surface profiles and nappe coordinates of the plane jet.

The measured characteristic lengths included the pool depth Y_p, pool length L_p, and jet inclination. Because of the factors that are

described in the next sections, the pool depth varied due to surface waves and has a downward slope from the drop wall to the nappe. Therefore, the pool depths were measured at different locations and times and the average values were used to represent the profile. Since it was not possible to measure the pool length directly in the center of the channel, an indirect method is selected with the aid of a grid on the wall. The velocity distributions across the sliding jet at two sections were measured and the section lines were marked on the side wall. By computation, the thickness of the sliding jet and, therefore, the boundary between the main flow and the circulating flow was recorded. The centerline of the initial part of the sliding jet is drawn to intersect the channel bed reference to obtain the pool depth. Finally, the jet inclination was recorded at the intersection line. Careful measurements revealed 1-2% error depending on the flow rate. For the jet model, the jet inclinations at two locations were measured: (i) at the height of hypothetical pool depth that is obtained from drop model; and (ii) at the bed where the sliding jet strikes.

4.4.2. Experimental Data

The photographic analysis revealed some important features of the air entrainment mechanism. Plates 4.5 to 4.7 show some close-up pictures for various models. The jet flow is extremely agitated after the intersection line and the sliding jet is retarded by the main vortex in the pool. The flow at the base of the drop is supercritical and has a disturbed surface that is referred as a partial hydraulic jump. For the plane jet model, the effect of the side wall caused the backwater flow to splash to a considerable height. The free falling jet oscillated because of

Plate 4.5 Observed flow agitation and air entrainment for model I
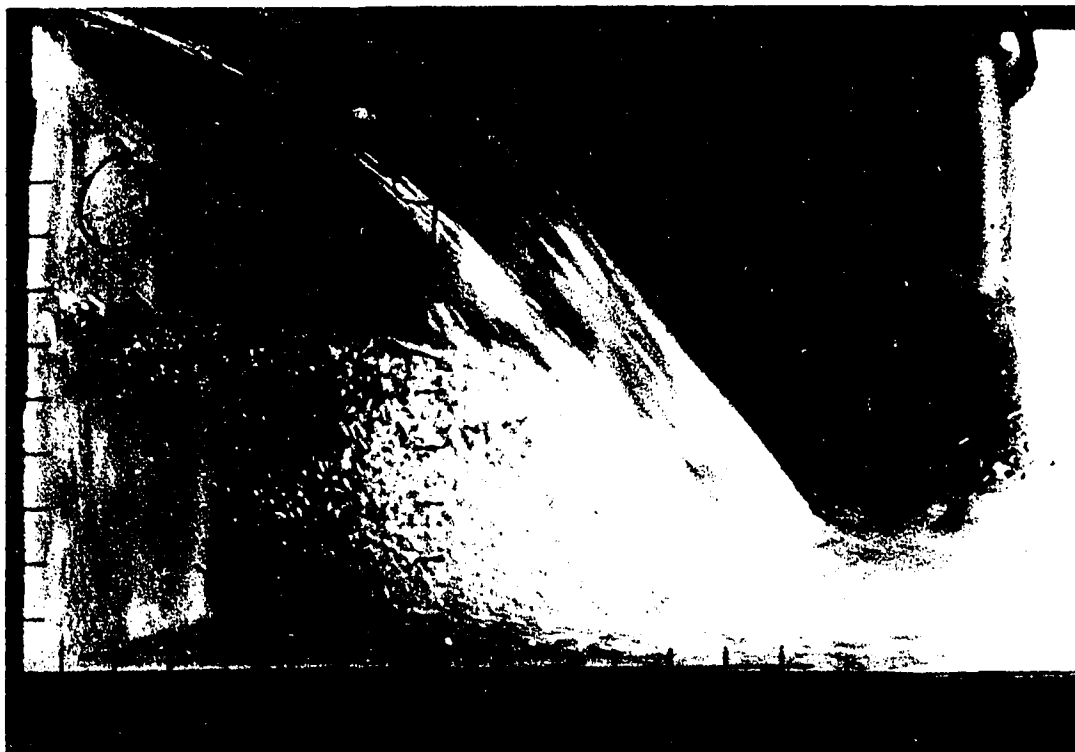
Plate 4.6 Observed flow agitation and air entrainment for model II

Plate 4.7 Observed flow agitation and air entrainment for model III

the pressure difference across the nappe. This flow pattern affected the energy dissipation characteristic of the drop. With the aid of video filming, the mechanism of the surface wave at the pool location was carefully studied. The video film frames were converted into computer figures to track down the water surface fluctuation. Figure 4.4 shows the variation of pool water surface profiles at different times for a discharge of 15.84 L/s for model I.

Besides the photographic work, the flow and the velocity profiles at different locations were also measured. Figure 4.5 shows the results for model II for Y_c/H value of 0.20. The results for other values of Y_c/H are given in Appendix II. From these measurements, some flow parameters like pool height and bed hitting length can be compared to those of previous investigations. The velocity distributions at the base of the models for various Y_c/H are shown in Figures 4.6 to 4.8. By knowing the velocity distributions upstream and at the drop base, the energy loss can be calculated.

A more detailed explanation of nappe oscillation, pool surface wave, air entrainment characteristics, and energy loss mechanism are presented in the following section.

4.5 Analysis

4.5.1 Observations

Except for a brief explanation of air to water momentum transfer presented by Horner (1969), there are no other previous investigations that describes the behavior of air-water mixture in the drop. The flow is complicated by the air entrainment and flow circulation and this hinders any attempt to quantify flow characteristics by measurement. The main

Fig. 4.4 Variation of pool water surface profile at diffirent times
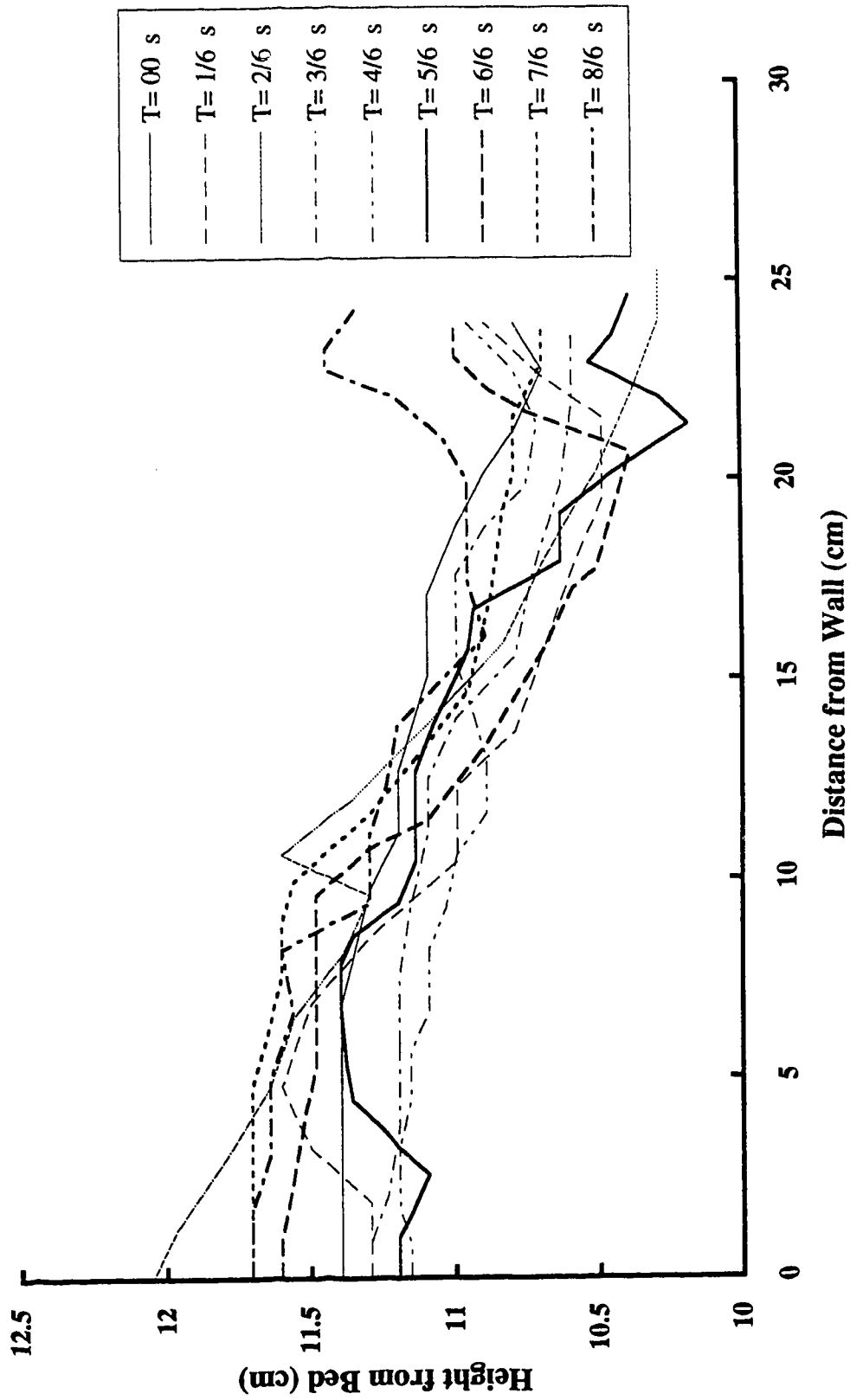
Fig. 4.5 Water and velocity profiles at various locations for Yc/H= 0.20
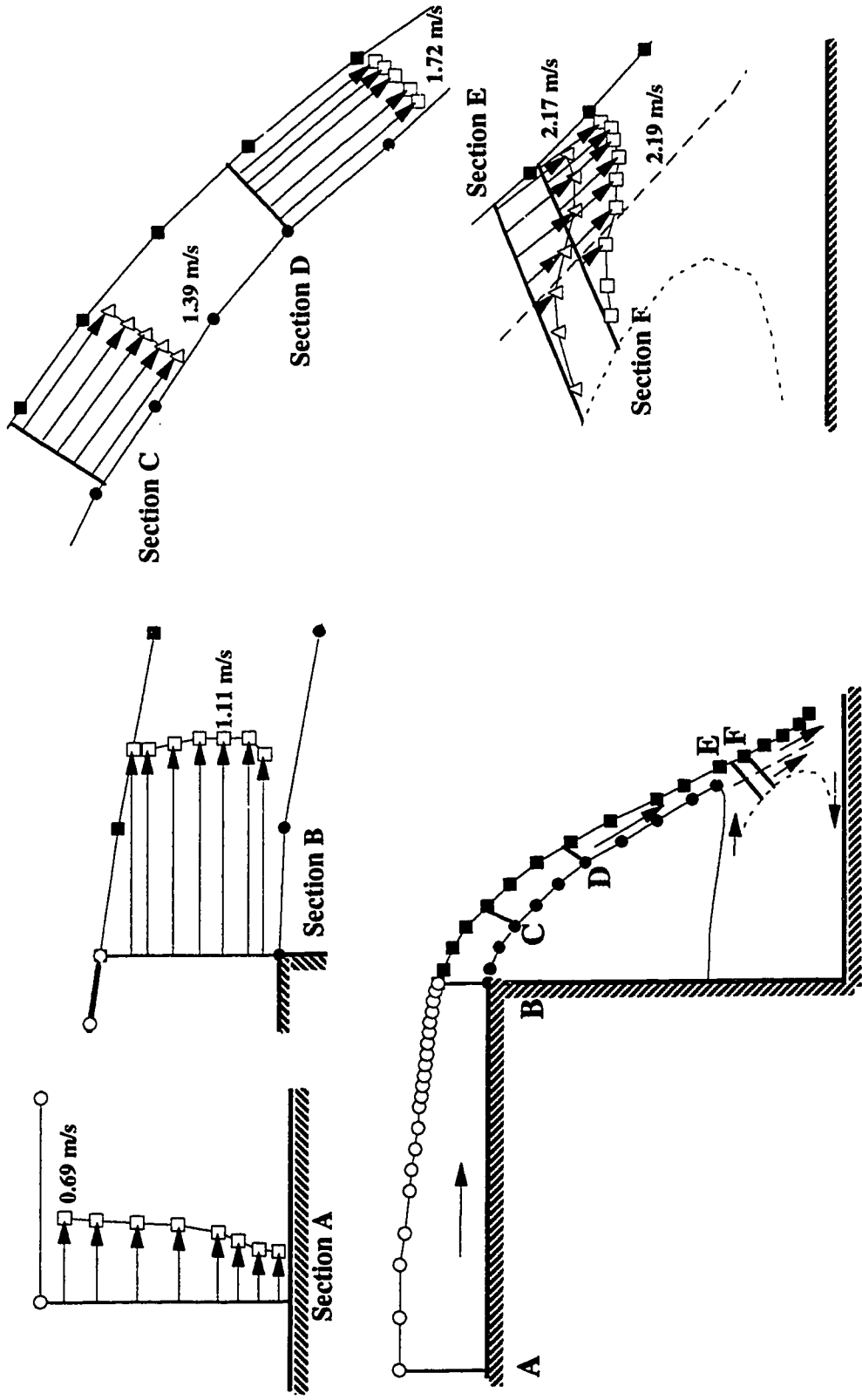
Figure 4.6 Velocity distribution at the base of model I
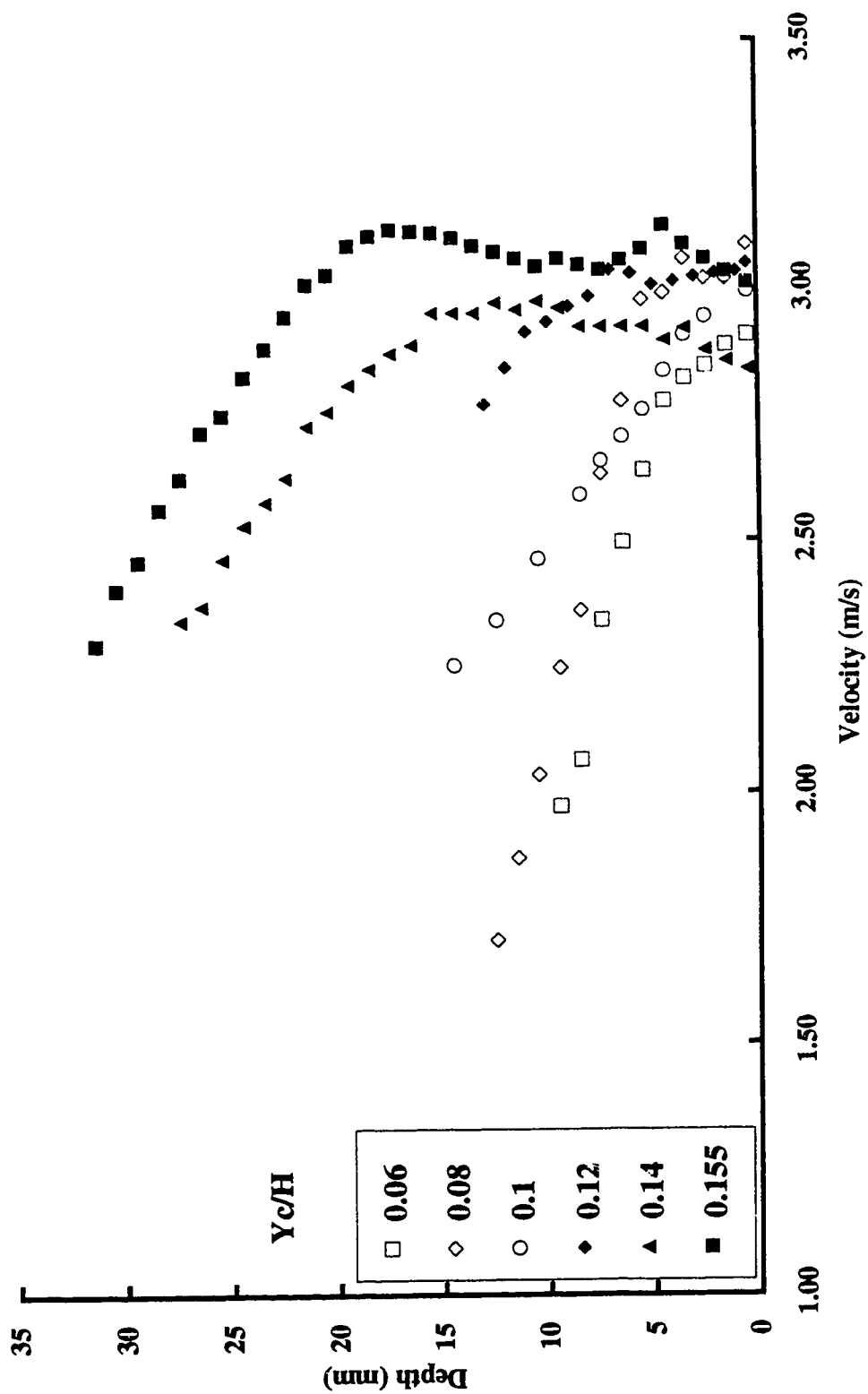
Figure 4.7 Velocity distribution at the base of model II
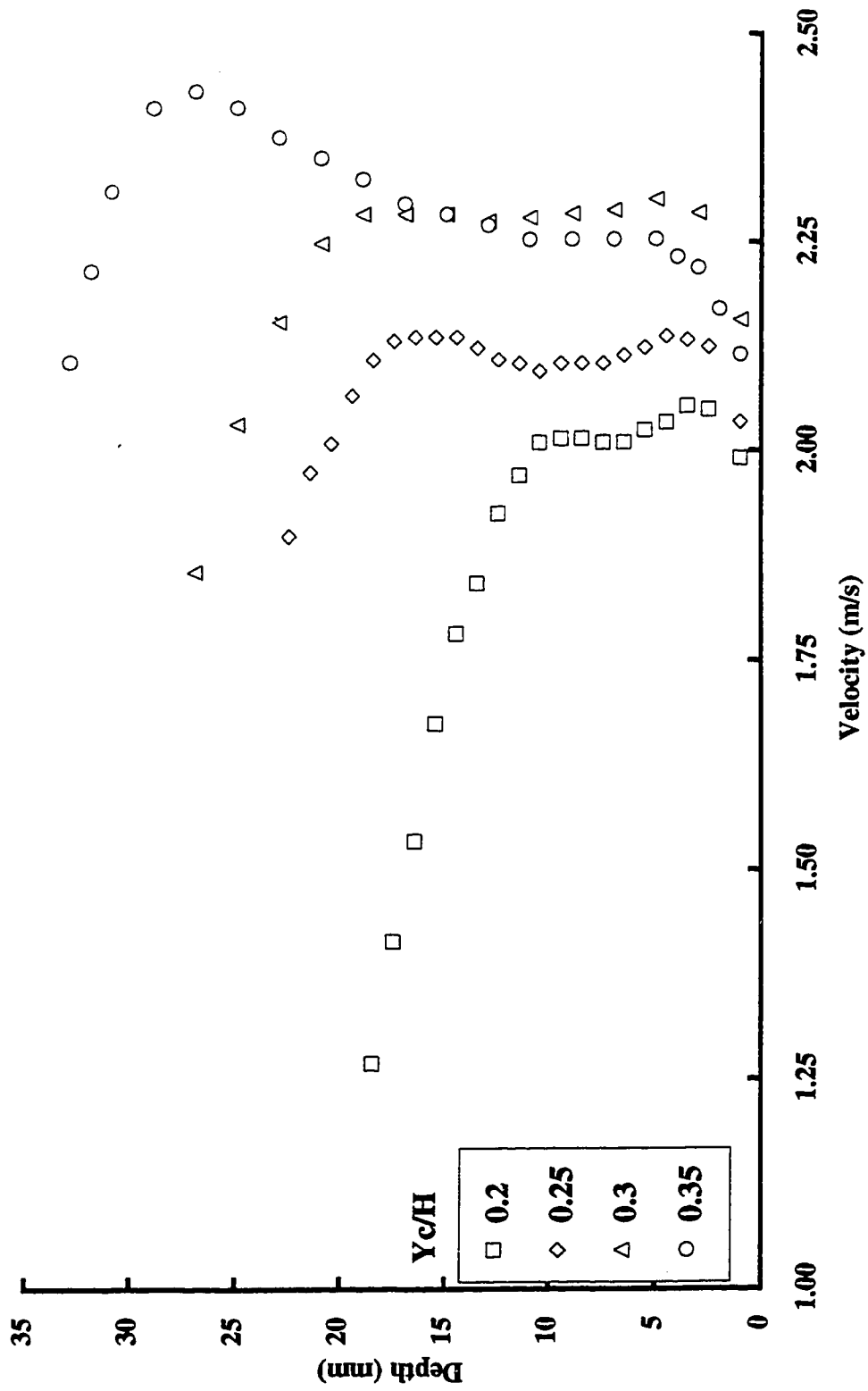
Figure 4.8 Velocity distribution at the base of model III
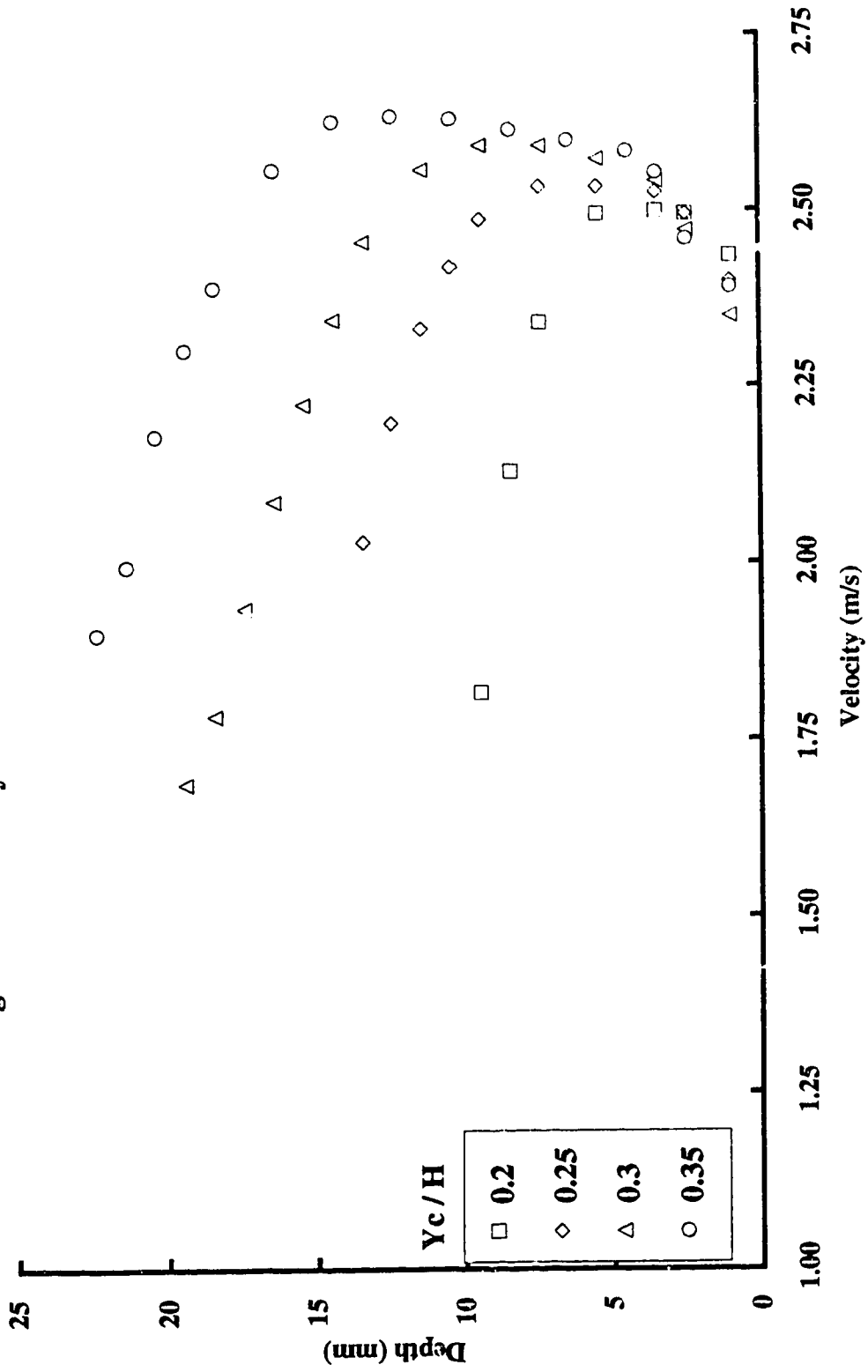
intention of flow observation is to identify some air entrainment and energy dissipation characteristics. Most flow visualization was done at the pool location. With the aid of photographic work, video filming, and dye injection, it will be shown that the presence of pool and nappe oscillation are considered as the major factors in energy dissipation.

At upstream end, the subcritical flow turns supercritical as it approaches the drop. As the flow leaves the drop, the free falling jet with increasing velocity exerts shear forces on the surrounding atmosphere. This shear drives the upper and lower air layers to move along the free falling jet. The nappe oscillation initiated by the pressure difference across the nappe, causes only small amount of air to be entrained into the free falling jet. Horner (1969) argued that the fragmentation of the jet entrained significant amount of air in this region. When the jet reaches the pool surface, the moving lower air layer strikes the pool. The entrained air gyrates in the vortices beside the sliding jet in the form of air bubbles (Plates 4.5 to 4.7). Some of the air bubbles are entrained into the sliding jet while the rest are released into the area behind the free falling jet. Figure 4.9 demonstrates these main features. Close to the bed hitting point, the upper air layer hits the horizontal flow and the flow is again aerated. Beyond this point, the air-water flow releases the air and the flow has a spray-like appearance. This argument is further supported by Horner (1969).

The nappe oscillation was studied by Petrikat (1958) and Schwartz (1963). Some experimental results on the frequencies of nappe oscillation were published by Schwartz (1963). These frequencies were determined with the aid of a stroboscope in the Civil Engineering Laboratory at the University of Witwatersrand, South

94

Figure 4.9. Diagrammatic section showing air entrainment

Air entrained by
nappe oscillation

Air is ejected after
hitting point

Aeration pipe

Air layer strikes and
significant amount is
entrained into the pool

Air is ejected after
rotating in vortices
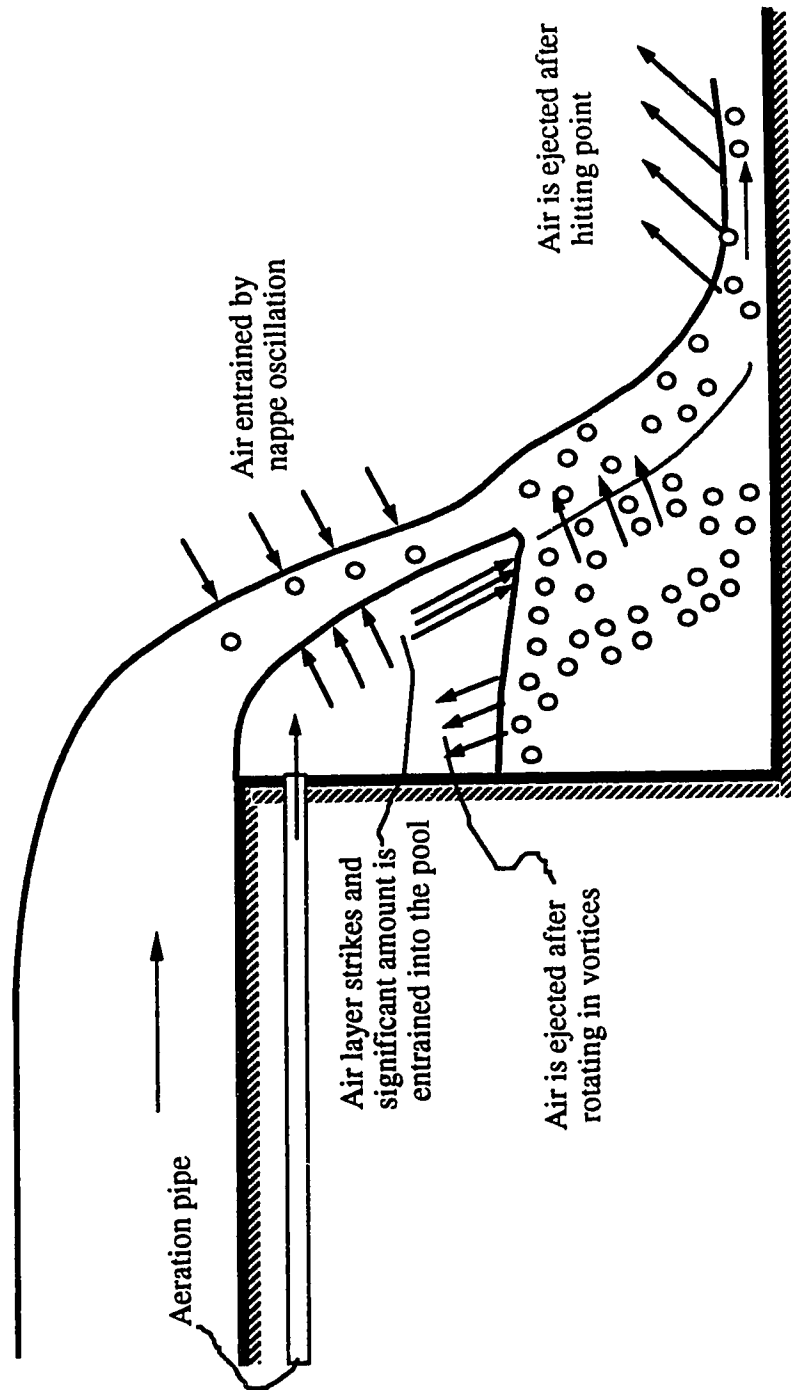
Africa. It was found that the nappe might oscillate at three stable frequencies. These frequencies ranged from six to ten cycles per seconds for fall heights of only three to four feet. Although, there was no intention to measure the frequency of nappe oscillation, in this study, observation of the video film in slow motion gave some estimate of the mean frequencies. Table 4.2 shows the frequencies of nappe oscillation for the three models. The oscillation of nappe results in the undulation

Model	H m	Q L/s	Y_c/H	Period Second	Frequency Cycles/Second
I	0.618	22.13 "	0.1 "	0.122 0.108	8.2 9.2
II	0.25	37.29 " 22.51 " "	0.35 " 0.25 " "	0.143 0.140 0.167 0.150 0.173	7.0 7.1 6.0 6.7 5.8
III	0.25	37.29 " 22.51 "	0.35 " 0.25 "	0.129 0.129 0.150 0.142	7.8 7.8 6.7 7.1

Table 4.2 Nappe oscillation frequencies for various models

of pool surface. It is believed that the pool surface has a downward slope toward the nappe. But, as it will be explained, this slope changes during the undulation of the pool surface. The cause of the nappe oscillation is the entrainment of air by the lower nappe and by the jet impingement into the pool. When air is entrained by the jet, the pressure falls below the atmospheric pressure, forcing the nappe to move

towards the wall. Because the nappe is aerated, the consumed air is replaced, thereby raising the pressure underneath to atmospheric and pushing the nappe forward. This oscillation is perhaps also due to the inertia of the nappe. Schwartz (1963) presented a theoretical solution for nappe trajectory and showed that even a small pressure difference across the nappe affected the nappe appreciably. The frequency of nappe oscillation is also affected by its reaction to pool water surface. As the nappe oscillates backwards in each cycle, it pushes back the pool water mostly at the upper part where the hydrostatic pressure of the pool is insignificant and the surface wave moves toward the wall. This results in the increase of water level at the pool location. When the nappe oscillates forward, the adjacent water layer flows toward the nappe and the water level falls. Figure 4.4 clearly shows how the water surface fluctuates with time. The moving flow strikes the nappe when the latter oscillates backward and might slow down the nappe oscillation. This appears to explain the reason for having different frequencies for a given discharge and fall height. Another important feature of this phenomenon is the energy that is dissipated during the nappe impact with the moving flow. In addition, the air-water mixture is also exchanged at the boundary between the sliding jet and the pool. After the surface wave hits the wall, the reflected wave may strike another incoming wave. This process may continue until the energy of the waves is dissipated and the water level becomes steady.

In spite of the observations from photographic, video, and dye injection methods, the analysis of flow characteristics in the pool is still very difficult. Air entrainment, nappe oscillation, and vortices are occurring simultaneously and can not be studied separately. However, a

close visualization of the flow in the pool reveals some important features of flow patterns. Figure 4.10 shows the general pattern of flow observed in the pool. The sliding jet exerts some shear on the pool and starts the vortex A. The size of vortex A depends on the pool height and
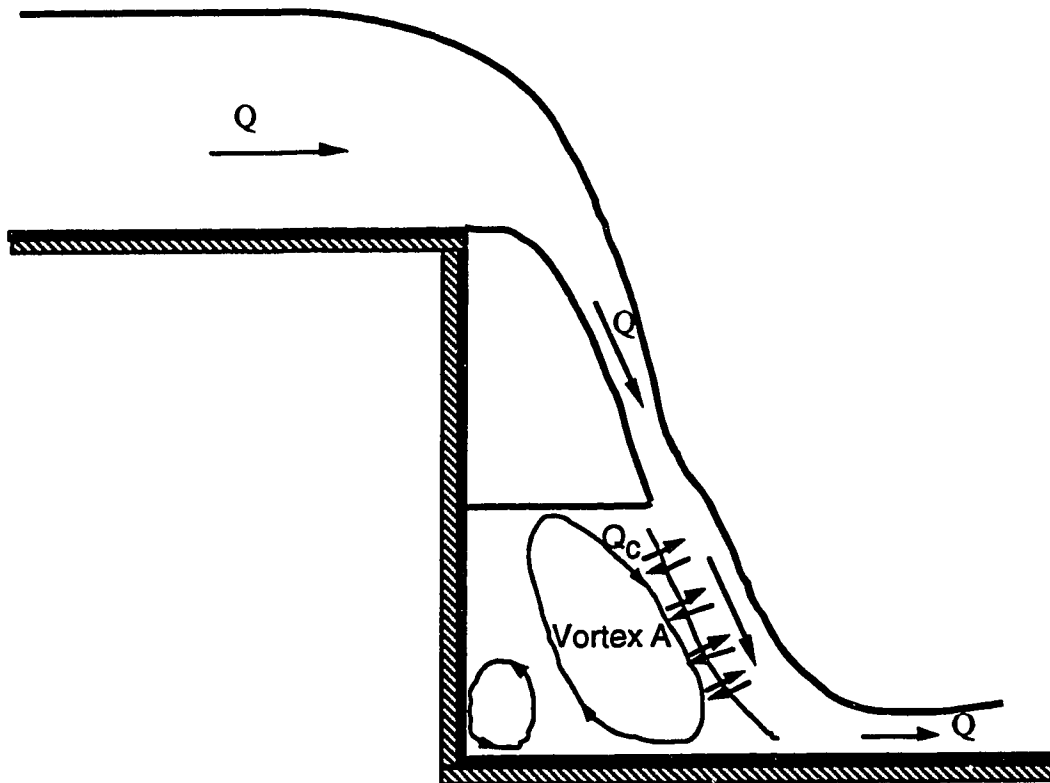
Figure 4.10 Diagrammatic section through the general flow patterns observed in the drop

hence, on the discharge. For all runs, the boundary between the sliding jet and the vortex is specified in Appendix I. It was noticed that the upper part of the sliding jet was approximately straight up to the inflection point where the curvature of the jet changes. It is believed that the flow is only interchanged between the sliding jet and the pool in

the upper part and near the bed. The use of dye injection reveals that flow is exchanged along the boundary, but at an insignificant rate. However, it was not possible to measure the interchanging discharge. The nappe oscillation plays a major factor in this phenomenon.

Finally, it must be borne in mind that the methods of observation, used in this study, may not reveal all aspects of flow patterns and better techniques are needed to improve the visualization and confirm some of the ideas presented herein.

4.5.2. Flow Analysis

4.5.2.1. Energy Loss at the Base of the Drop and Plane Jet

The downstream flow remains supercritical, so the energy loss can be easily studied because it is unaffected by any downstream disturbance. The relative energy loss ΔE is expressed as

$$\frac{\Delta E}{E_0} = \frac{E_0 - E_1}{E_0} = 1 - \frac{E_1}{E_0} \qquad (4.1)$$

where E_0 and E_1 are the specific energies upstream and at the base of the drop or the plane jet, respectively.

E_0 can be approximated by the following relation

$$E_0 = H + 1.5 Y_c \qquad (4.2)$$

Since the upstream velocity distribution was carefully measured, it is recommended that E_0 be evaluated by the relation

$$E_0 = H + Y_0 + \frac{\sum v_0^3 \, \Delta A}{2g \sum v_0 \, \Delta A} \tag{4.3}$$

where:

Y_0 is the upstream depth of flow

v_0 is the upstream point velocity

ΔA is the area element

E_1 can be determined from either method using the velocity or the depth of flow at the base:

$$E_1 = Y_1 + \frac{\sum v_1^3 \, \Delta A}{2g \sum v_1 \, \Delta A} \tag{4.4}$$

$$E_1 = Y_1 + \frac{Y_c^3}{2Y_1^2} \tag{4.5}$$

where v_1 is the average point velocity at the base associated with area element ΔA and Y_1 is the flow depth at the base. It should be noted that Equation (4.5) is very sensitive to the value of Y_1 used. The thin and spray-like flow at the base prevents the accurate measurement of Y_1. In addition, Equation (4.5) is based on the uniformity of flow. The velocity measurement at the base revealed that the velocity distribution is not uniform, so Equation (4.4) is used to evaluate the downstream energy.

Figure 4.11 shows the variation of the energy loss for the drop and plane jet along with the data of Moore (1943) and Rand (1955) for the drop. Equation (4.2) has to be used to evaluate the upstream energy

Figure 4.11 Variation of energy loss for the drop and the plane jet
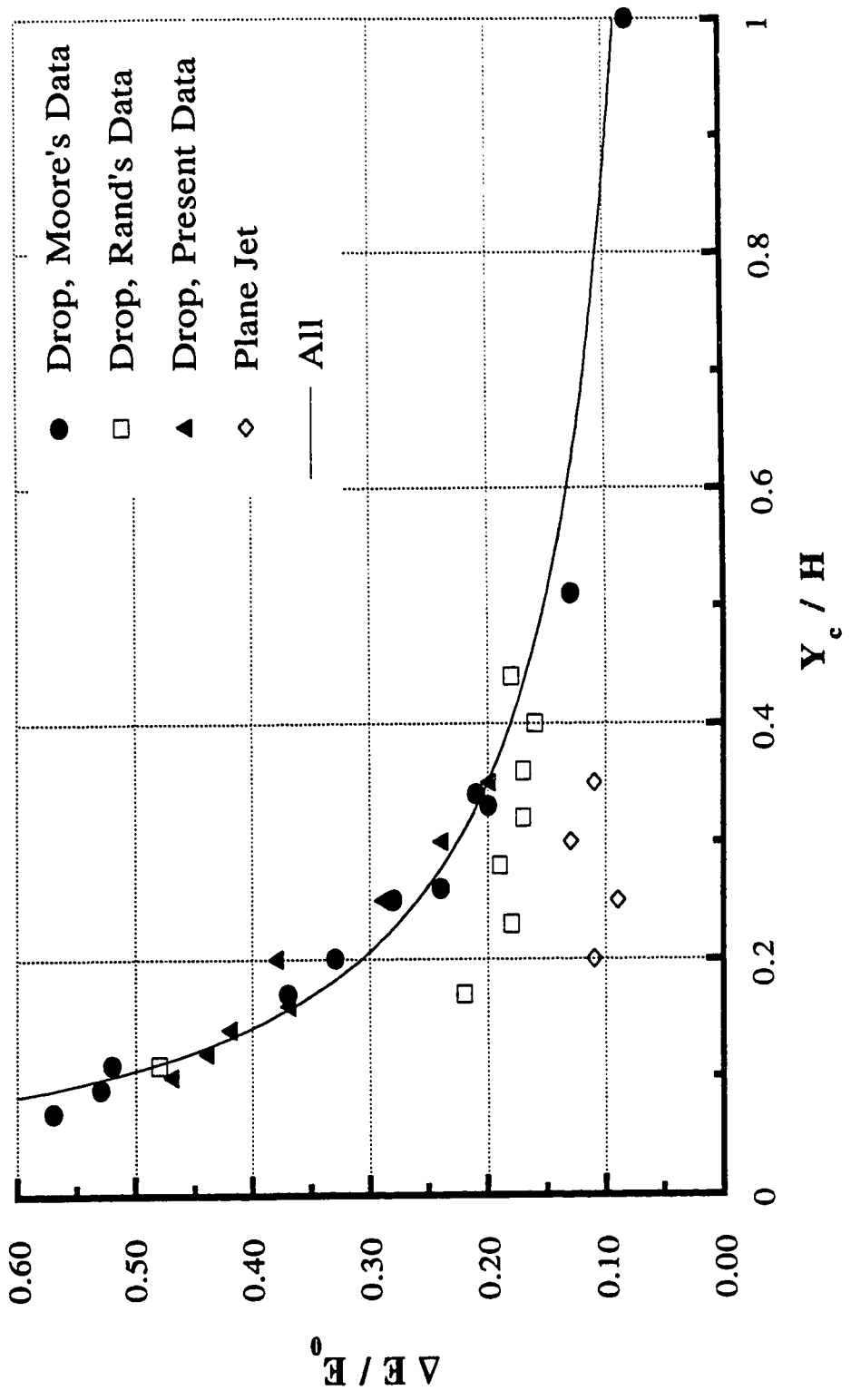
for the data of Moore and Rand. Equation (4.5), based on depth measurement, is used to evaluate E_1 for Rand's data. The discrepancy in Rand's data supports the previous argument about evaluating E_1 from Equation (4.5). Although measurements were only taken on the centerline, the experimental results for the drop agree well with the Moore careful observations. A study of Figure 4.11 shows that $\Delta E/E_0$ for the drop decreases from a relatively large value of about 0.52 for Y_c/H equal to 0.10 to about 0.17 for Y_c/H approximately equal to 0.50. It was found that the variation of $\Delta E/E_0$ with Y_c/H is well described by the equation

$$\frac{\Delta E}{E_0} = 0.0896 \left(\frac{Y_c}{H} \right)^{-0.766} \tag{4.6}$$

The correlation factor for the above relation is 0.970.

It seems that for the plane jet, the energy loss is not sensitive to the changes in Y_c/H. The energy loss varies from 0.09 to 0.13 for the plane jet. This argument supports the idea that the pool beneath the jet contributes to energy loss at the base of the drop.

4.5.2.2. Pool Depth and Length, Y_p & L_p

The geometry of the pool beneath the jet is easily influenced by the aeration system. If the jet is not aerated, the pressure in the area behind the jet falls below the atmosphere and the water level of the pool rises until it reaches the brink. In this investigation, the jet was well aerated, so the pool depth and length were unaffected.

It is known that the pool depth is always greater than the water

depth in the downstream channel. This considerable difference in water level stems from the change of horizontal momentum of the sliding jet as it is deflected at the bottom. The pool depth and length can be made dimensionless by the drop height and hereafter called the pool depth ratio, D_r, and pool length ratio, L_r Rand (1955) suggested the following empirical relation for D_r based on his experimental data and the results of Moore (1943)

$$D_r = \left(\frac{Y_c}{H}\right)^{0.66} \tag{4.7}$$

Figure 4.12 shows the variation of D_r and L_r against Y_c/H along with the data of Moore and Rand. Equation (4.7) is also plotted to be compared with the data. It is seen that D_r and L_r vary mainly with Y_c/H and increase continuously with Y_c/H, with the maximum value of Y_c/H equal to 1. At this value, the pool depth reaches the brink and the area behind the jet is filled with water. The following relation established for D_r gives a better correlation for most of the data,

$$D_r = 1.107 \left(\frac{Y_c}{H}\right)^{0.719} \tag{4.8}$$

The correlation factor for the above relation is 0.995. A power equation for L_r obtained in terms of Y_c/H reveals the following relation with a correlation factor of 0.981

$$L_r = 2.47 \left(\frac{Y_c}{H}\right)^{0.621} \tag{4.9}$$

Fig. 4.12 Variation of pool depth and length ratio with drop ratio
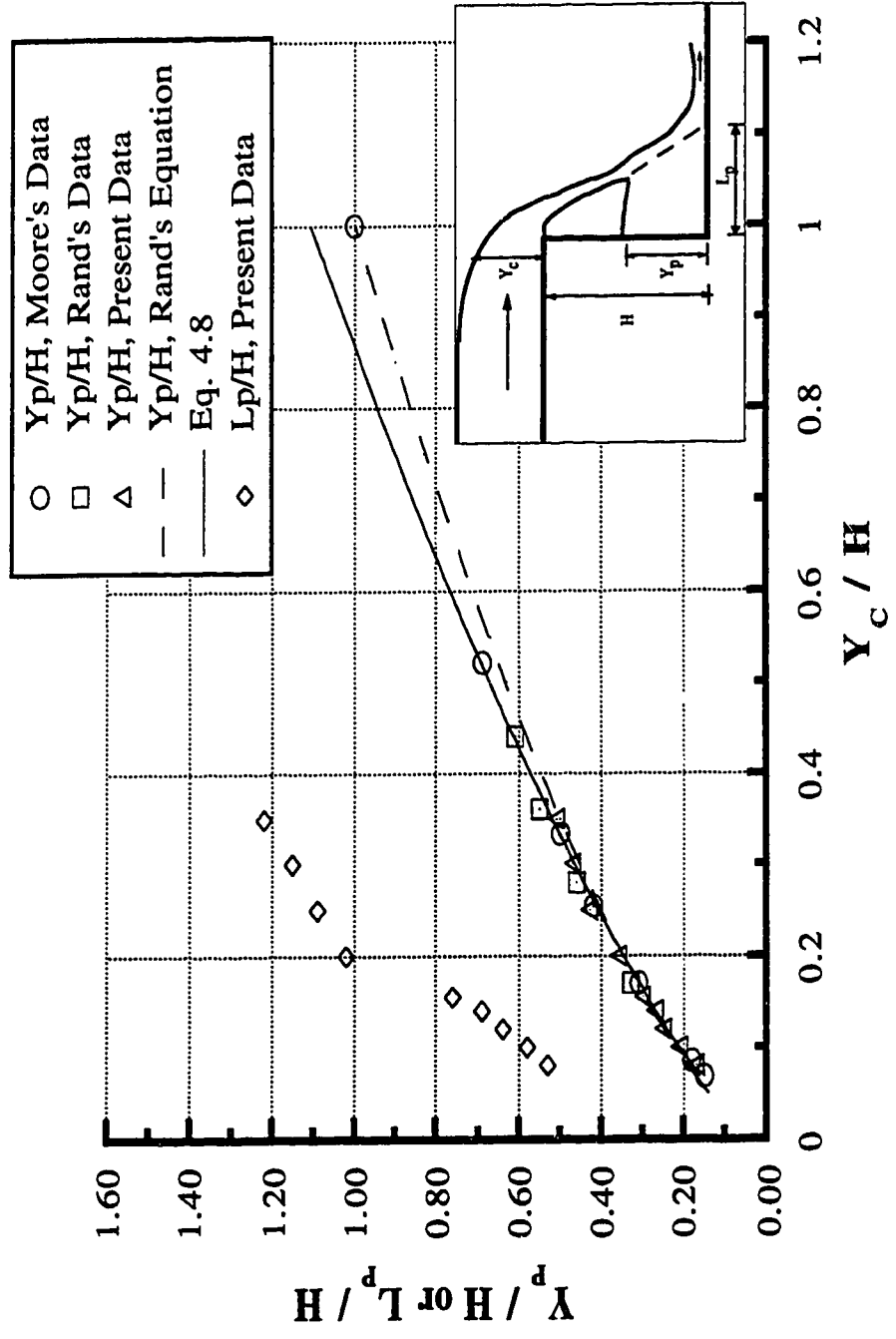
Later in this chapter, an attempt is made to evaluate D_r analytically by applying the momentum equation.

4.5.2.3. Circulating Discharge Q_c

There has been no previous attempt to measure the circulating discharge in the pool. The presence of nappe oscillation, air entrainment and vortices, makes it difficult to obtain any data regarding the circulating flow. The circulating flow is affected by the mechanism of nappe oscillation responsible for flow exchange between the circulating discharge and sliding jet. This flow behavior is clearly described in section 4.5.1. There are a lot of air bubbles in the pool. They get entrained into the Prandtl tube and make velocity measurements difficult. This was overcome by using a very small tube. Vortices also produce lateral currents which impinge on the static holes of the tube, thereby affecting the accuracy of the measurement.

Despite these difficulties, the velocity distribution of the circulating flow was measured and it is shown in Appendix II. The total discharge Q is used to make Q_c dimensionless and it is called the circulating discharge ratio, Q_r:

$$Q_r = \frac{Q_c}{Q} \tag{4.10}$$

Figure 4.13 shows the resulting relationship between Q_r and Y_c/H. The variation of the dimensionless backwater discharge ratio Q_{br} for the plane jet is also shown in Figure 4.13 for comparison. A study of Figure 4.13 shows that Q_r can be as large as 0.60 for Y_c/H

Fig. 4.13 Relationship established for circulating and backwater discharge ratio
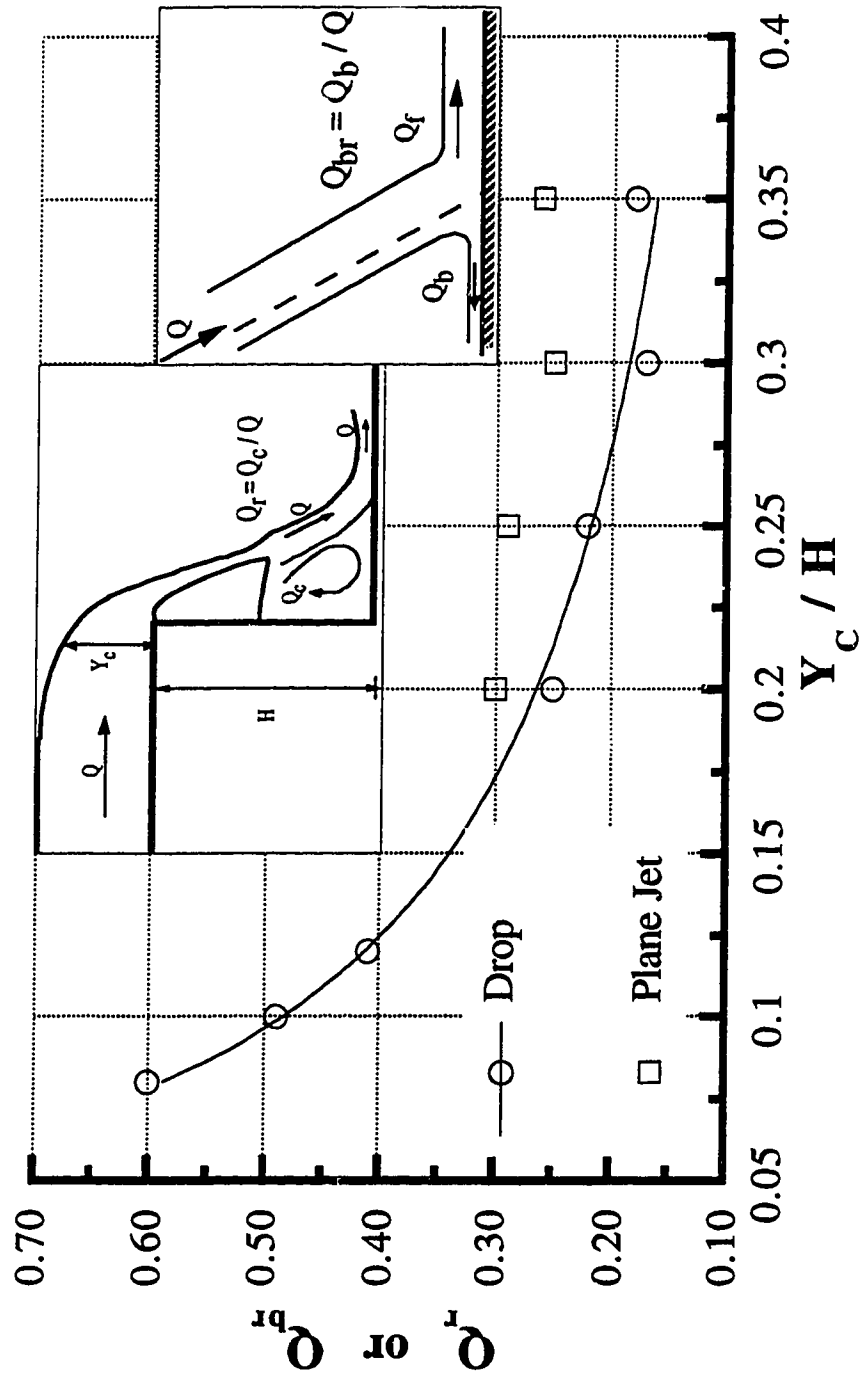
equal to about 0.06 and decreases as Y_c/H increases. It is reasonable to assume that the dissipated energy in the drop is proportional to the energy of the circulating flow. So, the reduction trend in the reduction of the energy loss with the increase in Y_c/H is anticipated for Q_r. It is also found that the variation of Q_r with Y_c/H is well described by the equation

$$Q_r = 0.065 \left(\frac{Y_c}{H}\right)^{-0.872}$$

(4.11)

The correlation factor is 0.998 for the above equation.

It is seen that the value of Q_{br} is greater than the value of Q_r for a given value of Y_c/H between 0.20 to 0.35. In this range, Q_{br} remains almost invariant.

4.5.2.4. Theoretical Approach to Flow Characteristics of the Drop

Figure 4.14 shows a drop with all the necessary parameters. It was indicated that the circulating flow slows down the increase in velocity of the sliding jet.

To simplify the analysis, the following assumptions are made:

(i)   The upstream flow approaches the drop structure at critical depth.

(ii)   The approaching flow is assumed to have a uniform velocity distribution and hydrostatic pressure at the critical section.

(iii) The energy loss and bed shear force between the critical section and the brink of the drop structure are ignored. This assumption is not far from the actual condition because the distance between these two sections is relatively small.
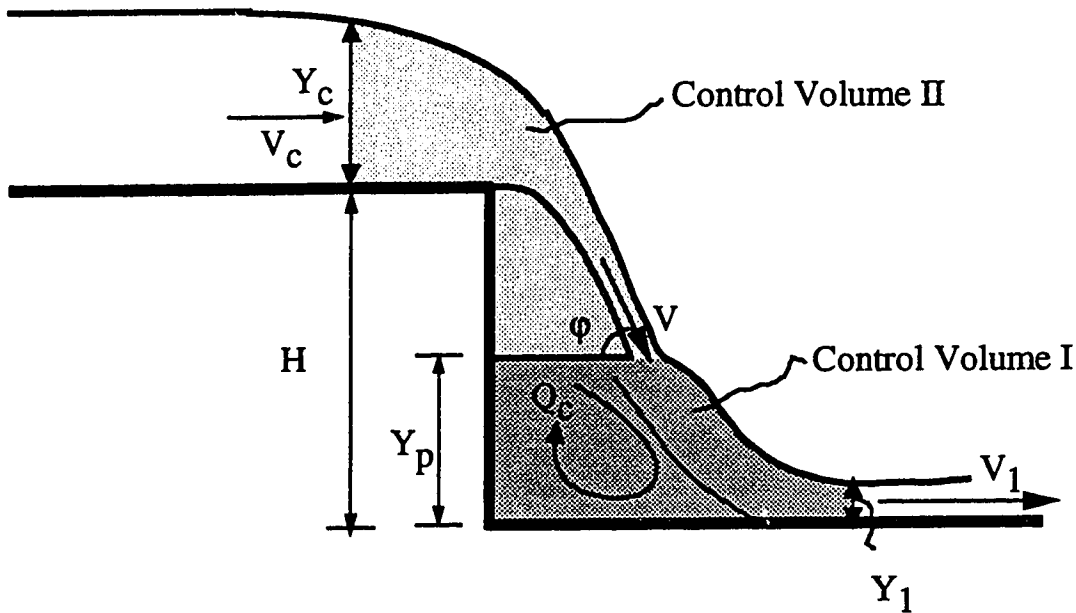
Figure 4.14 Sketch of a drop showing parameters and control volumes for the analysis

(iv)   The effect of air entrainment on flow characteristics is ignored.

(v)   The bed shear force at the base of the drop is also ignored.

The three basic equations of momentum, energy, and continuity are applied to assess the flow characteristics of the drop. Referring to Figure 4.14, the momentum equation in the horizontal direction for the control volume I gives

$$\rho q V \cos \varphi + \frac{1}{2}\gamma Y_p^2 = \rho q V_1 + \frac{1}{2}\gamma Y_1^2 \qquad (4.12)$$

The horizontal momentum and energy relations for the control volume II provide the following equations

$$\frac{1}{2}\gamma Y_c^2 + \rho q V_c = \rho q V \cos \varphi \qquad (4.13)$$

$$H + \frac{3}{2}Y_c = \frac{V^2}{2g} + Y_p \qquad (4.14)$$

The last relation is the continuity equation which reduces to

$$q = Y_c\sqrt{gY_c} \qquad (4.15)$$

For this set of equations, five unknowns V, $\cos\varphi$, Y_p, V_1, and Y_1 exist while only four equations are available. There are two suggestions to develop the required fifth equation. Firstly, it is convenient to use an empirical equation that relates one of the unknown parameters to a known factor. This method is then referred to (for convenience) as the Semi-Empirical theory. Equation (4.7) is used as the complementary equation that gives the relation for the pool depth. The second method is to apply Equation (3.5) from White's theory, referred to as the Modified theory. As pointed out earlier, White assumed that Q_r is approximately equal to Q_{rb} and the velocity distribution across the sliding jet and the circulating flow is uniform. Although the measurements show that this assumption is far from the actual condition, this assumption is reasonable for predicting the circulating discharge ratio.

The five simultaneous non-linear equations can now be solved to determine the hydraulic characteristics of the drop. The results of such computation are given in Table 4.3 for a wide range of Y_c/H from 0.08 to 1. The results from the present experimental study are also given in Table 4.3 for comparison. Figures 4.15 and 4.16 show the variation of jet inclination at the pool level φ and the energy loss, respectively,

Table 4.3 Comparison between calculated and experimental values

Y_c/H	Y_1/H Present Experiment	Y_1/H Semi-Empirical	Y_1/H Modified	$cos\,\varphi$ Present Experiment	$cos\,\varphi$ Semi-Empirical	$cos\,\varphi$ Modified	Y_p/H Present Experiment	Y_p/H Semi-Empirical	Y_p/H Modified	$V_1(m/s)$ Present Experiment	$V_1(m/s)$ Semi-Empirical	$V_1(m/s)$ Modified
0.06	0.017	0.013	0.017	-	74.5	74.7	-	0.15	0.12	2.45	2.69	2.16
0.08	0.023	0.020	0.025	72	72.0	72.3	0.17	0.18	0.15	2.47	2.79	2.24
0.1	0.026	0.027	0.034	71	69.8	70.2	0.21	0.21	0.17	2.55	2.88	2.30
0.12	0.038	0.035	0.043	69	67.7	68.3	0.25	0.24	0.20	2.63	2.96	2.37
0.14	0.047	0.042	0.053	67	65.9	66.6	0.27	0.27	0.22	2.75	3.04	2.43
0.155	0.053	0.048	0.061	66	64.6	65.4	0.30	0.29	0.23	2.88	3.10	2.47
0.165	0.057	0.053	0.066	64	63.7	64.6	-	0.30	0.24	2.82	3.14	2.50
0.2	0.078	0.068	0.085	60	60.9	62.1	0.36	0.35	0.27	1.86	2.07	1.65
0.25	0.094	0.090	0.113	57	57.4	59.0	0.43	0.41	0.32	2.09	2.17	1.73
0.3	0.116	0.114	0.143	53	54.2	56.3	0.47	0.47	0.36	2.20	2.26	1.80
0.35	0.140	0.139	0.173	51.5	51.3	53.8	0.51	0.52	0.40	2.29	2.34	1.87

Figure 4.15 Variation of jet inclination at pool surface
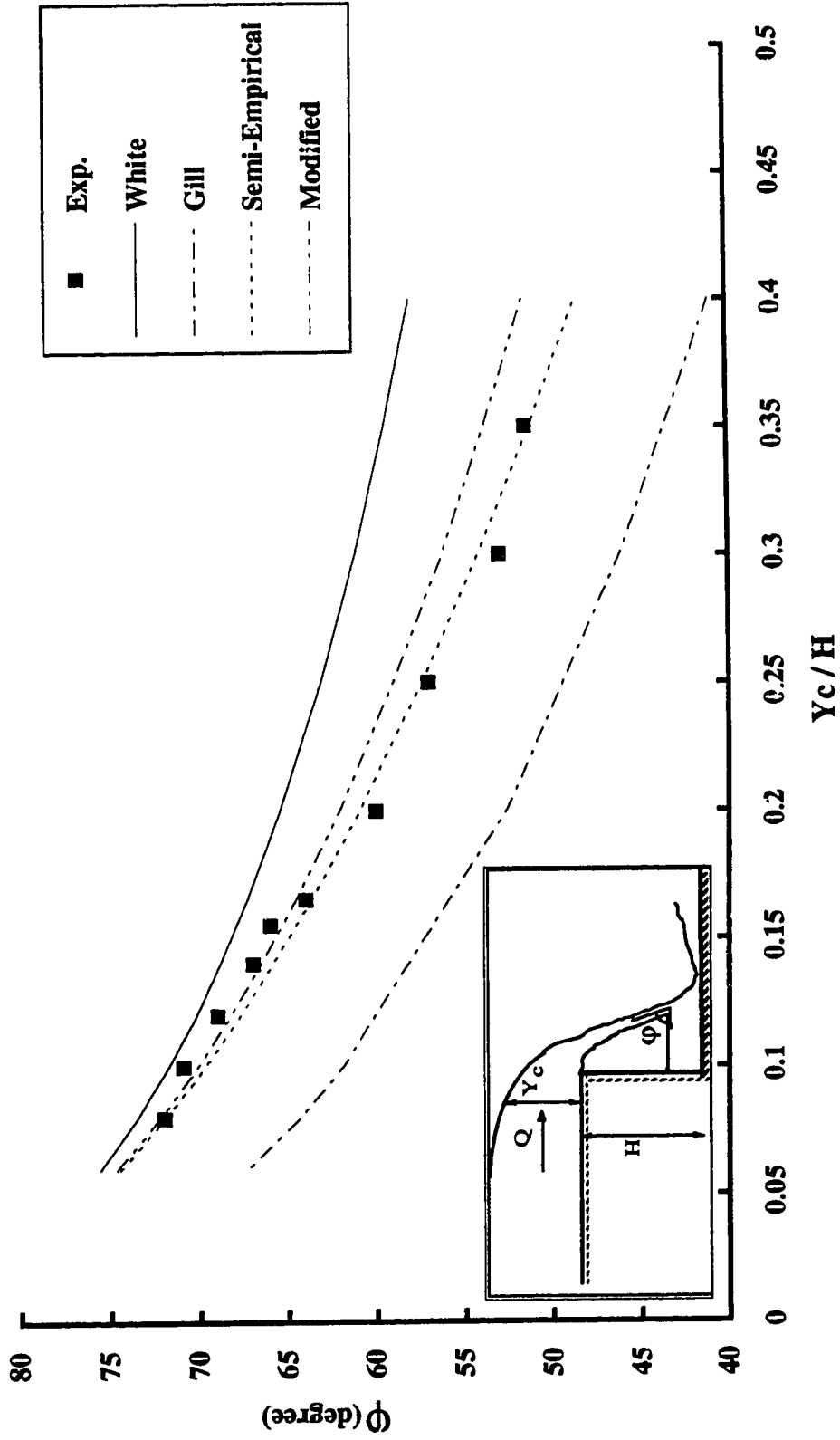
Figure 4.16 Variation of the relative energy loss at the base of the drop
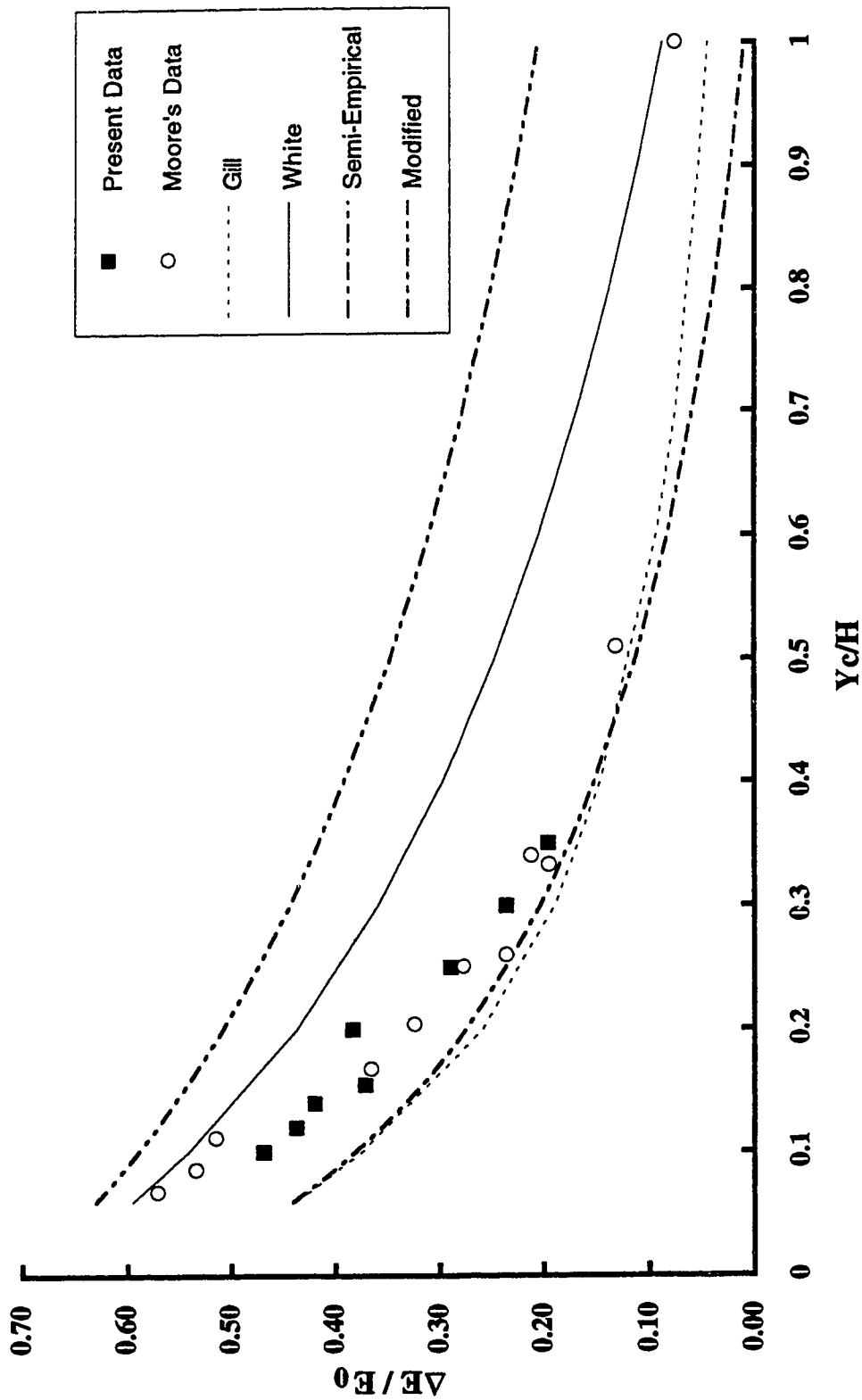
for the present experiment and Moore's data. In addition, the theoretical results from Gill, White, Semi-Empirical, and Modified methods are also presented for comparison.

It can be noted that in the modified theory, the values of Y_1/H are always greater than those of the experimental data. The difference between the values of Y_1/H using the Semi-Empirical theory and the observed data is smaller than that of the Modified theory and the observed data. The computed values of Y_p/H by Modified theory are consistently lower than the corresponding values from experiments. This difference becomes appreciable at higher values of Y_c/H. In this case, the observed data are very close to predictions from the Semi-Empirical theory.

As it is seen in Figure 4.15, White's theory always overestimated while Gill's theory significantly underestimated the values of φ. For a range of Y_c/H from 0.08 to 0.16, predicted results from the Modified theory are closest to the observed data while in the remaining range, predictions from the Semi-Empirical method agree very well with the observed data. In general, predictions from the Semi-Empirical theory have been shown to be in much better agreement with the experimental data.

Figure 4.16 shows that the computed values of the energy loss by Gill's theory are very close to those of the Semi-Empirical method. In a range of Y_c/H from 0.08 to 1, the experimental data are located between the values calculated by the Semi-Empirical and White's theories. The Modified theory does not predict the energy loss well. The estimated values using this theory are significantly and consistently greater than the observed data.

It is reasonable to assume that Q_r would be proportional to the relative energy loss. The energy source for flow circulation in the pool is only provided by the sliding jet. So, the energy dissipated in the drop is consumed by the circulating flow- that is

$$\frac{\Delta E}{E_0} \approx Q_r \qquad (4.16)$$

Figure 4.17 shows the consolidated results of Q_r and $\Delta E/E_0$ along with the theoretical curve of Q_r obtained from the Modified theory. A study of Figure 4.17 shows that the values of $\Delta E/E_0$ are greater than those of Q_r, indicating that the circulating flow consumes only a part (which is rather significant) of the energy dissipated in the drop. This indicates that another factor contributes to the energy loss. This supports the idea that the oscillating jet impact on the pool surface could dissipate some energy. This phenomenon is well described in section 4.5.1. The Modified theory overestimated the value of Q_r, but it has a good agreement with the values of $\Delta E/E_0$. It seems that the difference between the experimental and theoretical values of Q_r is somewhat balanced for the contribution of nappe impact to the energy dissipation. Therefore, Equation (4.16) gives a good estimate for $\Delta E/E_0$ if Q_r is calculated by the Modified theory. There is no parameteric solution for Equation (4.16). However, if Equation (3.4) from White's theory is combined with the Semi-Empirical theory, the parameteric solution for Equation (4.16) produces the following relation

Figure 4.17 Relationships established for the relative energy loss based on the circulating discharge ratio
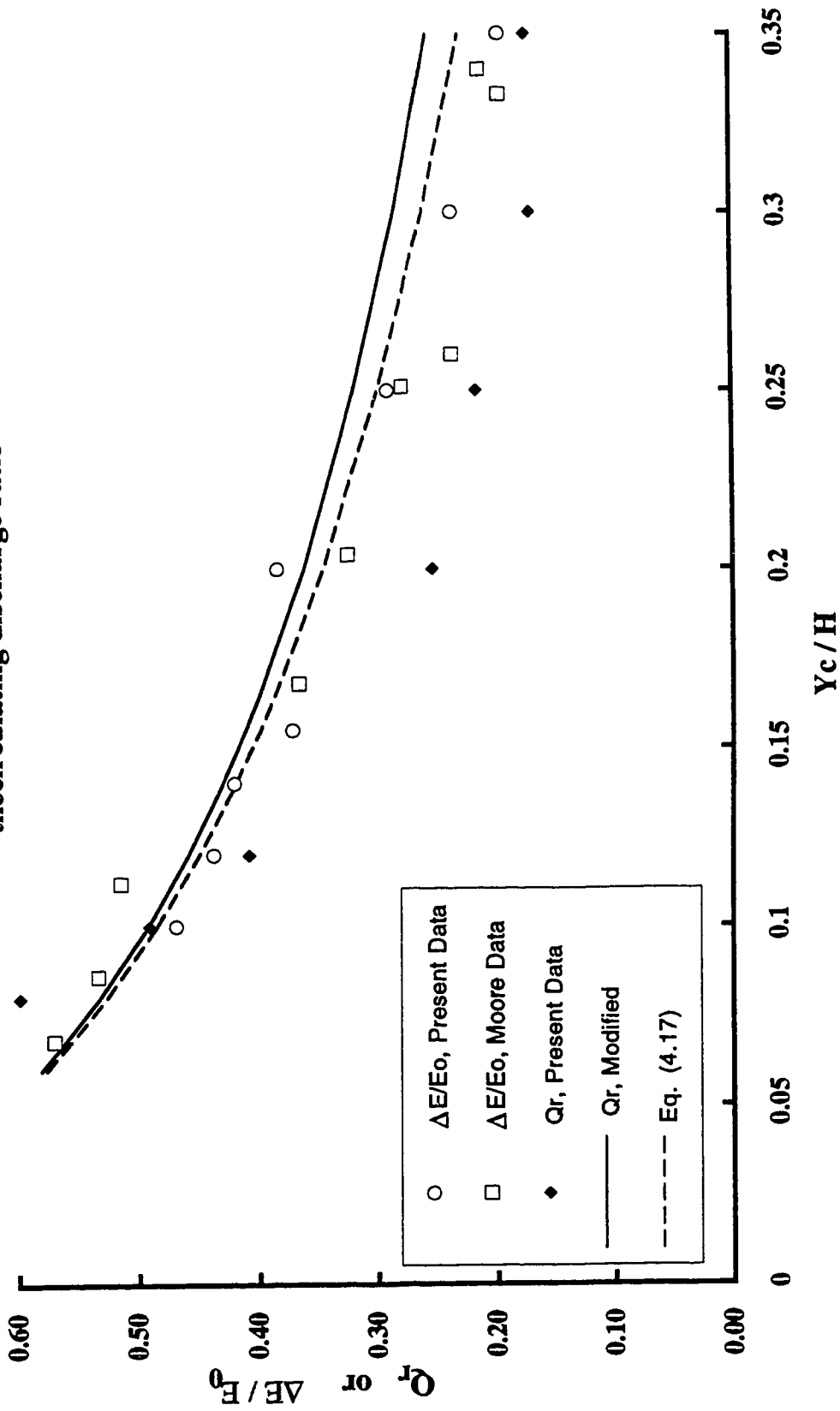
$$\frac{\Delta E}{E_0} = \frac{A - B}{A + B} \qquad\qquad (4.17)$$

where:

$$A = \sqrt{2\left(1 + 1.5(Y_c/H) - 1.107(Y_c/H)^{0.719}\right)} \qquad (4.18.a)$$

$$B = \sqrt{1.5(Y_c/H)} \qquad\qquad (4.18.b)$$

Figure 4.17 shows that the relative energy loss calculated by Equation (4.17) gives a much better agreement than the Modified method with the observe data. In addition, energy loss can be easily calculated from Equation (4.17) whereas it has to be determined numerically for the Modified method.

Finally, it must be borne in mind that Equation (4.17) should not be extended to conditions outside those that were mentioned. Although, the method of analysis appears crude in some parts, the final results show practical and useful relationships to estimate the flow characteristics of the drop.

Chapter 5

CONCLUSIONS

5.1. Jet Flow on Stepped Spillways

1. The experimental results of Horner (1969) were used to estimate the energy loss on a stepped spillway in the jet flow regime, where the flow impinges on the treads of steps. The upstream flow was subcritical and approaches the spillway at critical depth. Both horizontal and inclined step configurations were included in this investigation.

2. The earlier investigation by Horner (1969) revealed that the remaining energy at the base of a stepped spillway does not depend on the number of steps N. This misleading conclusion is in contrast to the nature of this type of flow and experimental results.

3. The energy loss in jet flow regime appears to be mainly due to the jet circulation in the pool beneath the nappe. The formation of a partial hydraulic jump on every step is considered as the secondary factor in energy dissipation.

4. It was also possible to develop an asymptotic expression to show that energy loss in jet flow regime could be significant, especially with a large number of steps; for the case of thirty steps, $H/L = 0.421$, and Y_c/H approximately equal to 0.3, the relative energy loss was 0.97.

5. The idea of assessing the proportion of energy lost per step α was shown to be useful for analysis. It was found that α varied with Y_c/H and H/L. Equations have been developed to estimate α for horizontal and inclined steps.

6. The boundary between jet flow and skimming flow appears to vary from $Y_c/H=$ 0.78 to 0.83. It was taken as 0.80 for further analysis.

7. The energy dissipated on a stepped spillway in jet flow regime for maximum discharge with horizontal steps was found to be a function of H/L and N. A generalized equation has been developed to describe this variation.

5.2. Jet Flow on Drops

1. Some flow patterns of a drop or free overfall are evaluated by model study. The mechanism of energy dissipation is carefully studied with the aid of measurements and observations. The plane jet model is also carried out because of its similarity to the drop condition.

2. The flow visualization observations revealed that the nappe oscillation is an important factor in the flow exchanging process between the sliding jet and the circulating discharge. The nappe oscillates because of the pressure difference across the jet. During the oscillation process, the jet impact on the pool surface might dissipate some energy.

3. The energy loss at the base of the drop is not constant and varies mainly with Y_c/H. An empirical equation is derived to estimate the relative energy loss based on the present investigation and Moore's data. The relative energy loss at the base of the plane jet is approximately constant and is about 11%.

4. The pool depth, resulting from the change of momentum of the deflected jet, is appreciably greater than the depth downstream. Empirical relationships are derived to evaluate the pool depth using the present data as well as those of Rand and Moore.

5. The velocity distributions in the sliding jet and the circulating flow are not uniform and decrease continuously toward the pool. This is a good indication that the shear force acting between the sliding jet and circulating flow may be considered as a main factor in energy dissipation. An equation is introduced to determine the variation of circulating discharge with Y_c/H.

6. It has been possible to measure the circulating discharge and study its variation with the main parameters of the drop.

7. The momentum, energy, and continuity principles are applied to determine some flow characteristics of the drop. The analytical solution shows satisfactory results when compared to predictions from other theories and observed data.

REFERENCES

Blaisdell, F. W., "Equation of the Free Falling nappe". Proceedings, ASCE, Vol. 80, Paper No. 482, 1954.

Diez-Cascon, J., Blanco, J. L., Revilla, J., "Studies on the Hydraulic Behavior of Stepped Spillways". Journal of International Water Power and Dam Construction, Vol. 43, No. 9, 1991, pp 22-26.

Frizell, K. L., "Stepped Spillway Design with a RCC Dam". Proceedings, National Conference on Hydraulic Engineering, 1987, pp 122-127.

Frizell, K. H., "Stepped Spillway Design for Flow over Embankments". Proceedings, National Conference on Hydraulic Engineering, 1991, pp 118- 123.

Frizell, K. H., "Hydraulics of Stepped Spillways for RCC Dams and Dam Rehabilitations". Proceedings, Roller Compacted Concrete III, 1992, pp 423-439.

Gausmann, Madden, "Experiments with Models of Gilboa Dam". Transactions, ASCE, Vol. 86, 1923, pp

Gill, M. A., "Hydraulics of Rectangular Vertical Drop Structures". Journal of Hydraulic Research, Vol. 17, No. 4, 1979, pp 289-302.

Horner, M. W., "An Analysis of Flow on Cascades of Steps". Thesis submitted to the University of Birmingham, England, in partial fulfillment of the requirement for the degree of Ph. D., 1969.

Moore, W. L., "Energy Loss at the Base of Free Overfall". Transactions, ASCE, Vol. 108, 1943, pp 1343-1360.

Petrikat, K., "Vibration Tests on Weirs and Bottom Gates". Journal of Water Power, Vol. 10, 1958, pp

Peyras, L., Royet, P., and Degoutte, G., "Flow and Energy Dissipation over Stepped Gabion Weirs". Journal of Hydraulic Engineering, Vol. 118, No. 5, 1992, pp 707-717.

Rajaratnam, N., "Skimming Flow in Stepped Spillways". Journal of Hydraulic Engineering, Vol. 116, No. 4, 1990, pp 587-591.

Rand, W., "Flow Geometry at Straight Drop Spillways". Proceedings, ASCE, Vol. 81, 1955, Paper 791.

Robinson, K. M., "Predicting Stress and Pressure at an Overfall". Transactions, ASAE, Vol. 35, No. 2, 1992, pp 561-569.

Schwartz, H. I., "Projected Nappes Subject to Transverse Pressure". Journal of the Hydraulics Division, Vol. 89, No. HY4, 1963, pp 97-104.

Schwartz, H. I., "A Contribution to the Study of Nappe Oscillation". Transactions, South African Institution of Civil Engineers, Vol. 5, 1963, pp 253-254.

Sorensen, R. M., "Steeped Spillway Hydraulic Model Investigation". Journal of Hydraulic Engineering, Vol. 111, No. 12, 1985, pp 1461-1472.

Stephenson, D., "Energy Dissipation down Stepped Spillways". Journal of International Water Power and Dam Construction, Vol. 43, No. 9, 1991, pp 27-30.

The Societe d'emergie dela Baie James, "The La Grande Riviere Hydroelectric Complex". 1988, Montreal.

White, M. P., Discussion of Moore(1943), <u>Transactions</u>, ASCE, Vol. 108, 1943, pp 1361-1364.

Young, M. F., "Feasibility Study of a Stepped Spillway". <u>Hydraulic Division Specialty Conference</u>, Jackson, MS, 1982, pp 96-105.

APPENDIX I

RESULTS OF TESTS ON STEPPED SPILLWAY MODELS (adapted from
Horner, 1969)

Model	L mm	h mm	E_s/L	Y_c/L
Eight Steps	1066.8	3594.2	0.142	0.045
			0.164	0.055
			0.176	0.059
			0.201	0.065
			0.233	0.071
			0.265	0.082
			0.284	0.090
			0.304	0.100
			0.324	0.104
			0.343	0.108
Ten Steps	241.3	1016.0	0.235	0.073
			0.284	0.086
			0.343	0.098
			0.373	0.112
			0.412	0.125
			0.466	0.135
			0.515	0.147
			0.549	0.157
Twenty Steps	120.7	1016.0	0.500	0.143
			0.578	0.159
			0.672	0.173
			0.735	0.184
			0.804	0.200
			0.873	0.212
			0.961	0.225
			1.088	0.235
			1.157	0.251
Thirty Steps	68.9	871.0	0.407	0.129
			0.578	0.163
			0.755	0.196
			0.917	0.222
			1.142	0.249
			1.338	0.276
			1.505	0.300
			1.608	0.353
			1.951	0.400
			2.127	0.447

Table I.1 Tests results of horizontal steps for $H/L = 0.421$

Model	L mm	h mm	E_s/L	Y_c/L
Ten Steps	241.3	1270.0	0.225	0.071
			0.245	0.078
			0.275	0.086
			0.304	0.094
			0.333	0.098
			0.353	0.106
			0.373	0.114
			0.402	0.120
			0.422	0.124
			0.451	0.133
Thirty Steps	68.9	1088.1	0.471	0.137
			0.520	0.151
			0.647	0.176
			0.912	0.222
			1.392	0.278
			1.569	0.306
			2.020	0.353
			2.500	0.402

Table I.2   Tests results of horizontal steps for $H/L = 0.526$

Model	L mm	h mm	E_s/L	Y_c/L
Ten Steps	241.3	1524.0	0.164	0.071
			0.201	0.078
			0.225	0.085
			0.260	0.093
			0.301	0.100
			0.331	0.106
			0.375	0.112

Table I.3   Tests results of horizontal steps for $H/L = 0.631$

Model	L	h	E_s/L	Y_c/L
	mm	mm		
Ten Steps	241.3	1778.0	0.235	0.071
			0.265	0.076
			0.284	0.084
			0.314	0.090
			0.333	0.098
			0.363	0.104
			0.382	0.110
			0.402	0.118
			0.431	0.125
			0.461	0.131
			0.471	0.137
			0.520	0.147
			0.559	0.157
			0.608	0.167
			0.647	0.176
			0.716	0.186
Thirty Steps	68.9	1524.0	0.490	0.141
			0.500	0.145
			0.765	0.192
			1.000	0.233
			1.255	0.263
			1.314	0.267
			1.422	0.276
			1.676	0.308
			2.059	0.335
			2.324	0.351
			2.588	0.390
			2.941	0.427
			3.804	0.518

Table I.4   Tests results of horizontal steps for $H/L = 0.736$

Model	L	h	E_s/L	Y_c/L
	mm	mm		
Ten Steps	241.3	2032.0	0.25	0.071
			0.28	0.078
			0.30	0.084
			0.32	0.092
			0.36	0.100
			0.39	0.106
			0.41	0.114
			0.43	0.118
			0.46	0.124
			0.48	0.129
			0.51	0.135
			0.57	0.147
			0.61	0.157
Thirty Steps	68.9	1741.2	0.55	0.147
			0.98	0.220
			1.22	0.247
			1.49	0.276
			1.75	0.304
			2.24	0.343
			2.84	0.392
			3.20	0.424
			3.88	0.475
			4.39	0.514

Table I.5   Tests results of horizontal steps for $H/L = 0.842$

Model	θ	L	h	E_s/L	Y_c/L
	Degree	mm	mm		
Ten Steps	5	241.3	1016.0	0.16	0.070
				0.17	0.078
				0.20	0.086
				0.22	0.094
				0.24	0.099
				0.25	0.105
				0.28	0.113
				0.33	0.125
				0.36	0.136
				0.41	0.148
				0.44	0.158
				0.49	0.168
				0.52	0.177
Thirty Steps	5	68.9	871.0	0.31	0.125
				0.46	0.162
				0.58	0.191
				0.77	0.218
				0.99	0.234
				1.15	0.275
				1.34	0.304
Ten Steps	10	241.3	1016.0	0.12	0.072
				0.15	0.086
				0.17	0.097
				0.20	0.115
				0.26	0.125
				0.31	0.136
				0.35	0.148
				0.39	0.158
				0.43	0.169
				0.47	0.177
Thirty Steps	10	68.9	871.0	0.31	0.136
				0.43	0.166
				0.58	0.195
				0.73	0.222
				0.86	0.251
				1.08	0.277
				1.22	0.306

Table I.6   Tests results of inclined steps for $H/L = 0.421$
(continued)

Model	θ	L	h	E_s/L	Y_c/L
	Degree	mm	mm		
Ten Steps	15	241.3	1016.0	0.19	0.111
				0.21	0.123
				0.26	0.134
				0.30	0.146
				0.35	0.156
				0.39	0.166
				0.42	0.175
				0.48	0.185
Thirty Steps	15	68.9	871.0	0.28	0.136
				0.40	0.168
				0.53	0.193
				0.67	0.220
				0.85	0.253
				1.04	0.279
Ten Steps	20	241.3	1016.0	0.23	0.136
				0.27	0.148
				0.32	0.160
				0.36	0.169
				0.40	0.177
				0.44	0.187
Thirty Steps	20	68.9	871.0	0.35	0.162
				0.47	0.187
				0.57	0.220
				0.79	0.263
				0.96	0.279
				1.09	0.310

Table I.6   Tests results of inclined steps for $H/L = 0.421$

Model	θ	L	h	E_s/L	Y_c/L
	Degree	mm	mm		
Ten Steps	5	241.3	1270.0	0.17	0.072
				0.19	0.078
				0.22	0.086
				0.24	0.094
				0.25	0.099
				0.28	0.107
				0.29	0.111
				0.32	0.117
				0.34	0.127
				0.37	0.136
				0.42	0.146
				0.46	0.156
Thirty Steps	5	68.9	1088.1	0.36	0.134
				0.50	0.158
				0.61	0.185
				0.85	0.216
				1.07	0.251
				1.25	0.275
				1.47	0.302
				1.82	0.347
				2.25	0.395
Ten Steps	10	241.3	1270.0	0.13	0.070
				0.14	0.076
				0.16	0.086
				0.17	0.092
				0.18	0.097
				0.21	0.103
				0.23	0.111
				0.27	0.125
				0.31	0.136
				0.36	0.148
				0.40	0.156
				0.44	0.166
				0.48	0.173
				0.55	0.185

Table I.7   Tests results of inclined steps for $H/L = 0.526$
(continued)

Model	θ	L	h	E_s/L	Y_c/L
	Degree	mm	mm		
Thirty Steps	10	68.9	1088.1	0.31	0.136
				0.49	0.173
				0.59	0.187
				0.75	0.214
				0.98	0.247
				1.19	0.279
				1.38	0.300
				1.75	0.347
				2.10	0.394
Ten Steps	15	241.3	1270.0	0.14	0.070
				0.15	0.078
				0.17	0.084
				0.19	0.092
				0.19	0.097
				0.20	0.105
				0.21	0.111
				0.24	0.123
				0.30	0.134
				0.34	0.146
				0.38	0.156
				0.43	0.166
Thirty Steps	15	68.9	1088.1	0.31	0.140
				0.43	0.164
				0.53	0.185
				0.77	0.220
				0.98	0.251
				1.10	0.269
				1.30	0.298
				1.75	0.349
				2.14	0.395
Ten Steps	20	241.3	1270.0	0.14	0.070
				0.15	0.078
				0.16	0.084
				0.17	0.090
				0.18	0.097

Table I.7   Tests results of inclined steps for $H/L = 0.526$
(continued)

131

Model	θ Degree	L mm	h mm	E_s/L	Y_c/L
Ten Steps	20	241.3	1270.0	0.20	0.105
				0.21	0.113
				0.23	0.123
				0.26	0.134
				0.31	0.146
				0.34	0.156
				0.39	0.164
Thirty Steps	20	68.9	1088.1	0.39	0.158
				0.55	0.189
				0.71	0.218
				0.93	0.247
				1.18	0.281
				1.35	0.304
				1.67	0.347

Table I.7   Tests results of inclined steps for $H/L = 0.526$

Model	θ Degree	L mm	h mm	E_s/L	Y_c/L
Ten Steps	5	241.3	1778.0	0.176	0.070
				0.225	0.086
				0.275	0.097
				0.324	0.111
				0.373	0.125
				0.402	0.134
				0.441	0.146
				0.529	0.166
				0.578	0.177
				0.627	0.187
Thirty Steps	5	68.9	1524.0	0.520	0.166
				0.627	0.187
				0.863	0.216
				1.108	0.245
				1.353	0.275
				1.578	0.300
				2.088	0.345
				2.559	0.392
				2.931	0.434
				3.314	0.475
				3.686	0.503

Table I.8   Tests results of inclined steps for $H/L = 0.736$ (continued)

Model	θ Degree	L mm	h mm	E_s/L	Y_c/L
Ten Steps	10	241.3	1778.0	0.137	0.070
				0.157	0.073
				0.186	0.086
				0.206	0.092
				0.225	0.097
				0.255	0.105
				0.284	0.111
				0.304	0.117
				0.324	0.123
				0.343	0.129
				0.363	0.134
				0.402	0.144
				0.441	0.154
				0.539	0.173
Thirty Steps	10	68.9	1524.0	0.461	0.160
				0.588	0.183
				0.784	0.205
				0.922	0.226
				1.069	0.247
				1.225	0.267
				1.461	0.296
				1.892	0.341
				2.127	0.370
				2.275	0.392
				2.873	0.431
				3.333	0.503
Ten Steps	15	241.3	1778.0	0.127	0.070
				0.157	0.086
				0.196	0.097
				0.225	0.111
				0.304	0.127
				0.382	0.146
				0.441	0.158
				0.451	0.169
				0.500	0.177

Table I.8   Tests results of inclined steps for $H/L = 0.736$
(continued)

Model	θ Degree	L mm	h mm	E_s/L	Y_c/L
Thirty Steps	15	68.9	1524.0	0.343	0.132
				0.451	0.166
				0.569	0.191
				0.824	0.222
				1.020	0.249
				1.245	0.277
				1.431	0.300
				1.775	0.331
				1.892	0.349
				2.333	0.392
				2.765	0.429
				3.167	0.473
				3.637	0.512
Ten Steps	20	241.3	1778.0	0.137	0.070
				0.157	0.078
				0.167	0.084
				0.176	0.092
				0.186	0.097
				0.196	0.103
				0.235	0.109
				0.265	0.117
				0.294	0.125
				0.314	0.129
				0.333	0.134
				0.363	0.144
				0.392	0.154
				0.431	0.164
				0.471	0.175
				0.520	0.183
				0.559	0.193
				0.647	0.203
Thirty Steps	20	68.9	1524.0	0.392	0.156
				0.510	0.179
				0.667	0.205
				1.118	0.253
				1.284	0.279
				1.461	0.294
				1.676	0.325
				1.951	0.353
				2.069	0.370
				2.363	0.392
				3.000	0.458
				3.167	0.489
				3.441	0.565
				3.745	0.600

Table I.8   Tests results of inclined steps for $H/L = 0.736$

Model	θ Degree	L mm	h mm	E_s/L	Y_c/L
Ten Steps	5	241.3	2032.0	0.186	0.072
				0.216	0.080
				0.235	0.086
				0.265	0.094
				0.284	0.099
				0.304	0.105
				0.324	0.111
				0.382	0.127
Thirty Steps	5	68.9	1741.2	0.471	0.156
				0.647	0.187
				0.902	0.218
				1.157	0.247
				1.333	0.275
				1.627	0.298
				2.167	0.356
				2.716	0.395
				3.304	0.434
				3.686	0.475
Ten Steps	10	241.3	2032.0	0.206	0.086
				0.235	0.094
				0.255	0.101
				0.284	0.107
				0.294	0.113
				0.324	0.119
				0.343	0.127
				0.402	0.134
Thirty Steps	10	68.9	1741.2	0.382	0.132
				0.569	0.168
				0.696	0.189
				0.912	0.220
				1.108	0.247
				1.333	0.273
				1.529	0.304
				2.010	0.347

Table I.9   Tests results of inclined steps for $H/L = 0.842$ (continued)

Model	θ Degree	L mm	h mm	E_s/L	Y_c/L
Thirty Steps	10	68.9	1741.2	2.598	0.395
				2.784	0.425
				3.333	0.475
				3.843	0.518
Ten Steps	15	241.3	2032.0	0.196	0.092
				0.225	0.099
				0.245	0.105
				0.275	0.113
				0.294	0.117
				0.324	0.125
				0.382	0.138
				0.412	0.144
				0.431	0.150
Thirty Steps	15	68.9	1741.2	0.343	0.131
				0.490	0.160
				0.637	0.185
				0.882	0.220
				1.098	0.249
				1.304	0.273
				1.500	0.300
				2.049	0.349
				2.510	0.395
				2.804	0.425
				3.431	0.473
				3.794	0.505
Ten Steps	20	241.3	2032.0	0.196	0.099
				0.225	0.107
				0.245	0.113
				0.265	0.119
				0.284	0.127
				0.304	0.131
				0.343	0.140
				0.392	0.150
Thirty Steps	20	68.9	1741.2	0.314	0.134
				0.529	0.175
				0.667	0.195
				0.843	0.220
				1.078	0.247
				1.265	0.275
				1.480	0.304
				1.961	0.347
				2.529	0.395
				2.902	0.434
				3.373	0.475
				3.892	0.508

Table I.9   Tests results of inclined steps for $H/L= 0.842$

APPENDIX II

VARIATION OF FLOW COORDINATES AND VELOCITY DISTRIBUTIONS
WITH Y_c/H AT DIFFERENT LOCATIONS

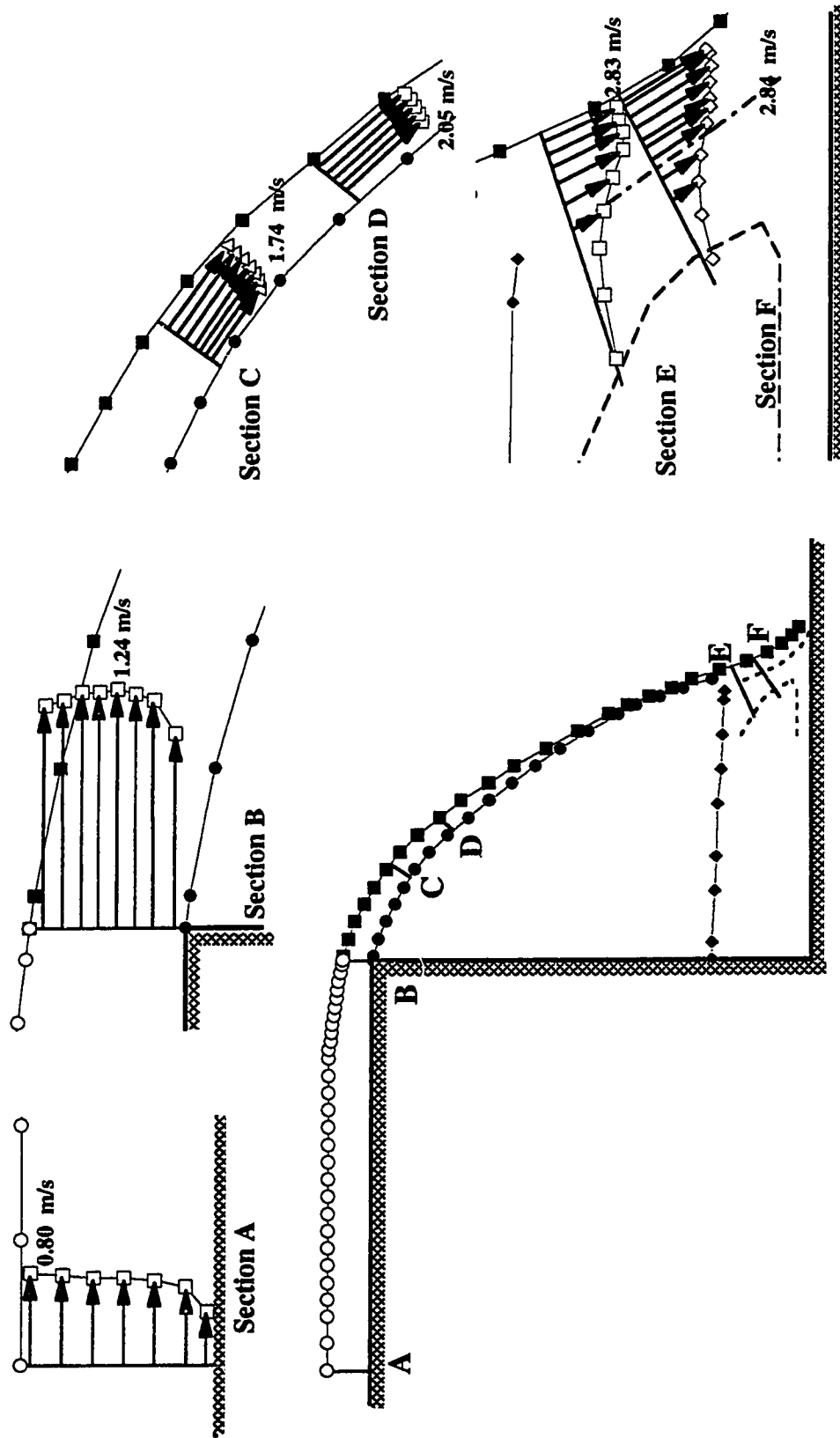Figure II.1 Water level and velocity profiles for Yc/H= 0.10

Figure II.2 Water level and velocity profiles for Yc/H= 0.12

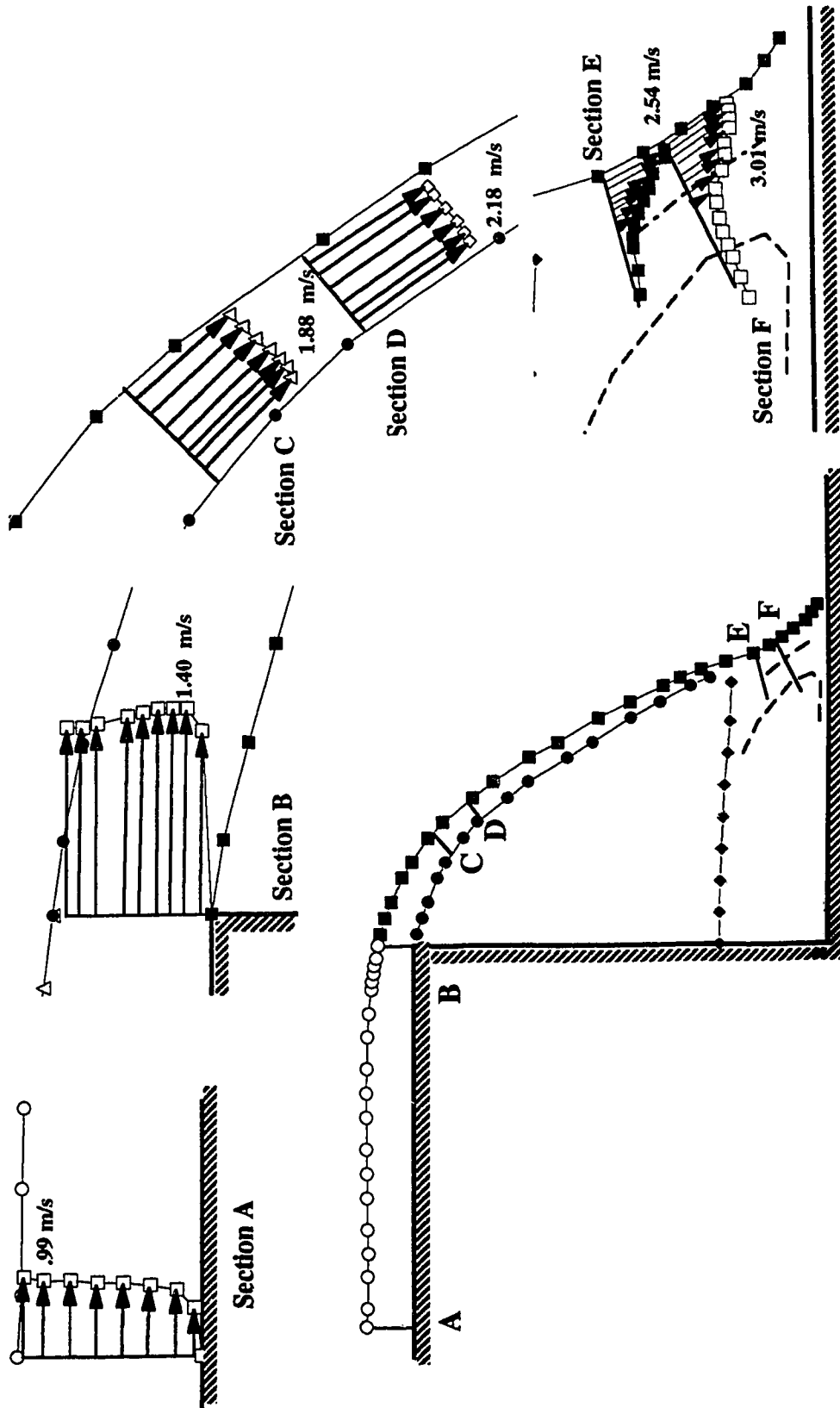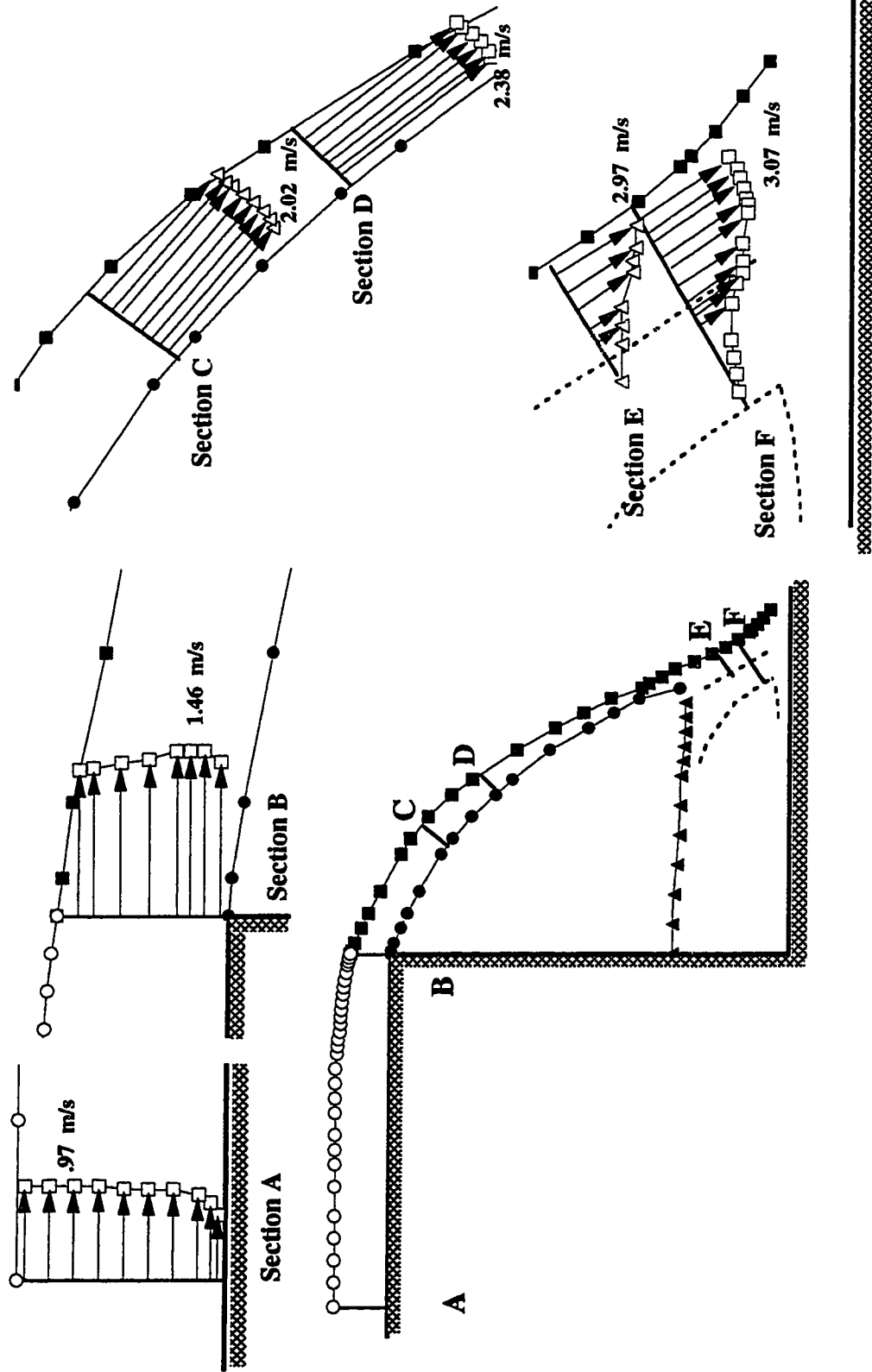Figure II.3 Water level and velocity profiles for Yc/H= 0.14

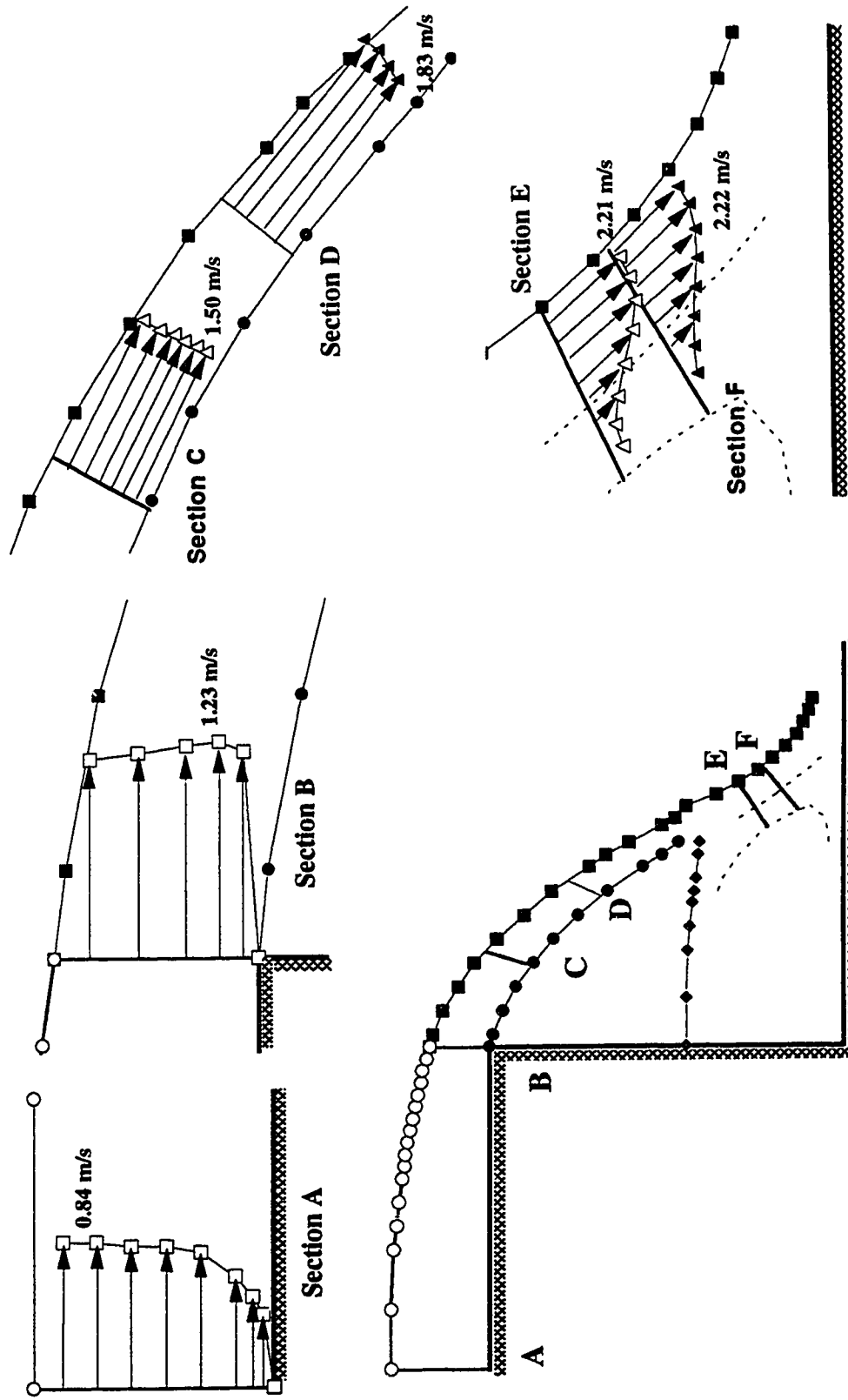Figure II.4 Water level and velocity profiles for Yc/H= 0.25
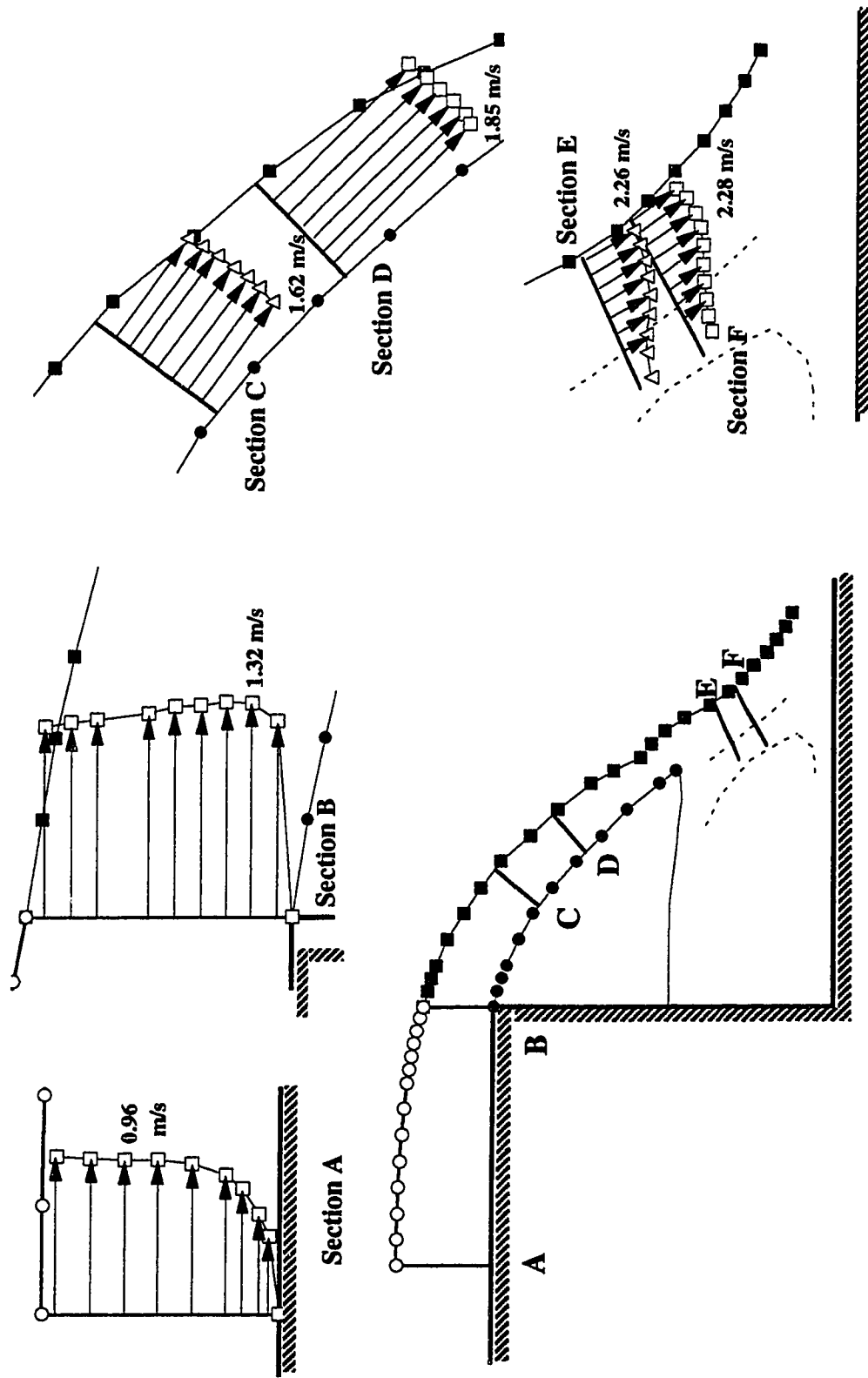
Figure II.5 Water level and velocity profiles for Yc/H= 0.30

Figure II.6 Water level and velocity profiles for Yc/H= 0.35